6-24-2020 2:30 PM

Iron(II) Metal-Ligand Cooperative Catalysts for Endo-Selective Intramolecular Hydrofunctionalization

Benjamin Bridge, *The University of Western Ontario*

Supervisor: Blacquiere, Johanna M., *The University of Western Ontario*
A thesis submitted in partial fulfillment of the requirements for the Master of Science degree in Chemistry
© Benjamin Bridge 2020

Abstract

Two new cationic Fe(II) $P^R_2N^{Ph}_2$ complexes, $[Fe(Cp^*)(P^{Cy}_2N^{Ph}_2)(MeCN)]PF_6$ (**3a**) and $[Fe(Cp^*)(P^{Ph}_2N^{Ph}_2)(MeCN)]PF_6$ (**3b**), were synthesized and characterized. The catalytic activity for intramolecular hydrofunctionalization was tested using the benchmark substrate 2-ethynylaniline (**EA)** and both catalysts effectively produced indole (**Ind**). The selectivity of catalysis was also tested using 2-ethynylbenzyl alcohol (**EBA**) and both catalysts formed only the *endo* product isochromene (**IC**). These complexes represent the first well-defined Fe(II) catalysts that are *endo* selective for the hydrofunctionalization of alkynes. An Fe(II) vinylidene complex, $[Fe(Cp^*)(P^R_2N^{Ph}_2)(=C=CHPh)]PF_6$ (R = cyclohexyl, **7**), was also characterized that suggests an analogous intermediate is responsible for catalytic selectivity. Catalyst decomposition was also probed and a possible off-cycle deactivation product was identified. On-cycle intermediates were potentially identified and proposed as resting-state species in the catalytic cycle. Preliminary studies were attempted to assess activity and selectivity on a small scope of substrates, but more optimization will be required.

Keywords

Summary for Lay Audience

Two iron compounds were made for the first time that were based on similar ruthenium compounds previously known. These iron compounds are catalysts that help to cause chemical reactions for making rings containing carbon atoms and either oxygen or nitrogen atoms. The ring size that the catalysts make is consistent and controlled by carefully designing the structure around the metal to do reactions in a specific way. These catalysts are the first ones made with iron that can make rings in a certain way that previously has been done with expensive metals. A similar iron compound was also made that showed how the catalyst was able to make the correct size of rings, and another compound was found that might be the catalyst breaking down. Understanding how the catalyst works and how it breaks down will help find ways to improve performance and lifetime. There could be a large reduction in the cost of catalysts if abundant metals like iron can continue to be used in well-designed compounds to do the jobs of precious metals.

Co Authorship Statement

Chapters 2, 3, 4, and 6 of the following thesis include work that has been submitted for review.

Chapters 2, 3, 4, and 6 were co-authored by B. J. Bridge, J. M. Blacquiere, and P. D. Boyle. All of the experimental work was performed by BJB with the exception of crystal data collection and refinement, which was performed by PDB. The manuscript was prepared by BJB and edited by JMB.

Chapters 1, 5, and 6 were written by B. J. Bridge and edited by J. M. Blacquiere.

Acknowledgements

First and foremost, I must acknowledge the unwavering support that I have received over the years from my partner, Morgan Lander. She has truly been a stable force throughout a turbulent time, inspiring me to challenge myself and guiding me with patience as I did. The goals I have accomplished would not have been possible without her. It has not been easy for either of us over the last few years as I have progressed through university, and I will never forget the sacrifices she has made to get us both through.

Before my graduate studies even began, I was fortunate enough to have had the opportunity to do laboratory work under the mentorship of Dr. Johanna Blacquiere. The opportunities that she afforded me from an early stage in my chemistry education were incredibly instrumental to my success in later years, and her fearless guidance through the challenging world of research will always be appreciated. I'm sure I challenged her at times with my pessimistic outlook, but ultimately I hope that I brought a meaningful and positive contribution to her lab and to the exciting chemistry that happens there.

Much appreciation also goes to Dr. James Stubbs, who was another early mentor and the one who referred me to Johanna when I was an undergrad. James had trust in me when I knew very little about chemistry, and everything that I learned from him had a huge impact on building my confidence and skills in the lab.

I am also grateful to have had the chance to work for Dr. Michael Kerr for my Honours Thesis during the last year of my undergraduate degree. A true gem, with such a passion for synthesis that he will never cease to inspire.

Thanks to Mat Willans for running a very fine NMR facility, to Paul Boyle for his crystallography work, and to Kristina Jurcic for the mass spec analysis.

To all of the d-orbitals, past and present, that I've had the pleasure of knowing along the way. David, Devon, Jonathan, Justin, J.W., Kyle, Matt, Meagan, Nick, Shane, Sophia; it has been a weird and crazy ride, and I appreciate you all for sharing it with me.

Table of Contents

List of Schemes

List of Tables

List of Figures

List of Charts

List of Appendices

List of Abbreviations

Å	Angstrom = 10^{-10} meters
Ar	Aryl
ATR-FTIR	Attenuated Total Reflectance – Fourier Transform Infrared
Bn	Benzyl
$BnNH_2$	Benzylamine
$C\alpha$	Alpha carbon
$C\beta$	Beta carbon
CHD	1,4-Cyclohexadiene
COSY	Correlation Spectroscopy
Cp	Cyclopentadienide
Cp*	1,2,3,4,5-pentamethylcyclopentadienide
Cy	Cyclohexyl
DCE	1,2-Dichloroethane
DCM	Dichloromethane
DHQ	1,4-Dihydroquinoline
DMF	Dimethylformamide
Dppm	Bis(diphenylphosphino)methane
EA	2-Ethynylaniline
EAD	2-Ethynylbenzyl amide

EADH	*N*-Methoxy-2-Phenylethynylbenzyl amide
EAM	2-Ethynylbenzyl amine
EBA	2-Ethynylbenzyl alcohol
GC-FID	Gas Chromatography Flame Ionization Detector
HMBC	Heteronuclear Multiple Bond Correlation
HSQC	Heteronuclear Single Quantum Coherence
IC	1*H*-Isochromene
Ind	Indole
IR	Infrared
M	Metal
MALDI-MS	Matrix Assisted Lase Desorption Ionization-Mass Spectrometry
MBF	1-methylene-1,3-dihydroisobenzofuran
Me	Methyl
MeCN	Acetonitrile
Mes	Mesityl
MeTHF	2-Methyl tetrahydrofuran
MI	2-Methylindole
MLC	Metal-ligand Cooperative
*n*BuNH$_2$	*n*-Butylamine
NHC	*N*-Heterocyclic carbene

NMR	Nuclear Magnetic Resonance
ORTEP	Oak Ridge thermal ellipsoid plot
PA	2-propynyl aniline
pK_b	Base dissociation constant
$P^R_2N^{R'}_2$	1,5-diaza-3,7-diphosphacyclooctane
py	Pyridine
TBAF	Tetrabutylammonium fluoride
THF	Tetrahydrofuran
TMS	Trimethylsilyl
TON	Turnover Number

Chapter 1

1   Introduction

1.1   Principles of Catalyst Design

Homogeneous transition-metal catalysts have allowed a large degree of control over reactivity through the ability to fine-tune specific variables of catalyst structure.[1-7] Altering the steric and electronic properties of ligands and using different metals has had significant impact on the activity and selectivity of catalytic transformations. The insight gained from systematic tuning has led to an increasing number of well-defined catalysts that have been rationally designed for specific needs. Improvement in activity and selectivity through ligand design has been well established for precious metals, and there is a large body of evidence that the right ligand environment can control base metals to be used for many complementary transformations.[8-23]

1.2   Catalytic Intramolecular Hydrofunctionalization of Alkynes

Hydrofunctionalization is the addition of an EH group (E = O, NH, S, PH, and others) across a double or triple bond.[24] This thesis will focus specifically on the intramolecular hydrofunctionalization of alkynes. Since both the alkyne and the nucleophile are part of the same substrate, the product formed is a heterocycle, which contains a double bond that may be located outside (*exo*) or within (*endo*) the new ring (Scheme 1.1). This regioselectivity is determined by which carbon atom of the alkyne is attacked by the heteroatom during the reaction. This reaction does not typically occur spontaneously and catalysis can be employed to facilitate transformation.
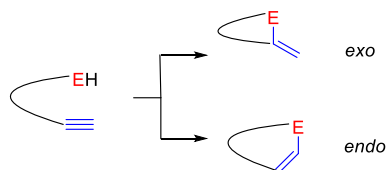
Scheme 1.1: Intramolecular hydrofunctionalization of alkynes will lead to *exo* or *endo* heterocycles.

Intramolecular hydrofunctionalization was catalyzed using a strong base to selectively form *exo* products.[25] 2-Ethynylbenzyl alcohol (**EBA**) was base-activated by deprotonation of the heteroatom to make it a better nucleophile, and the alkyne was attacked at the β-position due to closer proximity than to the α carbon (Scheme 1.2). The resulting carbanion deprotonated the conjugate acid of the base catalyst to regenerate the catalyst and form the *exo* heterocyclic product 1-methylene-1,3-dihydroisobenzofuran (**MBF**). The 6-membered *endo* product **IC** was not observed.
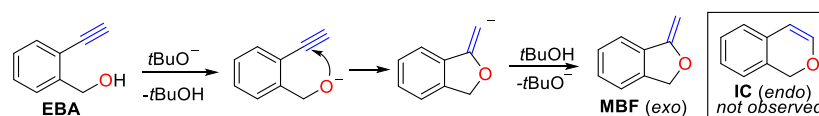
Scheme 1.2: *Exo*-selective hydrofunctionalization can be accomplished using strong base as a catalyst.

While effective at forming *exo*-selective heterocycles, strong bases will react with acidic functional groups and could be incompatible with many substrates. Use of transition metals as catalysts for hydrofunctionalization of alkynes can be effective on a broad range of substrates and allows a much more controlled approach than simple deprotonation.[26-33]

Transition metals can activate a substrate for hydrofunctionalization by π-coordination of the alkyne to a Lewis acidic metal (Scheme 1.3).[24] This activates the substrate by increasing the electrophilicity of the alkyne so the heteroatom can attack more favourably. The metal alters the shape of the alkyne by donating electrons into an anti-bonding orbital of the triple bond, and the extra flexibility that results can allow nucleophilic attack on either of the two carbon atoms in the alkyne. Through this type of activation, the carbon atoms may have similar electrophilicity and therefore the resulting product may be either *exo* or *endo*. Often, the electronic characteristics of the substrate will influence the resulting regioselectivity, and control over the final products can be difficult to achieve.
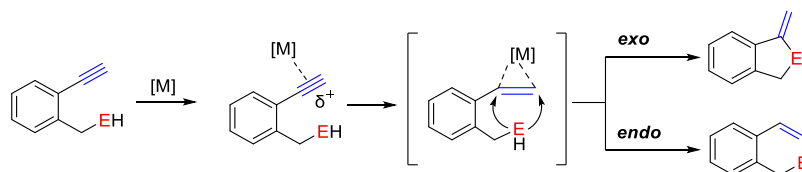
Scheme 1.3: Alkyne coordination can activate the substrate to increase electrophilicity, but products may form either *exo* or *endo*.

Copper(II) triflate has catalyzed the hydrofunctionalization of an internal alkynol to form the *exo* product through a π-activation mechanism that involved the alkyne coordinating to the Cu(II) metal center (Scheme 1.4).[34] The phenyl substituent on the alkyne provided resonance stabilization for only one carbon of the triple bond, resulting in polarization of the intermediate that led to a selective attack.
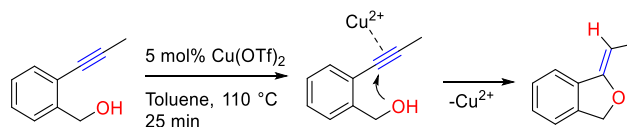
Scheme 1.4: Cu(II) is proposed to coordinate to both the alkyne and the heteroatom to form *exo* heterocycles.

Pt(IV) chloride has been effective as a catalyst to hydrofunctionalize a methoxy amide substrate through π-activation to form a 6-membered *endo* product (Scheme 1.5).[35] Two Pt(IV) cations were proposed to interact with the substrate in a bimolecular catalytic mechanism. One equivalent of metal activated the alkyne while the other coordinated to the oxygen atoms in the substrate. This second interaction with the oxygen atoms affected the flexibility of the substrate and *endo* heterocycles were formed.
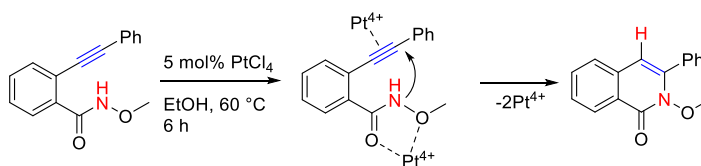
Scheme 1.5: Two Pt(IV) cations activate the substrate in tandem to form *endo* heterocycles.

Copper(II) chloride has been shown to catalyze the hydrofunctionalization of a 2-ethynyl amide derivative (**EADH**) through a radical mechanism (Scheme 1.6). A hydrogen atom was abstracted from the **EADH** and oxidized to a proton along with reduction of the Cu(II) to Cu(I). This redox resulted in radical species **EAD·** which underwent intramolecular hydrofunctionalization and was *endo*-selective for an isoquinolone derivative.[36]
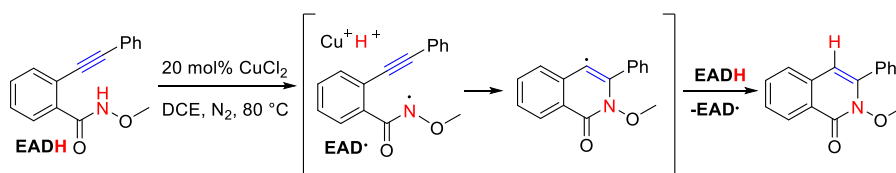
Scheme 1.6: Activation of a substrate for radical hydrofunctionalization has been demonstrated with Cu(II).

Iron has been shown to exhibit activity in the catalytic hydrofunctionalization of alkynes via π-activation. An Fe(III) chloride salt formed *exo* heterocycles when terminal alkynamines were heated in toluene (Scheme 1.7).[37] The *exo* regioselectivity was due to the number of carbon atoms between the nucleophile and the alkyne so only 5-membered rings could form favourably.
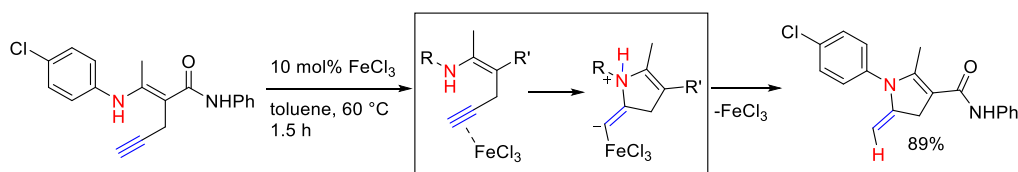
Scheme 1.7: Fe(III) has been shown to effectively catalyze the hydrofunctionalization of terminal alkynes to form *exo*-selective products.

Fe(II) has been demonstrated to initiate radical transformations as well (Scheme 1.8).[38] Fe(II) was oxidized to Fe(III) by di-tert-butyl peroxide ((tBuO)$_2$) and a radical species from the tetrahydrofuran (**THF**) solvent was formed. This radical coupled with two equivalents of indole (**Ind**) to form a bis-indolylmethane derivative. While not an

example of hydrofunctionalization, this type of unwanted reactivity may be avoided by careful control of reaction conditions and catalyst structure.
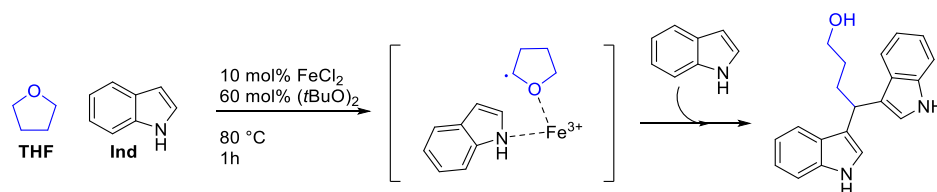
Scheme 1.8: A radical mechanism involving Fe(II) to Fe(III) oxidation using (tBuO)$_2$ has been demonstrated to couple tetrahydrofuran (**THF**) to indole (**Ind**).

Divergent reaction pathways were observed with the use of exogenous bases and an Fe(III) salt for the hydrofunctionalization of alkynyl phenols to form benzofuran (*exo*) and chromene (*endo*) derivatives (Scheme 1.9).[39] Using *n*-butylamine (*n*BuNH$_2$) as a base resulted in selectivity for the *exo*-heterocycle. Switching the base to aniline (PhNH$_2$) gave a roughly even mixture of both *exo* and *endo* regioisomers. When aniline was used along with Fe(III), however, the reaction was completely selective for the *endo* product. The alkyne had to be activated by the Lewis-acidic Fe(III) for *endo*-selectivity to occur, otherwise the mechanism was base-mediated and *exo*-heterocycles would result.
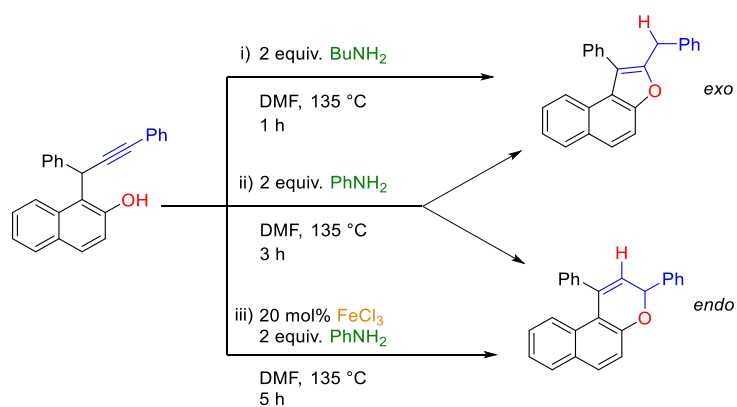
Scheme 1.9: i) Use of *n*BuNH$_2$ mediated the hydrofunctionalization of alkynol phenols to form *exo* heterocycles. ii) Aniline produced a mixture of *exo* and *endo* heterocycles. iii) Fe(III) used with aniline was successful for *endo*-selective hydrofunctionalization.

Fe(0) catalyst **A** successfully catalyzed the hydrofunctionalization of alkynols to produce *exo* heterocycles by π-activation (Scheme 1.10).[40] This complex is an example of metal-ligand cooperative (MLC) catalyst, in which a supporting ligand participates in catalytic steps (see Section 1.3).[41-46] Proton-transfer was assisted by the cyclopentadienone ligand, which converted to a hydroxyl group during an intermediate step in catalysis. Subsequent deprotonation of this hydroxyl group facilitated product release and regenerated the active catalyst.
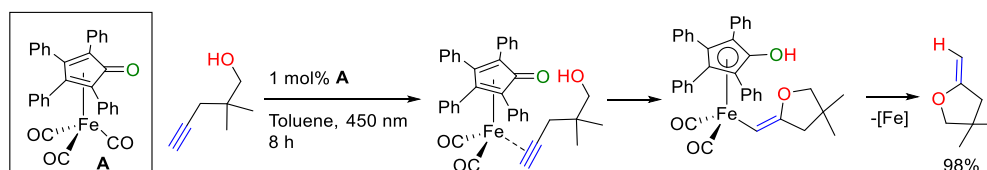
Scheme 1.10: Fe(0) catalyst **A** exhibits metal-ligand cooperativity.

Certain metals, such as Fe(II), Ru(II), Os(II), Mo(0) and Ir(III), have been shown to react with both terminal and internal alkynes to form a vinylidene complex (Scheme 1.11).[47-55] These complexes result from a 1,2-shift of an alkyne R group to the β carbon position, which has been demonstrated to be much more facile on terminal alkynes due to the relatively small size of a proton.[56-60] Catalytic hydrofunctionalization through a vinylidene intermediate is therefore typically accomplished using terminal alkynes as substrates.
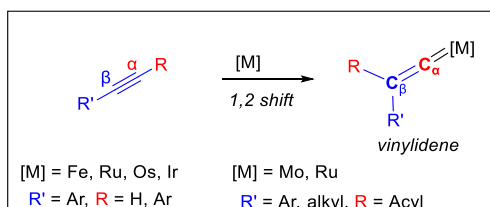
Scheme 1.11: Vinylidene intermediates have been formed from terminal and internal alkyne with the use of certain metals.

The structure of a vinylidene contains a highly polarized C=C bond with an electrophilic α carbon. When vinylidene intermediates were formed during hydrofunctionalization

catalysis, the electrophilic α carbon was attacked by the tethered nucleophile and e*ndo* heterocycles were selectively produced (Scheme 1.12). [53] [61]
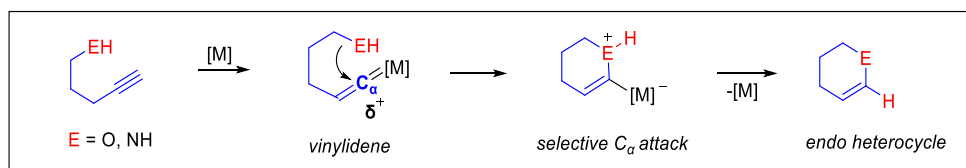
Scheme 1.12: *Endo*-selective heterocycles have been formed through a vinylidene intermediate.

Multiple proton-transfer steps were determined to be part of the catalytic cycles for hydrofunctionalization of terminal alkynes that go through a vinylidene intermediate (Scheme 1.13).[57-60] Isomerization to the vinylidene and product release both involved proton-transfer steps that were assisted by bases.
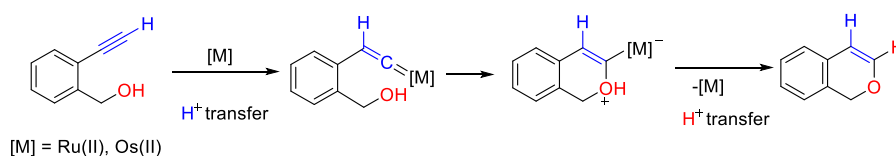
Scheme 1.13: Proton-transfer steps occur multiple times during catalysis that goes through a vinylidene intermediate

Piano-stool Ru(II) catalyst **B**, for intramolecular hydrofunctionalization and oxidative cyclization on aliphatic alkynol substrates, demonstrated that both *exo* and *endo* heterocycles were produced (Scheme 1.14i).[62] Two regioisomers of heterocycles were observed because both π-activation and vinylidene mechanisms were operative (Scheme 1.14ii). The sodium salt of *N*-hydroxysuccinimide was used as a base to promote hydrofunctionalization, but also acted as an oxidant in a separate pathway that formed lactones (not shown). The choice of electron-withdrawing *P*-substituents favoured hydrofunctionalization over oxidative cyclization. The presence of excess PAr$_3$ ligand pushed the regioselectivity to form more of the *endo* product by favouring the formation of a metal-vinylidene intermediate. This indicates that bulky phosphine ligands on piano-

stool Ru(II) complexes, such as **B**, create a steric environment favourable for vinylidene formation.
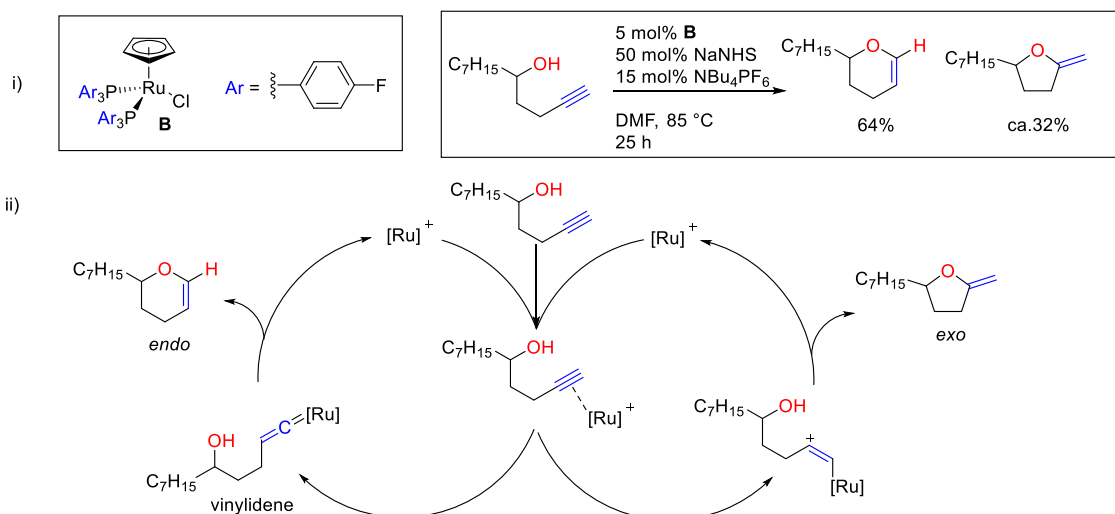
Scheme 1.14: i) A piano-stool Ru(II) complex **B** catalyzed the hydrofunctionalization of alkynes. ii) Both vinylidene (left) and π-activation (right) mechanisms were evident.

Piano-stool Ru(II) complex **C** was found to be highly selective for *endo* hydrofunctionalization of terminal aryl alkynols (Scheme 1.15).[60] 2-Ethynylbenzyl alcohol (**EBA**) was catalytically converted into 1*H*-isochromene (**IC**), without any formation of the *exo* product, 1-methylene-1,3-dihydroisobenzofuran (**MBF**). Basic amine solvent assisted in proton-shuttling steps and was required for catalytic activity to be achieved.
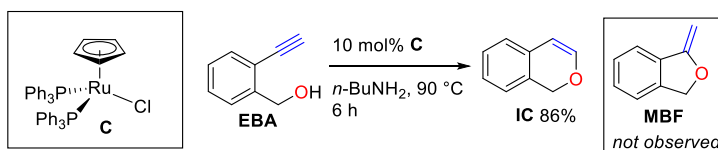
Scheme 1.15: Bulky P-substituted ligands on piano-stool Ru(II) complex **C** allowed catalysis of *endo* selective heterocycles.

Hydrofunctionalization with catalyst **C** using deuterium isotope-labelled substrate also confirmed that the terminal alkyne proton was incorporated into the β-position of the

vinylidene (Scheme 1.16i). Internal alkynes were not cyclized under the conditions that were effective for terminal substrates using catalyst **C** (Scheme 1.16ii). This is highly suggestive that the mechanism does not follow π-activation of the alkyne. This observation along with the *endo* selectivity of the reaction both indicate that the alkyne is activated through a metal-vinylidene intermediate.
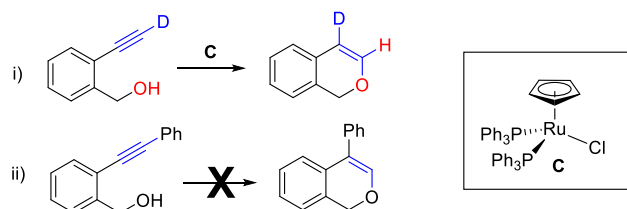
Scheme 1.16: i) Deuterium was transferred into the β-position during catalysis of isotope labelled **EBA**. ii) Internal alkynes failed to hydrofunctionalize using Ru(II) complex **C**.

Aryl alkynamides were hydrofunctionalized to isoquinolones using the same piano-stool Ru(II) complex **C** (Scheme 1.17i).[58] Only *endo* selectivity was observed and internal alkynes failed to cyclize. A vinylidene route is therefore highly probable. The complex was also unable to cyclize the benzylamine derivative, unlike the analogous alcohol substrate. This is a consequence of competitive coordination of the amine to the metal center due to strong Lewis basicity (Scheme 1.17ii). As a result, only amides and anilines were effectively cyclized.
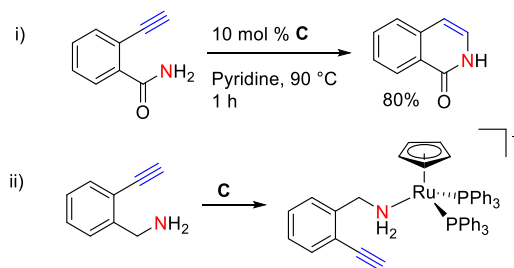
Scheme 1.17: i) *Endo*-selective hydrofunctionalization of alkynyl amides can be accomplished with bulky Ru(II) catalyst **C**. ii) Proposed coordination of 2-ethynylbenzyl amine to catalyst **C**.

The importance of the specific structure of **C** in directing regioselectivity was demonstrated with the hydrofunctionalization of a 2-propynylaniline derivative (Scheme 1.18, **PA**) to form the *endo* product dihydroquinoline (**DHQ**). In contrast, the dimer catalyst [RuCl$_2$(*p*-cymene)]$_2$, in the presence of tri-*n*-butylphosphine (P*n*Bu$_3$), formed only the *exo* product, 2-methylindole (**MI**) through a π-activation mechanism of the alkene.
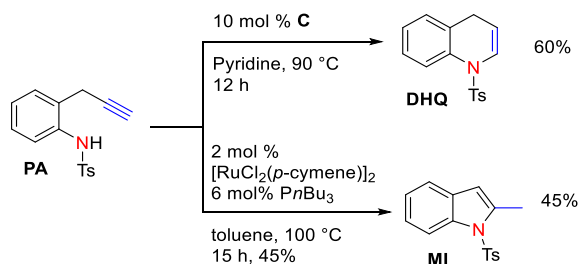
Scheme 1.18: Different Ru(II) catalysts are capable of the hydrofunctionalization of alkynes through both vinylidene and π-activation mechanisms.

If the number of carbon atoms on the substrate between the heteroatom nucleophile and the alkyne is increased to four or more, *endo* heterocycles can be formed selectively through vinylidene intermediates. However, increased flexibility of the alkyl chain, coupled with the unfavourable ring strain of 7- vs 6-membered rings, often makes this catalytic reaction more difficult to achieve when compared to substrates such as **EBA**.

A piano-stool Os(II) catalyst (**D**) is able to perform this catalysis and has been used to hydrofunctionalize alkynols into 7-membered *endo* benzoxepeines and secondary alkynamines into 7-membered *endo* benzazepines (Scheme 1.19i-ii).[59] The proposed mechanism was distinct from Ru(II) catalysts, in that it first involved oxidative addition of the terminal alkyne onto the Os(II) center before vinyilidene formation (Scheme 1.19iii).
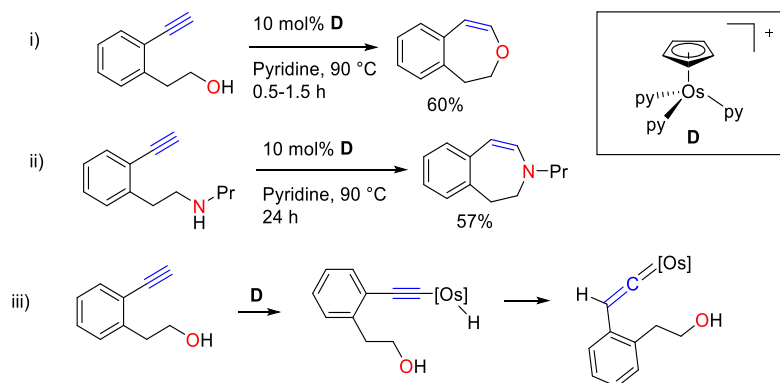
Scheme 1.19: Os(II) catalyst (**D**) is effective at *endo* formation of i) benzoxepine and ii) benzazepine in basic solvent. iii) Os(II) complex **D** can activate substrates through oxidative addition.

Os(II) is larger and more easily oxidized than Ru(II), and thus able to access an Os(IV) oxidation state more readily.[57] This ability was observed in osmacyclopropene complex **E** that was isolated and characterized after being trapped from the catalytic cycle with potassium *tert*-butoxide (*t*BuOK) (Scheme 1.20). The formation of such an intermediate was a direct result of the regioselective nucleophilic attack on the α carbon of a vinylidene. Proton-shuttling steps in the catalytic cycle were accomplished with pyridine solvent, which was required for catalytic activity.
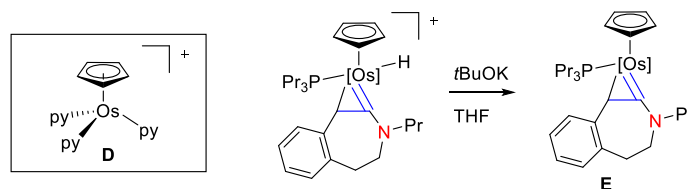
Scheme 1.20: An Os(IV) intermediate **E** was trapped from the catalytic cycle using a strong base.

A Ru(II) dimer complex (**F**) was recently employed for making *endo*-selective 7-membered *O*-heterocycles (Scheme 1.21i).[56] The monomeric Ru(II) active catalyst (**G**) was reacted with substrate under milder conditions than used for catalysis and oxocarbene intermediate (**H**) was formed (Scheme 1.21ii). This intermediate was formed after nucleophilic attack on the α carbon of a vinylidene. Unlike the Os(II) catalyst **D** that has

been previously used for this transformation, no basic solvent was required for catalysis. While not proposed by the authors, it is reasonable to hypothesize that the ligand assists in proton-transfer steps in the role that exogenous amine bases have previously been discussed (see Section 1.3).
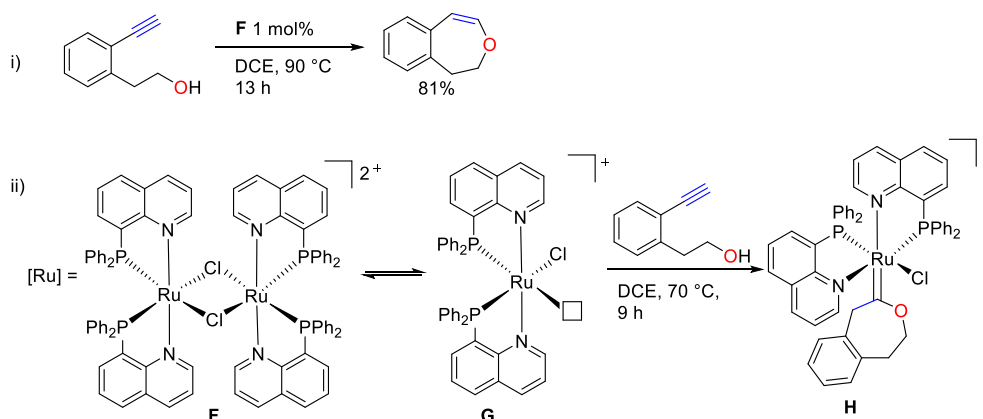
Scheme 1.21: i) 7-membered *endo*-selective heterocycles were formed with a well-defined Ru(II) catalyst. ii) Precatalyst dimer **F** dissociated into active catalyst **G** and formed oxocarbene **H** from an alkynol substrate.

1.3   Proton-Transfer MLC Catalysts for Hydrofunctionalization

Selectivity can thus be directed to form *endo* heterocycles with the right choice of catalyst, typically a piano-tool Ru(II) or Os(II) complex. This regioselectivity is directed by a vinylidene intermediate, and proton-transfer by a base has been established as key in formation of the metal-vinylidene and in subsequent steps of the catalytic cycle (Scheme 1.22).
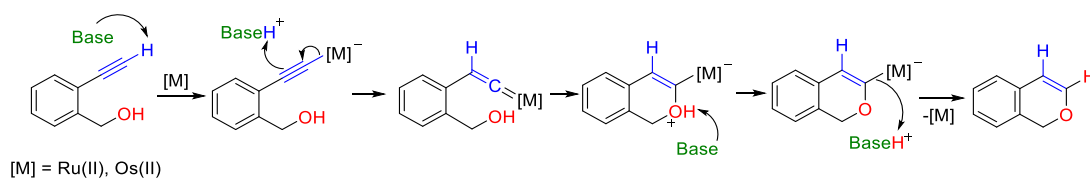
Scheme 1.22: Proton-transfer steps occur in vinylidene formation and product release during *endo*-selective intramolecular hydrofunctionalization.

Proton-transfer for hydrofunctionalization catalysis has often been mediated by exogenous amine bases, but activity can be improved by incorporating the basic functionality directly into the ligand structure. Early work developing metal-ligand cooperative (MLC) catalysts for hydrofunctionalization utilized phosphine ligands with pyridyl or imidazolyl functional groups to act as bases (Scheme 1.23, **J**).[63-65] The hydrofunctionalization of 2-ethynylaniline (**EA**) to indole (**Ind**) was achieved with a catalyst loading of **J** five times lower than the previous Ru(II) catalyst **C** (Scheme 1.23).[58, 66] These transformations did not require basic additives and were effective in THF, indicating that proton transfer was assisted by the basic site on the ligand structure.
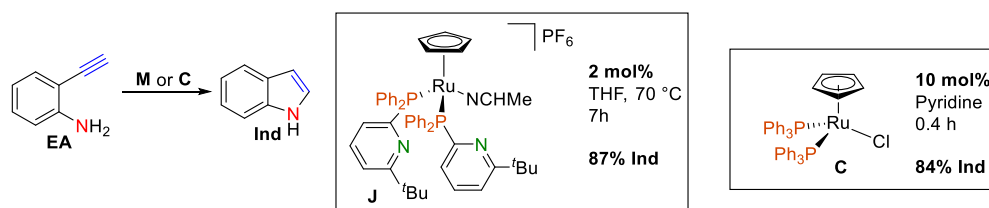
Scheme 1.23: Metal-ligand cooperative (MLC) catalyst **J**, in the absence of base, shows improved activity over non-MLC catalyst **C** for the hydrofunctionalization of **EA** to **Ind**.

Direct evidence of the ligand interaction of **J** with protons was observed through ^{15}N NMR spectroscopy studies of analogous vinylidene complex **K** reacting with water as a nucleophile (Scheme 1.24).[67] Hydrofunctionalization with water resulted in the protonation of the pyridyl ligand and a distinct upfield shift was observed in the ^{15}N NMR spectrum for two protonated species **L** and **M**. The proton was in equilibrium between these two hydrogen-bonded species (**L/M**) that both exhibited similar chemical shifts. Further studies using DFT calculations also supported the existence of similar species and indicated that several proton-transfer steps may occur during catalysis that directly involve the ligand.[68]
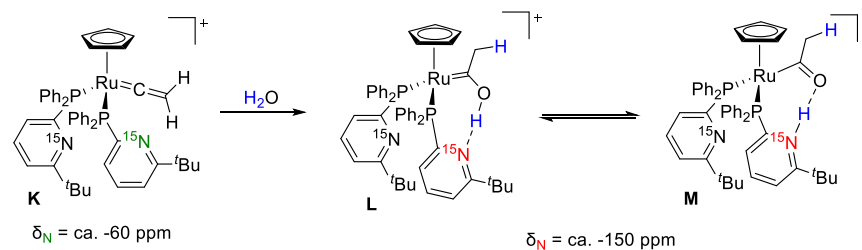
Scheme 1.24: Monitoring the hydration reaction of vinylidene **K** by ^{15}N NMR analysis provided direct evidence of protonation of the ligand in species **L** and **M**.

Further improvement of MLC catalyst activity for hydrofunctionalization has been possible by using the highly tunable 1,5-diaza-3,7-diphosphacyclooctanes ($P^R_2N^{R'}_2$) ligands on piano-stool Ru(II) complexes (Scheme 1.25).[69-71] The chelating phosphine donor ligands contained amine functional groups, which assisted in proton shuttling during hydrofunctionalization catalysis similar to previously studied MLC pyridyl ligands. The $P^R_2N^{R'}_2$ ligands were customized by the selection of *P*- and *N*-substituents used during synthesis, which allowed tunability of the steric and electronic characteristics. Coordination to [Ru(Cp/Cp*)(MeCN)$_3$]PF$_6$ then afforded [Ru(Cp/Cp*)($P^R_2N^{R'}_2$)(MeCN)]PF$_6$ complexes. The choice of a cyclopentadienyl (Cp) or the sterically bulky pentamethylcyclopentadienyl (Cp*) Ru(II) precursor also provided another dimension to the structural tunability.
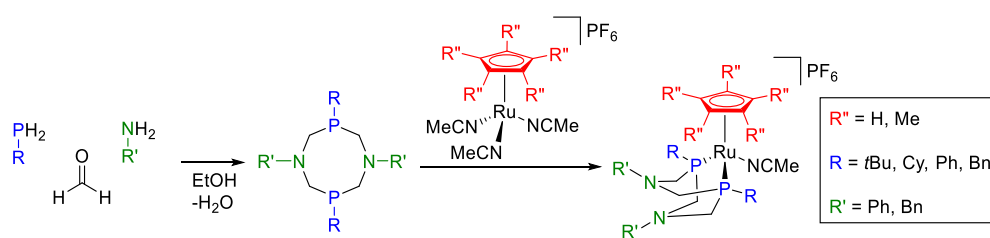
Scheme 1.25: General synthetic method for the synthesis of MLC complexes of the type [Ru(Cp/Cp*)($P^R_2N^{R'}_2$)(MeCN)]PF$_6$.

Such a high-degree of tunability has facilitated the development of these $P^R_2N^{R'}_2$ complexes to achieve significant improvements in catalytic activity for intramolecular hydrofunctionalization of alkynes. Testing of various *N*-substituents (R' = Ph, Bn, Mes, *p*-CF$_3$Ph, *p*-OMePh) revealed that the pK_b was an important factor for turnover number.

The less basic R' = *p*-CF₃Ph performed most poorly, indicating that the basicity of the ligand amine was critical for optimal performance. The *P*- substituent steric factors (R = *t*Bu, Cy, Ph, Bn) influenced performance more than electronics, and as a result bulky *P*-substituents gave the best results. Lower temperatures were required for the Cp* derivative to initiate into the catalytic cycle, but if higher temperatures were employed, the Cp derivative excelled and had almost twice the lifetime.

[Ru(Cp/Cp*)(P$^R_2$N$^{R'}_2$)(MeCN)]PF₆ complexes **N** (Cp) and **O** (Cp*) where R = *t*Bu and R' = Ph were found to be the most active catalysts for the intramolecular hydroamination of **EA** (Scheme 1.26). Due to the cooperative nature of the amine functionality, no exogenous base was required for catalysis. The highest turnovers for any of the catalysts studied was 20 times higher than the previous MLC catalyst **J**.
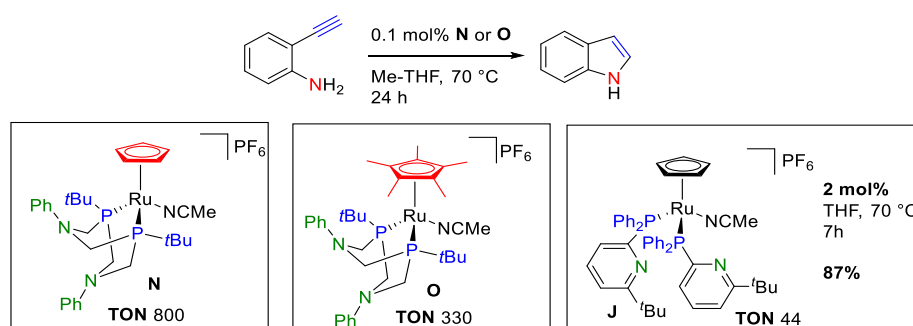
Scheme 1.26: Ru(II) P$^R_2$N$^{R'}_2$ MLC catalysts **N** and **O** have shown significant improvements in activity over Ru(II) catalyst **J**.

Complexes **N** and **O** also follow a vinylidene mechanism for intramolecular hydrofunctionalization, which was demonstrated with regioselective *endo* hydrofunctionalization of **EBA** to **IC** (Scheme 1.27). Catalysis was accomplished at a lower temperature than the optimal conditions used for **EA** and as a result the Cp* derivative performed with higher activity than the Cp.
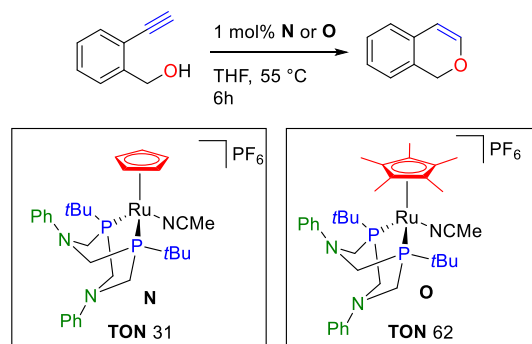
Scheme 1.27: *Endo* selective hydrofunctionalization of **EBA** to **IC** can be accomplished with Ru(II) $P^R_2N^{R'}_2$ catalysts.

1.4   Fe(II) Complexes

Fe(II) complex **P** has previously been used for dimerization catalysis of terminal alkynes (Scheme 1.28).[72] This activity illuminates a potential problem with chemoselectivity when hydrofunctionalization of those substrates is the goal. An Fe(II) piano-stool complex with an *N*-heterocyclic carbene (NHC) ligand catalyzed the dimerization of terminal alkynes to form *gem*-specific 1,3-enynes. The specialized NHC ligand was found to be essential to the activity of this catalyst and participated in C☐−H activation of one equivalent of substrate. This formed an acetylene complex **Q** while opening another coordination site, which allowed a second equivalent of substrate to bind. Migratory insertion formed a new C−C bond and the product was released through another C−H activation step involving the ligand.
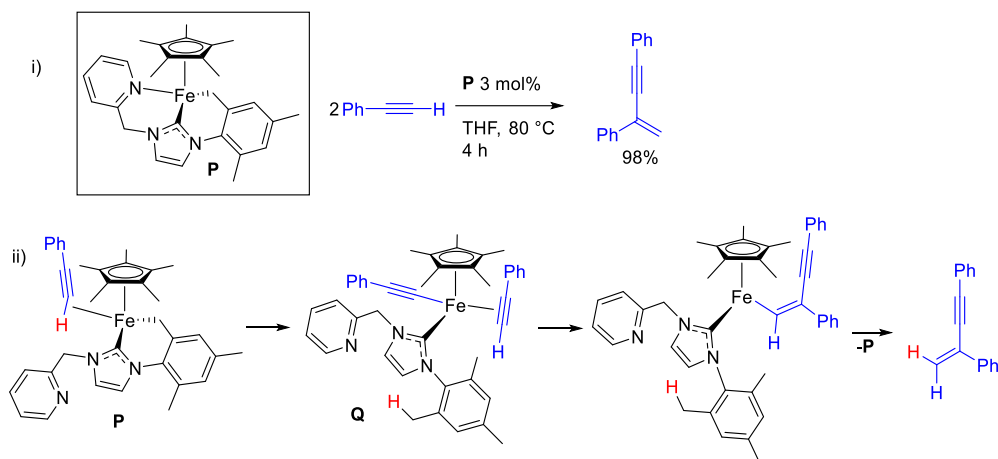
Scheme 1.28: i) Fe(II) catalyst **P** can form *gem*-specific 1,3-enynes from terminal alkynes. ii) The ligand played a role in substrate activation to form **Q**.

Fe(II) PNP pincer-type complex **R** also catalyzed the dimerization of terminal alkynes (Scheme 1.29i).[73, 74] The active catalyst is first formed from an Fe(II) hydride complex and two equivalents of substrate. A vinylidene intermediate formed from a third equivalent of substrate and nucleophilic attack occurred to form a new C−C bond (Scheme 1.29ii). Product release was facilitated by proton-transfer from a fourth equivalent of substrate, regenerating the active catalyst. There must be adequate space on the catalyst for substrates to react to produce alkyne dimers. This evidence suggests that steric bulk surrounding an Fe(II) center may prevent such dimerization from being favourable.
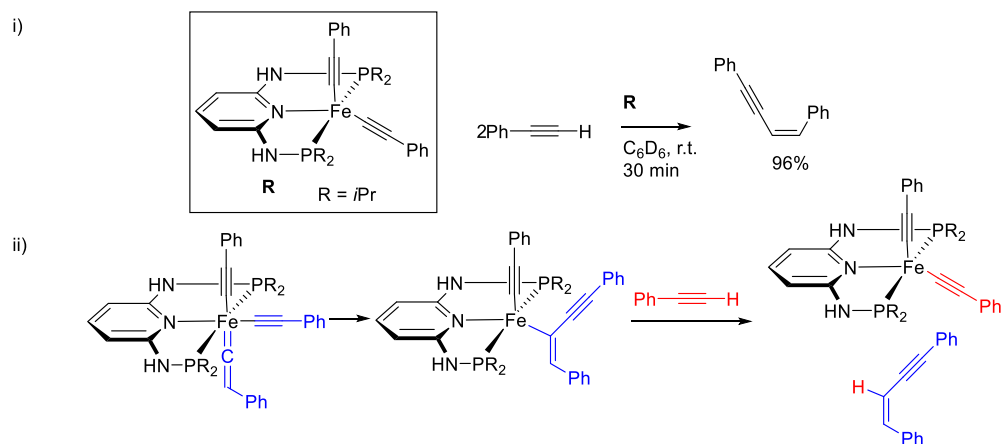
Scheme 1.29: i) Fe(II) PNP pincer-type complex **R** is active for dimerization of terminal alkynes. ii) Vinylidene intermediate during Fe(II) catalysis with **R** produced *Z*-selective 1,3-enynes from terminal alkynes.

A simple Fe(II) complex prepared from $FeCl_2$ and lithium hexamethyldisilazide (LiHMDS) was active under mild catalytic conditions for the trimerization of terminal alkynes to form substituted aromatics (Scheme 1.30).[75] Understanding any divergent pathways that reactions may take can help to achieve catalysis with high selectivity for only the desired transformations, by optimizing the reaction conditions and through careful catalyst design.
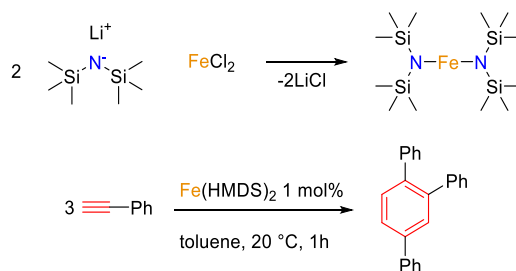
Scheme 1.30: A simple Fe(II) complex has been shown to form substituted aryl rings from terminal alkynes.

Fe(II) has been shown to be capable of forming stable vinylidene complexes, and a large variety has been reported (Chart 1.1).[49, 76-79] Despite the precedence for such structures,

there are currently no literature reports of iron being used for the catalytic hydrofunctionalization of alkynes through a vinylidene intermediate.
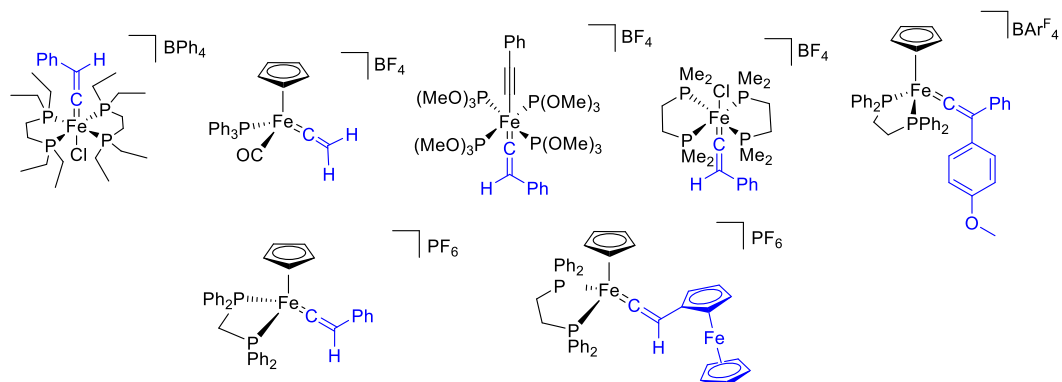
Chart 1.1: Several different types of Fe(II) vinylidene compounds have been reported.

The reactivity of an Fe(II) vinylidene complex **S** with nucleophiles demonstrated that all were regioselective for attack on the α carbon (Scheme 1.31).[77] A non-protic nucleophile, such as a tertiary phosphine or pyridine, added to the vinylidene at the α carbon to form vinyl phosphonium **T** or vinyl ammonium **U** derivatives, respectively, and the complex remained cationic. Use of a slightly stronger base resulted in deprotonation of the β proton of the vinylidene to give the neutral acetylene derivative **V**. Water had a combined effect, with both addition of the oxygen to the α carbon as well as deprotonation, to afford neutral Fe(II)-acyl derivative **W**. The addition of nucleophiles such as methanol and methylamine formed carbene species **X** that remained cationic.
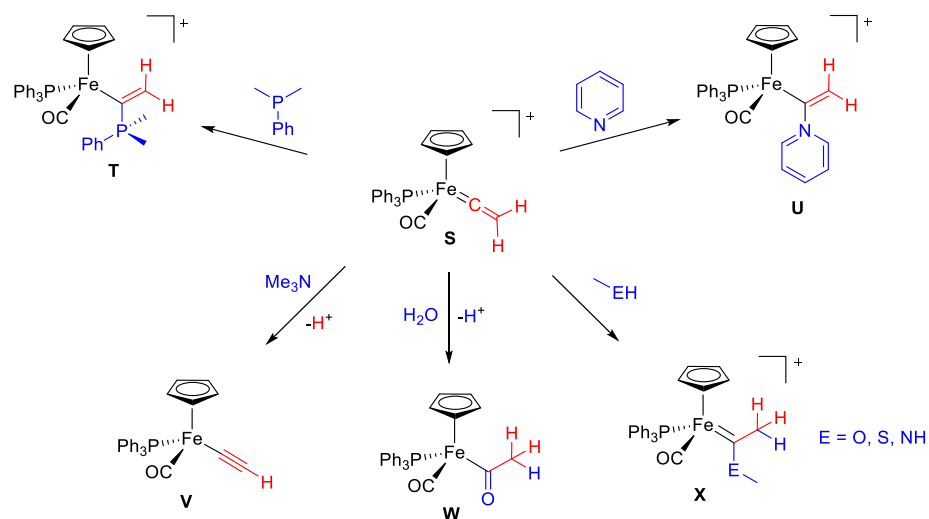
Scheme 1.31: Fe(II) vinylidene compound **S** reacted with nucleophiles were selective for attack on the α carbon.

Fe(II) complexes analogous to the Ru(II) $P^R_2N^{R'}_2$ catalysts described above have been reported.[80-83] The complexes are diamagnetic and have been used as catalysts for hydrogen production and oxidation. The basic amine functionality on the ligand assisted with proton-transfers just as in the Ru(II) $P^R_2N^{R'}_2$ hydrofunctionalization catalysts. Complexes **Y** and **Z** were synthesized from Fe(II) chloride (Scheme 1.32). A salt metathesis with LiCp* followed by coordination of ligand and *in situ* reduction produced the hydride derivatives **Y** and **Z**.
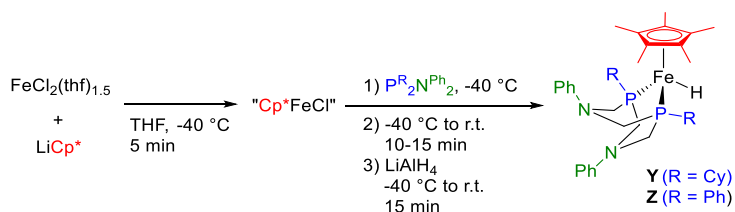
Scheme 1.32: Fe(II) $P^R_2N^{R'}_2$ complexes **Y** and **Z** have been synthesized and used for studies in H_2 activation.

1.5   Scope of Thesis

The elaboration of ligand substituents has allowed significant improvements in catalyst selectivity and activity. As we have seen, the selectivity of alkyne hydrofunctionalization can be controlled through the formation of a key vinylidene intermediate, accomplished using piano-stool Os(II) complex **D** and sterically crowded Ru(II) catalysts **B**, **C**, and **F** (Chart 1.2). The proper steric and electronic effects of the surrounding ligand environment can thus influence Ru(II) to exhibit increased activity and *endo* selectivity for intramolecular hydrofunctionalization and has allowed its applications to mirror those of Os(II). The use of MLC ligands on Ru(II) complexes **J**, **N**, and **O** has allowed even further development by incorporating basic functionality into the ligand structure, and in the case of $P^R_2N^{R'}_2$ catalysts by also adding multiple dimensions of tunability, garnering significant improvements in catalytic activity for intramolecular hydrofunctionalization of alkynes.
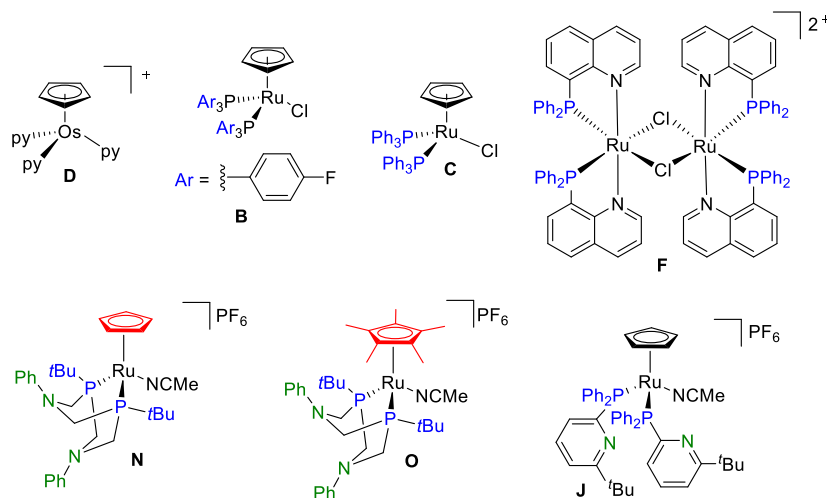
Chart 1.2: M(II) catalysts for the *endo* selective intramolecular hydrofunctionalization of alkynes (M = Ru, Os).

The potential for Fe(II) catalysts to be capable of similar improvements is also promising. The intramolecular hydrofunctionalization of alkynes using Fe(III) chloride and Fe(0) complex **A** (Chart 1.3) has previously been accomplished. The regioselective reactivity of Fe(II)-vinylidene **S** with nucleophiles is promising evidence that *endo*-selective

hydrofunctionalization is possible. Fe(II) $P^R_2N^{R'}_2$ diamagnetic complexes **Y** and **Z** have also been successfully synthesized, analogous to known Ru(II) catalysts. Despite such precedence with piano-stool Fe(II) complexes, no examples have previously demonstrated that Fe(II)-vinylidene intermediates have been involved in forming *endo* selective heterocycles. Promoting the formation of such an intermediate would allow catalysis of *endo* heterocycles with the same selectivity as Ru(II) and Os(II).
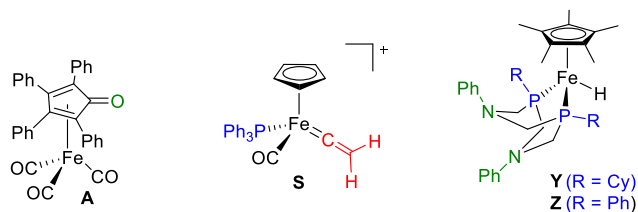
Chart 1.3: Piano-stool Fe(0) and Fe(II) complexes **A**, **S**, **Y**, and **Z**.

A well-defined ligand environment can serve to mediate the characteristics of Fe(II) for use in catalytic applications only previously accomplished by inherently more stable cations such as Ru(II), and would serve as a significant advance toward the widespread use of base-metals for homogenous catalysis. The following thesis outlines the synthesis and characterization of two such Fe(II) $P^R_2N^{R'}_2$ catalysts. These new complexes were tested for activity and selectivity for the catalytic intramolecular hydrofunctionalization of alkynes to form *endo* heterocycles. Intermediates relevant to catalysis were studied to confirm a vinylidene mechanism was responsible for selectivity and a catalyst deactivation product was observed.

Chapter 2

2 Synthesis and Characterization of Fe(II) $P^R_2N^{R'}_2$ Complexes and Substrates for Catalytic Hydrofunctionalization of Alkynes

2.1 Syntheses of [Fe(Cp*)($P_2^RN_2^{Ph}$)(MeCN)]PF$_6$ Complexes

The initial method used to synthesize the Fe(II) $P^R_2N^{R'}_2$ complexes was based on an established synthetic route for analogous ruthenium complexes.[69] This first involved synthesis of a cationic Fe(II) piano-stool precursor **1** according to a literature procedure (Scheme 2.1).[84] While this formed the desired cationic complex **1** in fair yield, the more stable product decamethylferrocene was also observed in approximately 30% yield by ^{1}H NMR spectroscopy. It has been observed that the iron complex **1** decomposes at room temperature in solvents other than MeCN.[85] Since the reaction is performed in a mixture of THF and MeCN, this decomposition pathway was impossible to avoid. Yields were negatively affected as a result and extra purification was necessary to remove decamethylferrocene.
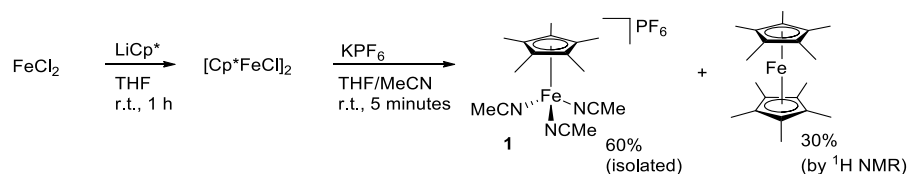
Scheme 2.1: Synthesis of piano-stool iron (II) precursor, **1**.[84]

Coordination of ligand **2a** or **2b** to the iron precursor **1** in acetonitrile produced Fe(II) $P^R_2N^{R'}_2$ complexes **3a** and **3b** in excellent yield (Scheme 2.2). **2a** was chosen as an alternative to the P-tBu substituted ligand previously used with Ru(II). Although they perform similarly, significantly lower cost is associated with the phosphine precursor needed for the Cy ligand synthesis over the tBu analog (see Scheme 1.25). The synthesis of the ruthenium analogues required heating at 65 °C for 4 h to facilitate ligand solvation. To avoid potential decomposition of starting material **1** the iron

reaction was attempted without heating. Complexes **3a/b** were successfully formed at room temperature within 24 hours in excellent yield. However, when the synthesis of iron precursor **1** was taken into consideration, the overall yields of **3a** and **3b** were only 57 and 54 %, respectively.
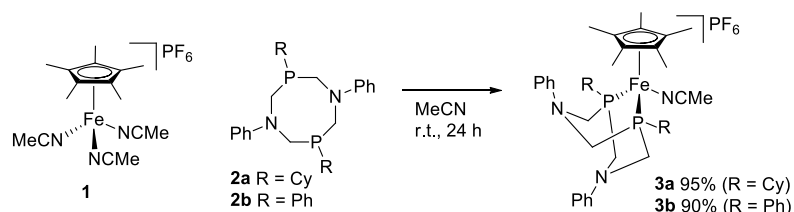
Scheme 2.2: Coordination of $P^R{}_2N^{Ph}{}_2$ ligands with piano-stool iron complex.

In an effort to avoid the synthesis of the unstable precursor **1** and to reduce the number of purification steps required, an alternate synthetic procedure for complexes **3a** and **3b** was developed. In this method, the $P^R{}_2N^{R'}{}_2$ ligand was coordinated directly to iron (II) chloride, after which Li[Cp*] was added to form the neutral iron (II) $P^R{}_2N^{R'}{}_2$ chloro complex **4a/b** (Scheme 2.3, top).[83] These are known Fe-Cl complexes that were used without isolation or characterization. In the same pot, complex **4a** or **4b** was then treated with KPF_6 followed by MeCN to achieve halide displacement and form the novel cationic iron (II) complex **3a** or **3b**, respectively, in high purity with very good yield (Scheme 2.3, bottom). Previous synthesis of a ruthenium analog from the related chloro complex required the use of $TlPF_6$ for successful halide displacement.[69] With iron, this general procedure worked well using KPF_6 and allowed the formation of potential catalysts in a one-pot procedure starting from commercially available iron (II) chloride.
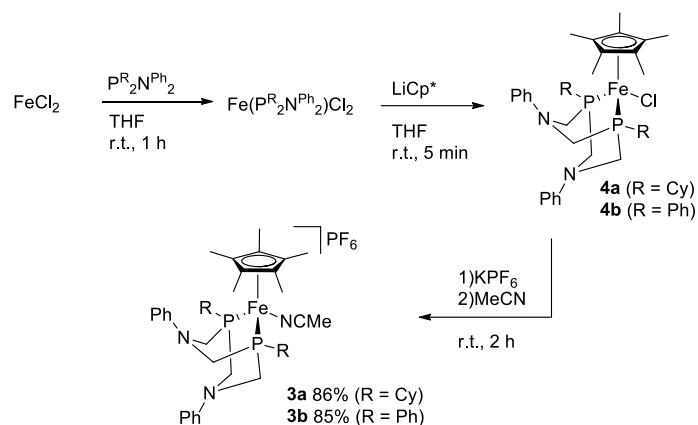
Scheme 2.3 One-pot synthetic procedure to access cationic iron $P^R_2N^{R'}_2$ complexes, **3a/b**, following an adapted literature procedure for Fe-Cl complexes **4a/b**.[83]

2.2 Characterization of $[Fe(Cp^*)(P_2^RN_2^{Ph})(MeCN)]PF_6$ Complexes

Complexes **3a** and **3b** each showed a singlet by $^{31}P\{^1H\}$ NMR spectroscopy in DCM-d_2 at 52.4 and 50.2 ppm, respectively. The relative chemical shifts are consistent with those reported previously for Fe-Cl complexes **4a** and **4b** in THF-d_8, with each showing a singlet in their $^{31}P\{^1H\}$ NMR spectra at 53.2 and 51.0 ppm, respectively.[83] The ^1H NMR spectra of **3a** and **3b** show the relative integrations of the methylene protons of the $P^R_2N^{Ph}_2$ ligand (each 2H) and the methyl protons of the Cp* (15H) and bound MeCN (3H) are consistent with the proposed formula for both complexes. MALDI-MS data also showed molecular ion peaks at m/z = 657.4 and 645.2 that correspond to $[\textbf{3a}\text{-MeCN-PF}_6]^+$ and $[\textbf{3b}\text{-MeCN-PF}_6]^+$, respectively. The experimental isotope pattern for $[\textbf{3a}\text{-MeCN-PF}_6]^+$ and $[\textbf{3b}\text{-MeCN-PF}_6]^+$ are consistent with simulated data (Figure 2.1).[86] Each signal contains six peaks, a result of the different isotopes of both iron and carbon. These data support successful coordination of the $P^R_2N^{Ph}_2$, MeCN, and Cp* ligands and represent the first examples of cationic iron (II) $P^R_2N^{R'}_2$ complexes. Complexes **3a** and **3b** were further characterized by $^{13}C\{^1H\}$ NMR and IR spectroscopy.
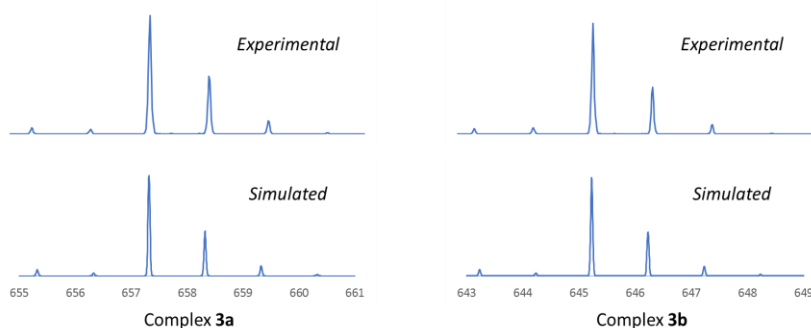
Figure 2.1: MALDI-MS data for complexes **3a** and **3b** acquired with a pyrene matrix showing simulated (bottom)[86] and observed (top) isotope patterns for [**3a**-MeCN-PF$_6$]$^+$ (*m/z* = 657.4) and [**3b**-MeCN-PF$_6$]$^+$ (*m/z* = 645.2).

Single crystals of complex **3a** were obtained and the structure was elucidated by X-ray diffraction (Chart 2.1, i). Comparison of **3a** to previously reported values for Fe-Cl complex **4a** shows very little difference in Fe-Cp* (centroid) distance or in Fe-P bond lengths and angles (Table 2.1).[83] Complex **3a** shows a closer interaction between the metal and the MeCN ligand than that observed for the analogous ruthenium complex **6** as would be expected.[87] However, in complex **3a** the C≡N bond is 1.142(1) Å compared to 1.144(6) Å in complex **6** and 1.141 Å for a free acetonitrile molecule,[88] indicating very little backbonding occurs with the ligand in either the iron or ruthenium complexes. The P-M-P angle and P-M-X angles (where X is acetonitrile) are all slightly larger for iron than for ruthenium. All three complexes crystallize with a ligand conformation typically seen for these types of complexes, with the 6-membered metallocycle proximal to the Cp* ligand in a boat conformation, and the metallocycle proximal to the active site of the complex in a chair conformation.
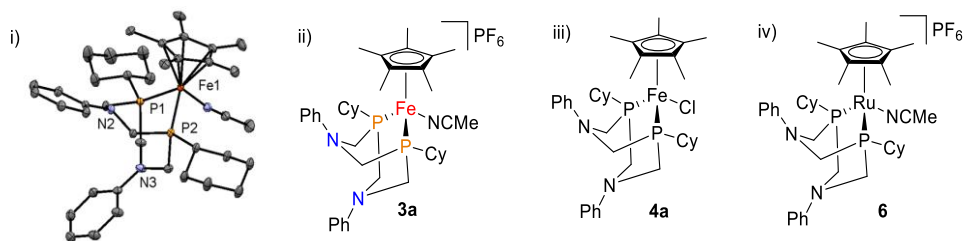
Chart 2.1: i) Thermal displacement plot of **3a** with ellipsoids at 50% probability (hydrogen atoms and PF_6^- counterion were removed for clarity). ii) Drawing of complex **3a**. iii) Analogous Fe(II) $P^{Cy}_2N^{Ph}_2$ chloride complex **4a**. iv) Analogous Ru(II) the $P^{Cy}_2N^{Ph}_2$ catalyst **6**.[87]

Table 2.1: Comparison of bond distances and angles for complexes **3a**, **4a**,[83] and **6**[87]

Bond	3a	4a[83]	6[87]
M-X (X = NCMe or Cl)	1.897(1) Å	2.3436(4) Å	2.046(4) Å
M-P1	2.1770(8) Å	2.1722(4) Å	2.2753(2) Å
M-P2	2.1800(7) Å	2.1881(4) Å	2.2615(2) Å
M-Cp*	1.736 Å	1.732 Å	1.869 Å
P1-M-P2	81.39(2)°	81.11(1)°	78.80(5)°
P1-M-X	93.72(3)°	92.14(1)°	90.7(1)°
P2-M-X	94.13(3)°	91.48(1)°	90.9(1)°

2.3 Synthesis of [Fe(Cp)($P_2{}^RN_2{}^{Ph}$)(MeCN)]PF$_6$ Complexes

Attempts to prepare the Cp analogs of the cationic Fe complexes (**5a** and **5b**) through coordination of the ligand to FeCl$_2$ followed by halide abstraction met with partial success (Scheme 2.4). After purification steps were performed to remove the KCl and LiCl salts and minor ferrocene by-products, the resulting solid exhibited a singlet by $^{31}P\{^1H\}$ NMR spectroscopy at 63.0 and 57.7 ppm for **5a** and **5b**, respectively. These signals were downfield (7-10 ppm) of the corresponding Cp* analogues, which is expected due to the increased electron-donating capability of the Cp* ligand that

increases shielding of the coordinated phosphine ligand. MALDI-MS further confirmed metallation of the $P^R_2N^{R'}_2$ and Cp ligands with [M-MeCN-PF$_6$]$^+$ peaks found at *m/z* = 587.3 and 575.2 for **5a** and **5b**, respectively, which matched the calculated mass and isotope patterns expected for these iron complexes. [86]
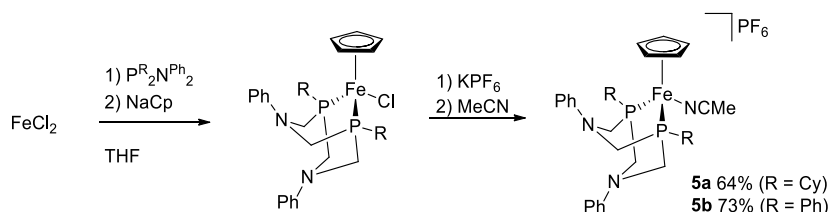
Scheme 2.4: One pot synthetic procedure for Cp derivatives **5a** and **5b**.

A multiplet signal at ca. 30 ppm for an unknown species also appeared in the ^{31}P{^{1}H} NMR spectra for both of the Cp complexes **5a** and **5b**. The singlet and the unknown multiplet appeared in unpredictable ratios after several attempts at synthesis. The large number of peaks and highly symmetric appearance of the multiplet suggests an AA'BB' spin system (Figure 2.2). Similar patterns have been observed for the [Pt$_2$Cl$_2$(μ-PPh$_2$)$_2$(PEt$_3$)$_2$] dimer complex, which contains bridging phosphido ligands (AA') with one phosphine ligand (BB') coordinated to each metal center.[89]
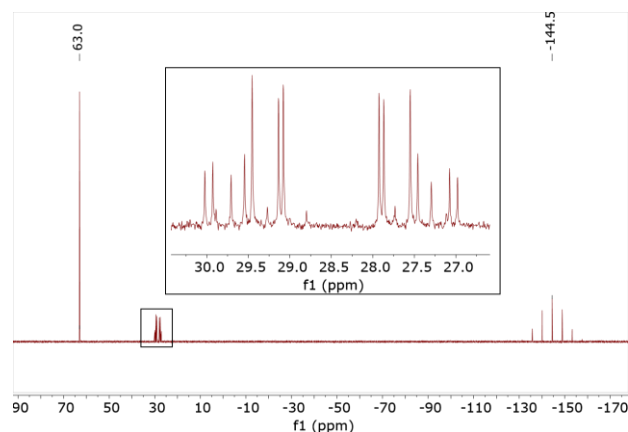
Figure 2.2: ^{31}P{^{1}H} NMR spectrum of **5a** with magnified region showing multiplet signal for unknown species

^{19}F NMR spectroscopy of **5b** showed a doublet that would be expected for coupling to the phosphorous atom in the [PF$_6$]$^-$ counterion. This doublet indicates that no

coordination occurs between the counterion and the metal complex that could give rise to additional coupling as observed by $^{31}P\{^{1}H\}$ NMR spectroscopy.

5a was dissolved in MeCN and heated to 55 °C for 2.5 hours. After the solvent was removed under vacuum, the solids were redissolved in CD_2Cl_2 for $^{31}P\{^{1}H\}$ NMR analysis, which showed ca. 10% increase in **5a** relative to the multiplet signal by integration. Repeating solvation and heating in MeCN at 70 °C for 3 hours resulted in further decrease of the multiplet (ca. 20% relative integration), along with a slight decrease in **5a** (ca. 5% relative integration) observed by $^{31}P\{^{1}H\}$ NMR analysis of the reaction mixture. A new unknown signal appeared at 49.4 ppm (ca. 20% relative integration), which was not previously observed when the material was dissolved in CD_2Cl_2 (Figure 2.3). This new signal may represent an MeCN adduct of the species that gives rise to the multiplet.
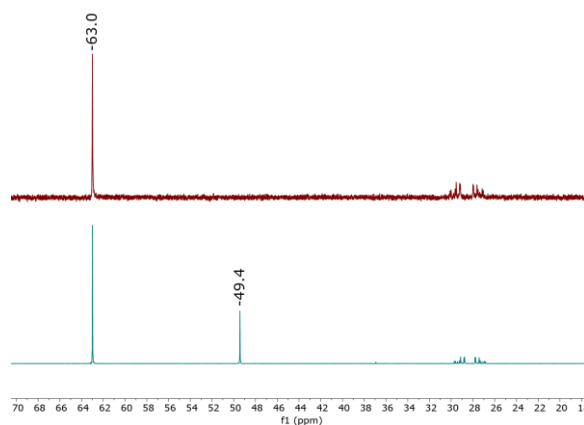
Figure 2.3: $^{31}P\{^{1}H\}$ NMR spectrum of crude **5a** in CD_2Cl_2 (top) and the reaction mixture of crude **5a** after heating to 55 °C in MeCN for 2.5 h then 70 °C for 3 h (bottom).

An AA'BB' pattern was occasionally observed in the $^{31}P\{^{1}H\}$ NMR spectrum for the Cp* complex **3b** when synthesized by the two-step procedure outlined in Scheme 2.3. Recrystallization attempts in MeCN with Et_2O also resulted in an increase in the amount of the multiplet. Solvation in MeCN and subsequent removal of solvent allowed complete conversion at room temperature to the desired complex **3b** (Figure 2.4).
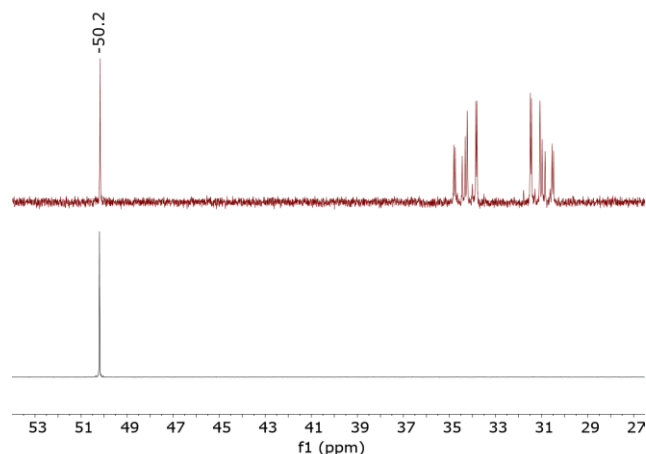
Figure 2.4: ^{31}P{^{1}H} NMR spectrum of **3b** following a recrystallization attempt in MeCN/Et$_2$O (top) and after addition and removal of MeCN at room temperature (bottom).

The combined evidence would suggest that the unknown multiplet signal arises from a species related to the parent complex of **3b**, **5a**, or **5b**, that lacks the labile MeCN ligand. An open coordination site and a coordinating ligand of one complex could then bind with the coordinating ligand and open site of another equivalent of complex to form dimer **8** (Scheme 2.5). This structure would be staggered due to steric clash of the bulky P-R substituents, and would therefore would lack mirror symmetry and have two distinct pairs of chemically equivalent P atoms (AA and BB). Since each atom couples to the others in a distinct way, these signals are not magnetically equivalent (AA'BB') and the complex splitting pattern emerges. Another possible structure is one that involves bridging P$^R_2$N$^{R'}_2$ ligands (**9**). A bridging bis(diphenylphosphino)methane iron complex Fe$_2$(μ-Ph$_2$PCH$_2$PPh$_2$)$_2$(NO)$_4$ has been previously synthesized,[90] and rhodium dimers with bridging, bidentate phosphines ligands have also been reported.[91] In the case of the second proposed structure for complexes **3b** and **5a/b**, the doubly bridging phosphine bond could be displaced by MeCN in solution in a slow equilibrium. Such a displacement would result in species **10**, which is proposed to give rise to the singlet oberved at 49.4 ppm after heating **5a** in MeCN.

Proposed structures
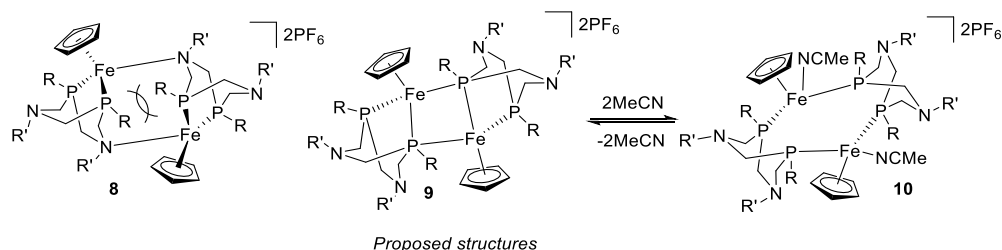
Scheme 2.5: Proposed structures of the unknown species observed as an AA'BB' in ^{31}P{^{1}H} NMR spectra of complexes **3b** and **5a/b**.

Difficulty converting the Cp analogs to the desired complex could be a result of a lower lability of ligands relative to the Cp* complexes, thus preventing MeCN from readily dissociating the proposed dimer into coordinatively saturated monomers. This difference in ligand lability would be consistent with what has been observed with the analogous ruthenium complexes as a result of increased steric bulk and electron donor capability of the Cp* ligand relative to Cp. However, the Cp Fe(II) derivatives appear to be much less stable as coordinatively unsaturated species when compared to both the Ru(II) and the Fe(II) Cp* analogs. This instability is a consequence of the smaller size of the metal cation relative to Ru(II) and a reduction in ligand stabilization relative to Cp*, respectively. As a result, dimerization seems to be a low energy state for these types of cations and could be a potential catalyst deactivation pathway that should be explored.

2.4   Synthesis of Substrates for Catalytic Hydrofunctionalization

In order to assess the regioselectivity of intramolecular hydrofunctionalization catalysis, substrates with three or more carbon atoms between the nucleophile and the alkyne must be employed. By increasing the potential size of the heterocycles formed, the ability for the product to be either *exo* or *endo* is introduced. 2-Ethynylbenzyl alcohol (**EBA**) has three carbon atoms between the alkyne group and the alcohol and is suitable for assessing the *endo* selectivity. **EBA** was synthesized in three steps following a literature procedure (Scheme 2.6).[92] Starting from 2-bromobenzaldehyde, a Sonogashira coupling with trimethylsilyl(TMS)-acetylene furnished a protected

alkyne in very good yield. Reduction with lithium aluminum hydride in dry THF gave the benzyl alcohol, which, upon deprotection and recrystallization in hexanes, afforded **EBA** in good yield.
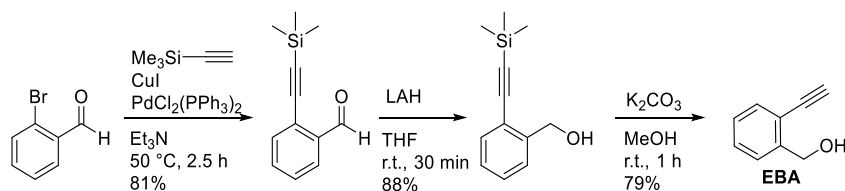
Scheme 2.6: Synthesis of **EBA** from 2-bromobenzaldehyde.

2-Ethynylbenzyl amide (**EAD**) also has three carbon atoms between the alkyne and the amide nucleophile and therefore is another substrate that is useful to test for regioselectivity. The compound was made starting from 2-bromobenzamide following a known procedure (Scheme 2.7). A Sonogashira coupling with TMS-acetylene gave a silyl alkyne, which upon deprotection with potassium carbonate initially gave the final amide product in poor yield after isolation by coloumn chromatography. The major by-product in the reaction was also isolated using column chromatography and was identified as the *exo* hydrofunctionalization product by ^{1}H NMR analysis. This compound was possibly formed due to catalysis by K_2CO_3 or residual palladium that carried over from the Sonogashira coupling step.[93]
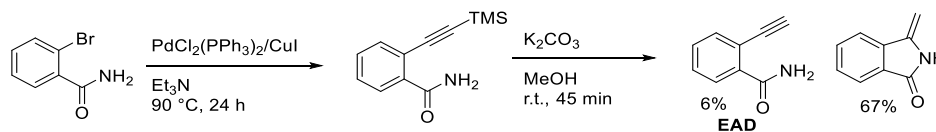
Scheme 2.7: Attempted synthesis of 2-ethynylbenzylamide (**EAD**) from 2-bromobenzylamide using potassium carbonate to deprotect the alkyne.

Repeating the deprotection with tetrabutylammonium fluoride (TBAF) afforded the desired amide product in better, but still poor yield of only 39% (Scheme 2.8). Again, a significant quantity of *exo* cyclized product was isolated from the reaction, but enough material was collected to do preliminary catalytic testing.
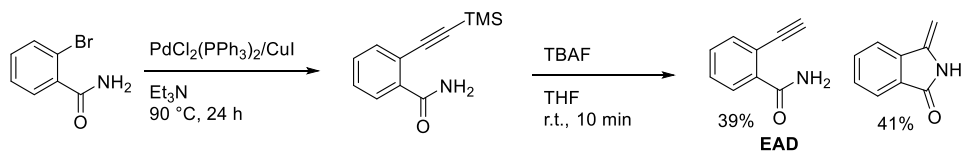
Scheme 2.8: Synthesis of **EAD** from 2-bromobenzylamide using TBAF to deprotect.

Analogous to **EBA**, 2-ethynylbenzyl amine could also potentially cyclize into two different regioisomers. This substrate was made in three steps from 2-iodobenzonitrile following a literature procedure. A Sonogashira coupling was used to produce the alkyne in excellent yield (Scheme 2.9). Deprotection was done using TBAF and afforded the nitrile in excellent yield, but reduction with LAH ultimately gave the final amine in poor yield. Fortunately, an adequate quantity of material was collected for preliminary catalysis trials.[58]
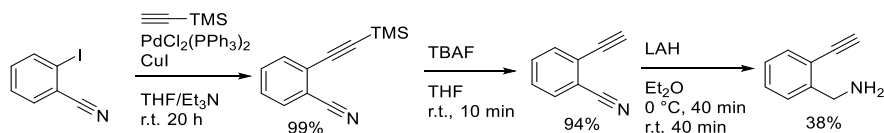
Scheme 2.9: Synthesis of 2-ethynylbenzylamine from 2-iodobenonitrile.

Substrates will typically only undergo intramolecular hydrofunctionalization to form 7-membered *endo* heterocycles if the catalyst is highly selective. A 6-membered *exo* product is relatively lower in energy since it exhibits less ring strain. The length of the alkyl chain between the heteroatom and the alkyne group on 2-ethynylbenzeneethanol is four carbons, so this challenging substrate is useful for assessing whether a vinylidene intermediate is involved in catalysis. The substrate was synthesized in two steps following a known procedure, starting with a Sonogashira coupling on an aryl bromide (Scheme 2.10). The silyl alkyne was made in fair yield, and deprotection with TBAF gave the alcohol in very good yield.[59]
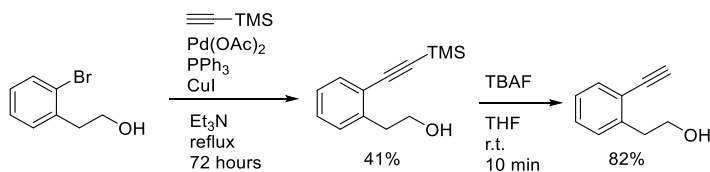
Scheme 2.10: Synthesis of 2-ethynylbenzeneethanol from 2-bromobenzeneethanol.

Synthesis of a biaryl alkynol with four carbon atoms between the alkyne and the nucleophile was attempted (Scheme 2.11) . This substrate should also be capable of forming 7-membered heterocycles and the rigid structure may make it suitable for hydrofunctionalization. A Suzuki coupling was successful in producing the biaryl phenol from an aryl boronic acid and an aryl iodide in 58% yield. A Sonogashira coupling was then attempted to form the biaryl alkynol, but after 24 hours no product had formed and starting material was recovered from the reaction mixture (ca. 50%). Because this reaction is two sequential aryl halide couplings, it may be more successful if the Sonogashira was performed first on the aryl iodide. For the second step, a Suzuki coupling of the aryl bromide may then furnish the TMS protected biaryl phenol. If successful, deprotection of the alkyne would be attempted with TBAF to avoid the possibility of unwanted hydrofunctionalization that may occur with a basic deprotection such as K_2CO_3.[94]
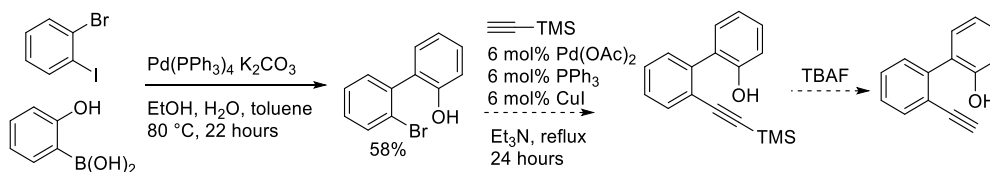
Scheme 2.11: Attempted synthesis of biaryl alkynol.

Chapter 3

3 Hydrofunctionalization with Cationic Fe(II) Catalysts

3.1 Conditions Optimization for Hydrofunctionalization of 2-Ethynylaniline

To establish if the Cp* iron complexes **3a** and **3b** are competent hydrofunctionalization catalysts, their performance was first evaluated with the benchmark substrate 2-ethynylaniline (**EA**). A benchmark substrate is used to test for catalyst activity and allows for a convenient way to compare different catalysts. Successful hydrofunctionalizaton will afford the 5-membered *endo* heterocycle, indole (**Ind**), regardless of the mechanism since there are only two carbon atoms between the nucleophile and the alkyne.

Hydrofunctionalization was attempted using 1 mol% of **3a** with mild heating at 40 °C in DCM and DCE (Table 3.1, Entries 1 and 2, respectively) and these reactions showed only trace consumption of substrate. Increasing the temperature to 70 °C using Me-THF, DCE, and anisole as solvents (Entries 3-5) showed an increase in consumption, but mostly starting material remained and a very poor yield of indole (**Ind**) was measured. The temperature was increased to 110 °C using the high boiling-point solvent anisole and this gave 78% **Ind** after 1 h (Entry 6). Lowering the catalyst loading to 0.5 mol% showed good yield of indole (Entry 7), but since the conversion was incomplete, **3a** was likely reaching the maximum turnovers possible under these conditions, giving a TON of 160. Complex **3b** was also screened at 0.5 and 1.0 mol% loading in anisole (Entries 8 and 9). Catalyst **3b** performed slightly better than **3a**, giving a TON of 170 at 0.5 mol%. This relative performance is consistent with the ruthenium analogues of these complexes, where catalysts with the phosphine substituents R = Cy or Ph show comparable activity in hydrofunctionalization of **EA** (TON of 330 and 450, respectively),[87] albeit with roughly twice the lifetime of the iron systems. With this information, the optimal conditions for catalysis were determined to be 1 mol% catalyst **3b** in anisole at 110 °C for 1 hour.

Table 3.1: Conditions optimization for the intramolecular hydrofunctionalization of 2-ethynylaniline (**EA**) to indole (**Ind**) with iron catalysts **3a** and **3b**.[a]
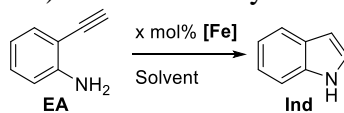
Entry	Solvent	Temp. (˚C)	[Fe] (mol%)	Conversion (%)[b]	Indole (%)[c]
1	DCM	40	**3a** (1)	2	0
				2 (24 h)	0 (24 h)
2	DCE[d]	40	**3a** (1)	4	2
				9 (24 h)	7 (24 h)
3	Me-THF	70	**3a** (1)	19	18
				36 (24 h)	15 (24 h)
4	Anisole	70	**3a** (1)	15	12
				33 (24 h)	10 (24 h)
5	DCE	70	**3a** (1)	17	17
				28 (24 h)	14 (24 h)
6	Anisole	110	**3a** (1)	85	78
				91 (24 h)	55 (24 h)
7	Anisole	110	**3a** (0.5)	79	72
8	Anisole	110	**3b** (1)	99	93
				94 (24 h)	64 (24 h)
9	Anisole	110	**3b** (0.5)	87	84
				92 (24 h)	70 (24 h)

[a]Conditions: **EA** (150 mM), reactions were heated for 1 hour prior to analysis by GC-FID unless otherwise stated. Tetralin was used as an internal standard, all data is an average of at least two trials, errors between the trials were all within +/− 7%. [b]Conversion of **EA**. [c]In-situ yields determined by calibrated GC-FID. [d]1,2-dichloroethane

All of the **EA** to **Ind** catalyic reactions showed a decrease in **Ind** yield when the reaction time was extended from 1 to 24 h (Table 3.1). Control reactions performed with catalyst **3a** and **Ind** did not show any consumption of product after 24 h, indicating that **Ind** was stable under those conditions and was not being consumed by the catalyst. Further tests were then performed by heating a 1:1 mixture of **EA** and **Ind** to 110 °C in anisole in the absence of catalyst. Analysis of these reactions at 1 hour and 24 hour time points confirmed that **Ind** was consumed in an unidentified competitive side reaction that occured in the conditions used for catalysis (Figure 3.1). Fortunately, at high temperatures and with the adequate catalyst loading, full conversion to **Ind** can be achieved in 1 hour with catalyst **3b** so the loss of product is negligible (ca. 5% indole).
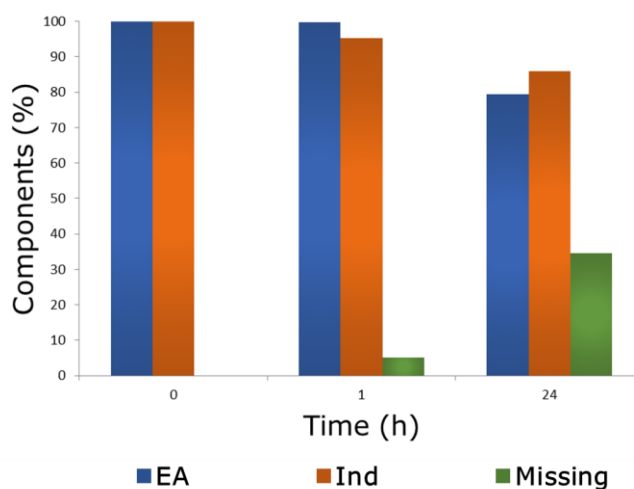
Figure 3.1: Control reaction of 1:1 **EA** and **Ind** in anisole at 110 °C in the absence of catalyst. Missing material was calculated by mass balance after analysis with calibrated GC-FID.

3.2 Intramolecular hydrofunctionalization of 2-Ethynylbenzyl Alcohol

Using the optimal conditions for formation of **Ind**, both catalysts **3a** and **3b** were used for the hydrofunctionalization of 2-ethynylbenzyl alcohol (**EBA**) to 1*H*-isochromene (**IC**) (Table 3.2). Catalyst **3a** was screened at 2.0 mol% and the substrate was fully

consumed in 1 hour (Entry 1). Analysis of the isolated product by ^{1}H NMR spectroscopy showed only the *endo* **IC** product was formed. The regioselectivity was further verified through GC-FID analysis by injection of independently synthesized *exo* product 1-methylene-1,3-dihydroisobenzofuran (**MBF**), which confirmed that no peak with the retention time for **MBF** was observed in the crude samples of the catalytic reactions. Dropping the loading of **3a** to 1.0 mol% revealed the lifetime of the catalyst under these conditions, giving a TON of 70 for **3a** (Entry 2). Extending the reaction time to 24 hours only led to a slight increase in the consumption of substrate with no further product being formed (Entry 2). Phenyl-substituted catalyst **3b** was also tested at the same two loadings and showed excellent activity, reaching nearly full conversion after 1 hour (Entries 3 and 4). Dropping the loading of **3b** to 0.5 mol% resulted in a conversion of 62%, which corresponds to a TON of 120 (Entry 5). This promising result is an improvement over the analogous ruthenium system by a factor of two.

Table 3.2: Intramolecular hydrofunctionalization of 2-ethynylbenzyl alcohol (**EBA**) to 1*H*-isochromene (**IC**) with iron catalysts **3a** and **3b**.[a]
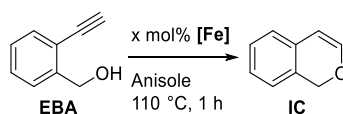
Entry	[Fe] (mol%)	Conversion (%)[b]	IC (%)[c]
1	**3a** (2)	96	75
2	**3a** (1)	70	62
		75 (24 h)	60 (24 h)
3	**3b** (2)	97	>99
		98 (24 h)	97 (24 h)
4	**3b** (1)	93	>99
		96 (24 h)	96
5	**3b** (0.5)	62	68

[a]Conditions: **EBA** (150 mM), reactions were heated in anisole at 110 °C for 1 h prior to analysis by GC-FID unless otherwise stated. Tetralin was used as an internal standard, all data is an average of at least two trials, errors were all within +/− 5%. [b]Conversion of **EBA**. [c]Yield determined by GC-FID analysis using internal standard and assuming a relative response factor for **EBA** to **IC** of 1.

3.3 Preliminary Scope Studies

Further assessment of the *endo* selectivity in hydrofunctionalization catalysis was attempted on a small selection of other substrates, using catalyst **3a** under the optimal conditions. Reaction aliquots were analyzed by GC-FID to quantify consumption of starting material. 2-Ethynylbenzyl amine was consumed fully in 1 hour with 2 mol% catalyst (Table 3.3, Entry 1). ^{1}H NMR analysis of the crude reaction mixture revealed only broad signals in the baseline, and a control experiment confirmed decomposition of this substrate occurs in anisole at the temperature used for catalysis. This substrate also has a heteroatom that is a better Lewis base than **EA** or **EBA**, so competitive

coordination to the metal is a concern. To circumvent this issue, amide substrates are often used in catalysis to form nitrogen-containing heterocycles.[58]

2-Ethynylbenzyl amide (**EAD**) was screened with 2 mol% **3a** and showed only 12% conversion (Entry 2). No evidence for either product regioisomer was found through ^{1}H NMR analysis of the reaction mixture. A control reaction without catalyst present confirmed the substrate was in fact stable under the conditions used for catalysis. Consumption was likely due to a catalytic process involving **3a**, so further experimentation should be performed with a higher catalyst loading. The analogous ruthenium complex [Ru(Cp)($P^{Ph}_2N^{Bn}_2$)(MeCN)]PF_6 was able to catalyze this hydrofunctionalization over 48 hours, but the increased basicity of the *N*-benzyl group of the ligand may be required for optimal activity.[71] This could ultimately mean both **3a** and **3b** will be ineffective at catalyzing this substrate, in which case the Fe(II) $P^{Ph}_2N^{Bn}_2$ derivatives should be explored.

Hydroalkoxylation of 2-ethynylbenzeneethanol was attempted using 2 and 10 mol% **3a,** which showed conversion of 13 and 30%, respectively (Entry 3). Increasing the temperature to 150 °C at 10 mol% showed a slight increase in conversion to 38% and leaving the reaction for 40 h doubled the conversion to 77%. No evidence for hydrofunctionalized product was detected by ^{1}H NMR analysis of the catalytic reaction mixtures; however, the substrate was clearly present. Catalyst **3b** should also be tested for activity on this substrate since it has been shown to be highly effective at hydrofunctionalization of **EBA**. Stoichiometric reactions with 2-ethynylbenzeneethanol and catalysts **3a/b** would also indicate whether the substrate could form a carbene product similar to those seen for Ru(II) complexes, which could account for some of the substrate conversion that was observed during trials.[56]

Table 3.3: Screen of *o*-alkynyl substrates for intramolecular hydrofunctionalization with iron catalyst **3a**.[a]
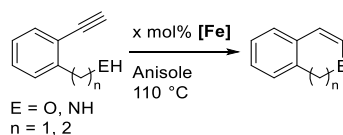
Entry	Substrate	*Endo* Product	Time (h)	Loading (mol%)	Conversion (%)[b]
1			1	2	>99[d]
			24	0	>99
2			1	2	12
3			1	2	13
			1	10	30
4			1[c]	10	38
			40[c]	10	77

[a]Conditions: **Substrate** (150 mM), reactions were heated in anisole at 110 °C for 1 h prior to analysis by GC-FID unless otherwise stated. Tetralin was used as an internal standard, all data is an average of at least two trials, errors were all within +/− 5%. [b]Conversion of **Substrate**. [c]150 °C. [d]Non-catalytic decomposition.

3.4 Catalysis Control Reactions

To assess whether the well-defined structure of catalyst **3a** or **3b** was indeed relevant in catalysis, control reactions with **EA** under optimized conditions were performed using $FeCl_2$ both with and without the $P^{Cy}_2N^{Ph}_2$ ligand present in solution (Table 3.3, entries 1 and 2). While the simple iron (II) salt did show noticeable consumption of **EA**, neither of the two conditions produced any amount of **Ind** product. These tests are strong evidence that the well-defined structures of **3a** and **3b** are responsible for the catalytic activity for hydrofunctionalization. Further controls were performed to gain some insight into whether the mechanism for **3a** was radical-mediated. Catalysis using 0.5 mol% **3a**, conducted in the absence of light, showed negligible difference to

reactions performed under ambient light (Table 3.4, Entries 3 and Table 3.1, Entry 7). 1,4-Cyclohexadiene (CHD) was added as a hydrogen-atom source to trap potential radicals and the catalyst performance was consistent with the standard conditions (Table 3.4, Entries 4 and Table 3.1, Entry 7). These results indicate that catalysis is not radical-mediated and thus likely involves π-activation or a vinylidene mechanism.

Table 3.4: Control Reactions for the intramolecular hydrofunctionalization of 2-ethynylaniline (**EA**) to indole (**Ind**).[a]
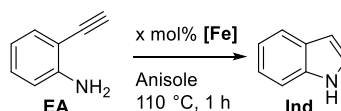
Entry	[Fe] (mol%)	Conversion (%)[b]	Indole (%)[c]
1	FeCl$_2$ (1)	17	0
2	FeCl$_2$ + P$^{Cy}_2$N$^{Ph}_2$ (1)	2	0
3	**3a** (0.5) in dark[d]	76	70
4	**3a** (0.5) + CHD[e]	76	70

[a] Conditions: **EA** (150 mM), reactions were heated for 1 h prior to analysis by GC-FID. Tetralin was used as an internal standard, all data is an average of at least two trials, errors were all within +/− 5%. [b] Conversion of **EA**. [c] In-situ yields determined by calibrated GC-FID. [d] Reaction vessel wrapped in foil to minimize light exposure. [e] 0.5 equiv cyclohexa-1,4-diene was added.

Chapter 4

4 Mechanistic Studies of Fe(II) $P^R_2N^{R'}_2$ Hydrofunctionalization Catalysts

4.1 Synthesis of [Fe(Cp*)($P^{Cy}_2N^{Ph}_2$)(=C=CHPh)]PF$_6$ Complex

To confirm that a vinylidene intermediate was responsisble for the regioselectivity of hydrofunctionalization of **EBA**, a reaction was performed with complex **3a** and phenylacetylene in order to synthesize a complex analogous to such an intermediate. Initial attempts to conduct this reaction included THF as a solvent and 10 equivalents of phenylacetylene relative to complex **3a**. Stirring overnight at room temperature resulted in formation of a viscous liquid, which upon removal of solvent furnished a rubbery product. ^{1}H NMR spectroscopy of the rubbery material showed multiplet signals at 3.4 and 1.6 ppm, which integrated to approximately equal amounts. These signals are consistent with reported data for poly(THF),[95] a result of solvent polymerization (Scheme 4.1). A control reaction was also performed using the same iron complex in THF in the absence of phenylacetylene and no polymerization was observed at room temperature. The ring-opening polymerization of THF is somewhat trivial and can be accomplished using both Brønsted and Lewis acids.[95, 96] In this case, it is interesting to note that complex **3a** itself was not acidic enough to polymerize the solvent at room temperature. However, when phenylacetylene was present the complex had a strong enough Lewis-acidic property that ring-opening polymerization was possible. This could be due to vinylidene formation, resulting in a highly electrophilic C_α.
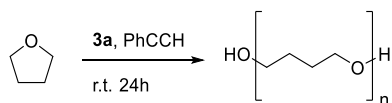
Scheme 4.1: Formation of poly(THF) from reaction of iron (II) complex **3a** with phenylacetylene in THF.

After the observation of polymerized THF in the phenylacetylene reaction above, the solvent was switched to DCM in a subsequent attempt to synthesize a vinylidene compound. After stirring **3a** and phenylacetylene for 24 hours at room temperature, an aliquot was removed and analyzed by ^{31}P{^{1}H} NMR spectroscopy. Two signals were observed, one for complex **3a** at 52.4 ppm and one slightly upfield at 51.1 ppm. Integration of the two corresponded to approximately 55% conversion of **3a** to the new complex. The same reactivity was observed using DCE as a solvent, but heating to 70 °C allowed complete conversion to the new species in 2 hours. The product was isolated in very good yield and upon further characterization was found to be consistent with vinylidene complex **7** (Scheme 4.2).
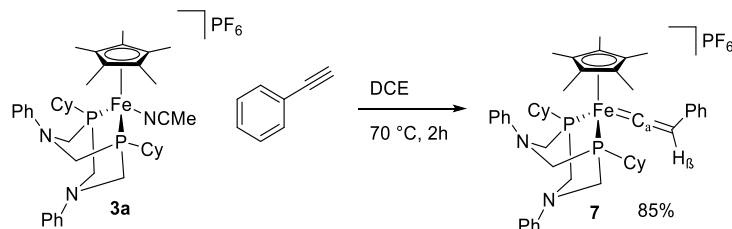
Scheme 4.2: Reaction of complex **3a** with phenylacetylene to form vinylidene complex **7**.

A MALDI-MS experiment of isolated complex **7** showed a molecular ion peak corresponding to [**7**-PF$_6$]$^+$ at m/z = 759.4 and the isotope pattern was consistent with that expected for iron complex **7** (Figure 4.1). A large peak at 1 m/z less than the molecular ion can be attributed to the loss of a proton during ionization. This proton loss occurred in only a fraction of the total ions as both isotope patterns, [**7**–PF$_6$]$^+$ and [**7**–PF$_6$–H]$^+$, are present.
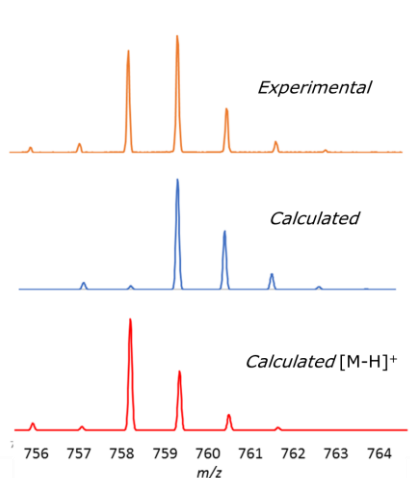
Figure 4.1: Zoom-in of the observed signal (top) with *m/z* = 759.4 in the MALDI-TOF mass spectrum of [Fe(Cp*)($P^{Cy}_2N^{Ph}_2$)(C=CHPh)]PF$_6$ (2a); simulations[86] of the isotope patterns for the fragment cations [Fe(Cp*)($P^{Cy}_2N^{Ph}_2$)(=C=CHPh)]$^+$ with *m/z* = 759.4 (middle) and [Fe(Cp*)($P^{Cy}_2N^{Ph}_2$)(=C=CHPh) – H]$^+$ with *m/z* = 758.4 (bottom).

The ^{1}H NMR spectrum of **7** showed that the Cp* methyl signals were shifted downfield ca. 0.2 ppm relative to **3a**, from 1.64 ppm to 1.86 ppm, due to a slight deshielding effect of the vinylidene ligand relative to MeCN. The ^{1}H-^{13}C HMBC spectrum showed a correlation between a ^{1}H signal at 6.01 ppm and a ^{13}C signal at 359.6 ppm corresponding to H$_\beta$ and C$_\alpha$, respectively. The signal for H$_\beta$ integrates to a single proton relative to methylene signals on the $P^R_2N^{R'}_2$ backbone, and the disappearance of the MeCN ligand is also evident by the ^{1}H NMR spectrum. The high frequency of this carbon signal is consistent with similar Fe(II) vinylidene complexes (364 to 380 ppm).[78, 97] This is much farther downfield than π-bound iron-alkyne complexes, which show ^{13}C{^{1}H} NMR signals around 58 to 63 ppm.[98, 99] The deshielding of the Cα signal is a result of a polarization of the Fe=C bond, creating a highly electrophilic carbon. Infrared spectroscopy further confirmed the existence of a C=C stretch at 1617 cm^{-1}, which was consistent with similar reported Fe(II) vinylidene structures (1615 to 1658 cm^{-1}).[76, 78]

Vinylidene **7** formed cleanly at 70 °C with no evidence of alkyne dimerization observed. Activity for alkyne dimerization has been demonstrated with Fe(II)

catalysts that are able to bind multiple equivalents of substrate during a catalytic cycle. In the case of the Fe(II) $P^R_2N^{R'}_2$ active catalysts, five of the six coordination sites in the octahedral complex are occupied by non-labile ligands. Once the vinylidene had formed, the complex was coordinatively saturated and unable to activate a second equivalent of substrate. As a result, the Fe(II) $P^R_2N^{R'}_2$ catalysts will not dimerize alkyne functional groups and are chemoselective for hydrofunctionalization.

4.2   Trapping of an On-Cycle Intermediate

To trap an on-cycle intermediate, reactions were performed at a milder temperature than needed for catalytic turnover in order to arrest the cycle at the resting state. Complex **3a** and 25 equivalents of substrate **EA** were dissolved in DCM and heated to 45 °C for 24 hours. $^{31}P\{^1H\}$ NMR spectroscopy revealed a new broad singlet 1 ppm upfield of **3a** (ca. 20% conversion by relative integration). Continued heating in DCM at 45 °C for an additional 48 hours resulted in nearly full conversion to the new species (ca. 90% by relative integration) (Figure 4.2).
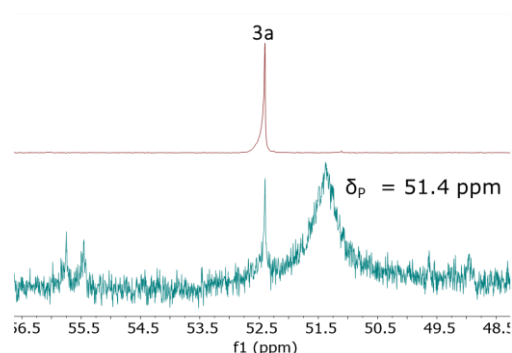
Figure 4.2: $^{31}P\{^1H\}$ NMR spectra of **3a** and **EA** in CH_2Cl_2 at room temperature (top) and $^{31}P\{^1H\}$ NMR spectra of reaction mixture **3a** and **EA** in CH_2Cl_2 after heating for 3 days at 45 °C (bottom).

The breadth of the new signal may be the result of an equilibrium between related species in solution. If a vinyilidene species (Scheme 4.3, **11**) had formed from **3a** and **EA**, an irreversible nucleophilic attack would occur since the amine would be in close

proximity and C_α is highly electrophilic. This attack would form a heterocyclic intermediate (**12**) that could be deprotonated by the basic site on the ligand to give ammonium or carbene complexes (**13a** and **13b**, respectively). Complexes **13a** and **13b** are proposed to be the resting state species of the catalytic cycle. Reversible proton-transfer between these species occurs fast enough at room temperature to account for the broad nature of the observed $^{31}P\{^1H\}$ NMR signal.
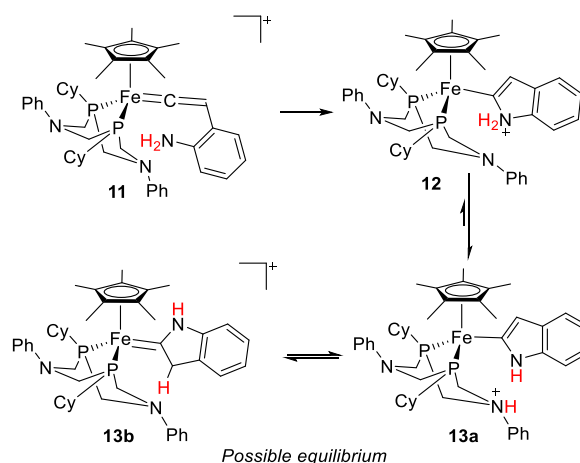
Scheme 4.3: Possible equilibrium between species in the catalytic cycle undergoing proton shuttling steps.

Cold temperature could potentially slow the equilibrium down enough to permit the observation of the proposed species through $^{31}P\{^1H\}$ NMR or ^1H NMR analysis of the diagnostic Cp* methyl protons. If the reaction between the species can be slowed down enough to see on the NMR time scale, the broad signals will resolve into distinct peaks, and the coalescence temperature would provide thermodynamic information about the equilibrium of the proton-transfer.

Since the equilibrium is proposed to involve proton shuttling, it could be possible to trap an intermediate by adding a base to the reaction (Scheme 4.4). Deprotonation from a cationic species in the catalytic cycle (**13a** or **13b**) would result in a neutral complex, **14**. If such a deprotonation was irreversible the resulting species would no longer be in equilibrium. This could allow isolation and characterization of the

possible intermediate and provide direct evidence of the rate-determining step in catalysis.
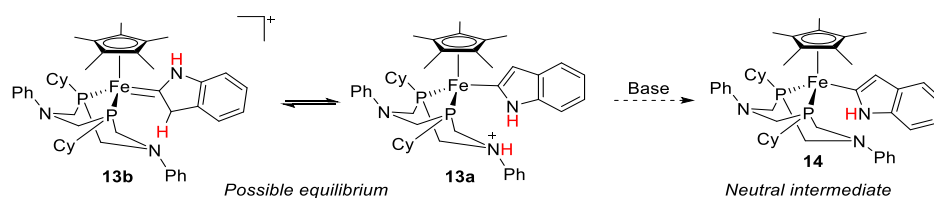
Scheme 4.4: A cationic intermediate in the catalytic cycle could potentially be deprotonated to form an isolable neutral complex.

A test reaction was performed by adding excess Et_3N to the reaction at room temperature after the broad signal had formed. Within minutes the compound had reacted and a singlet at 52.3 ppm appeared in the ^{31}P NMR spectrum. The location of the signal was consistent with regeneration of catalyst **3a**. This preliminary evidence suggests that Et_3N acted as a base and assisted in proton shuttling, promoting **Ind** product formation and release. MeCN, present in solution, was then able to bind to the open site on the catalyst and regenerate precatalyst **3a**. A stronger base will therefore be required to irreversibly deprotonate **13a/b** to allow for isolation and characterization.

4.3   Formation of a Catalyst Deactivation Product

Heating catalyst **3a** and **EA** at 70 °C in protio anisole for 2 days resulted in emergence of a set of new signals in the $^{31}P\{^1H\}$ NMR spectrum (Figure 4.3). The signals were a doublet slightly downfield of **3a** at 56.3 ppm ($J_{P\text{-}P}$ = 49 Hz) and a triplet at 4.3 ppm ($J_{P\text{-}P}$ = 49 Hz) in a 2:1 ratio, which are consistent with a single new compound. Almost full conversion of **3a** to the new species was achieved after increasing the temperature to 100 °C for an additional 24 hours. A control reaction in which **3a** was heated in anisole at 100 °C in the absence of **EA** formed the same product over 16 hours (ca. 50% by relative integration). The evidence supports this product as an off-cycle thermal deactivation product. The catalytic hydrofunctionalization data for **3a** indicates that turnover stops by 1 hour, which is consistent with fast deactivation of the catalyst.
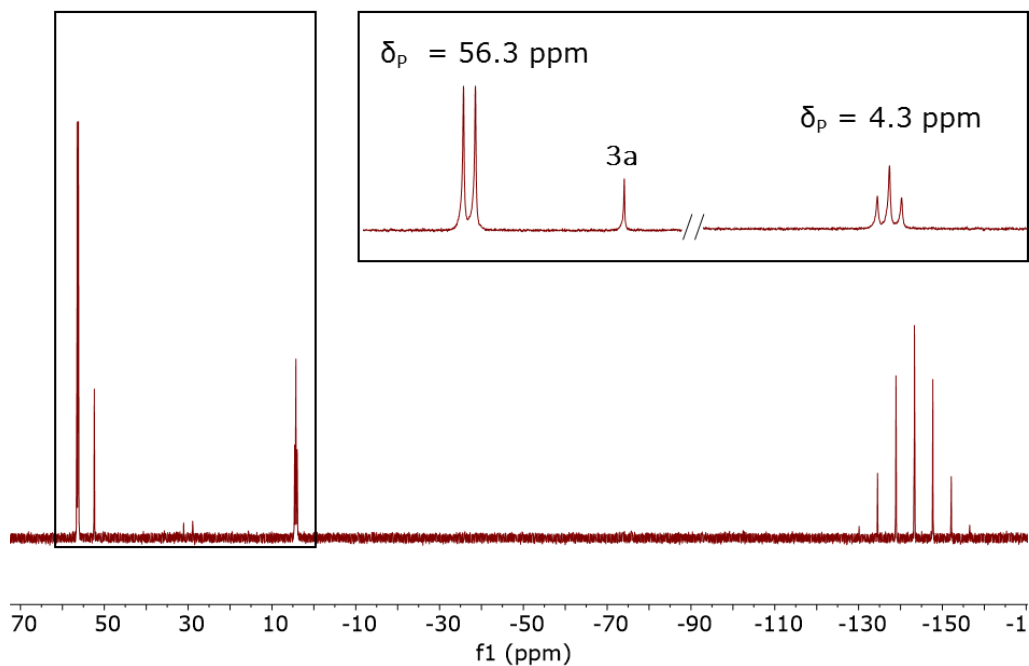
Figure 4.3: $^{31}P\{^1H\}$ NMR spectrum in anisole after heating **3a** and **EA** at 70 for 2 days then 100 °C for 24 hours. Deactivation species at 56.3 ppm (d, $J_{\text{P-P}} = 49$ Hz) and 4.3 ppm (t, $J_{\text{P-P}} = 49$ Hz) integrated in a 2:1 ratio.

A proposed structure for the deactivation product is based on the $^{31}P\{^1H\}$ NMR coupling and integration data (Scheme 4.5, **15a**). The 2:1 integration ratio means there is some multiple of three P atoms in the structure. Since a $P^R_2N^{R'}_2$ ligand contains only pairs of phosphines, there must be at least three equivalents of ligand involved. The multiplicity indicates that one P atom is coupled to two other equivalent P atoms. This suggests that one equivalent of free ligand has coordinated to the open coordination sites of two catalyst molecules. Since there are three equivalents of catalyst involved in the deactivation pathway, performing catalysis with a lower concentration of total reagents could extend the lifetime and allow for lower catalyst loadings to be employed.
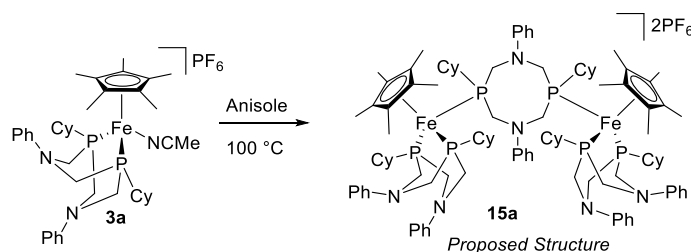
Scheme 4.5: Proposed deactivation product **15a** formed after heating complex **3a** in anisole.

4.4 Proposed Catalytic Cycle for the Hydrofunctionalization of Alkynes with Fe(II) Catalysts 3a/b

Based on the experimental evidence, a general catalytic cycle is proposed for the intramolecular hydrofunctionalization of alkynes with catalysts of the type $[Fe(Cp^*)(P^R_2N^{R'}_2)(MeCN)]PF_6$ (Scheme 4.6). Complex **3** first dissociates the labile MeCN ligand to form the active catalyst **16** with an open coordination site. Substrate binding and isomerization then forms vinylidene complex **17** which undergoes an irreversible regioselective nucleophilic attack at C_α to form a protonated iron-heterocycle complex **18**. Proton-transfer occurs between the iron-heterocycle on **18** and the ligand on complex **19** that is proposed to be the resting state in the catalytic cycle. The rate-determining step is proposed to be protonation of C_α of the iron-heterocycle on species **19** after a final proton-transfer from the ligand, allowing product release and regenerating active catalyst **16**. The off-cycle decomposition product **15** is produced in the absence of substrate, which means that it forms via the active catalyst **16**.
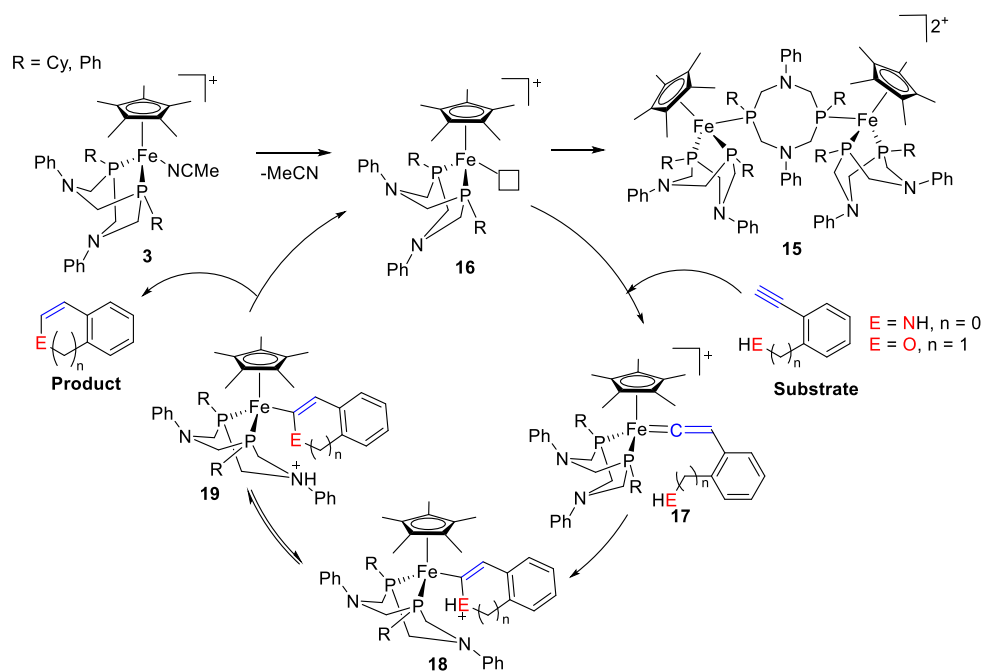
Scheme 4.6: Proposed catalytic cycle for *endo* selective intramolecular hydrofunctionalization of alkynes with catalyst **3**.

Chapter 5

5   Conclusions and Future Work

5.1   General Conclusions

Two new iron complexes **3a** and **3b** have been synthesized and characterized. These complexes are the first Fe(II) catalysts shown to be active for the *endo*-selective intramolecular hydrofunctionalization of alkynes to form *O-* and *N*-heterocycles. Control reactions showed the mechanism is not radical mediated and the well-defined structures of **3a** and **3b** are responsible for catalytic activity. *Endo*-selectivity was confirmed with the hydrofunctionalization of **EBA** to **IC**, where **3b** showed excellent activity with a lifetime of 120 TON, ca. twice that of the previous best $[Ru(Cp^*)(P^R_2N^{R'}_2)(MeCN)]PF_6$ catalyst. Establishing that a base-metal such as Fe(II) can achieve an improvement in activity over a precious-metal counterpart is a contribution toward environmental sustainablility as the use of catalysis continues to grow.

A vinylidene complex **7** has been isolated and characterized, which indicates that such an intermediate is responsible for the observed *endo*-selectivity. No evidence of alkyne dimerization was observed during the synthesis of vinylidene **7**. Preliminary work has established conditions that are suitable for the formation of catalytic intermediates, providing evidence for a resting state that is proposed to involve proton shuttling between the ligand and an iron-heterocycle. A deactivation product proposed to consist of one ligand equivalent coordinated to two catalyst equivalents has been observed to form cleanly as a result of thermal decomposition. This product forms quickly in the absence of substrate at catalytic temperature. Further characterization of this deactivation species would assist in understanding the mechanism involved. Once elucidated, methods to avoid the deactivation pathway could then be developed in order to extend catalyst lifetime.

The utility of ligands thus goes even beyond improvements in activity and selectivity. As shown, the specific environment that a properly selected ligand creates can allow the use of a base-metal such as iron in place of a more rare metal (i.e. Ru or Os) that

would typically be used. This illustration of the high level of control that a well-designed ligand can provide is a step forward to the utilization of abundant metals in homogenous catalysis.

5.2   Future Work

Since catalyst decomposition occurs quickly and cleanly, isolation and characterization of the deactivation species **15** should be pursued (Scheme 5.1). ^{1}H NMR spectroscopy should show a single strong peak for Cp* methyl protons if the structure has mirror symmetry as proposed. ^{1}H-^{31}P{^{1}H} HMBC NMR should show coupling between this Cp* methyl peak and both of the signals observed in ^{31}P NMR spectra. MALDI-MS data would also be useful in confirming the structure if the central ligand stayed bound to one or both metal centers.

Confirmation of the structure of the deactivation product will provide evidence as to the mechanism that is involved and may allow development of strategies to circumvent such a pathway. If the proposed structure is correct, the product is an off-cycle species that involves three equivalents of catalyst reacting together. This would indicate that the concentration of the total reaction mixture may be an important factor in extending catalyst lifetime. Analysis of the rate of decomposition can be accomplished by heating catalyst solutions of various concentrations. Because decomposition occurs quickly at optimal catalytic temperature, milder conditions must be used. This may be accomplished with *in situ* monitoring of a high temperature reaction by ^{31}P{^{1}H} NMR.
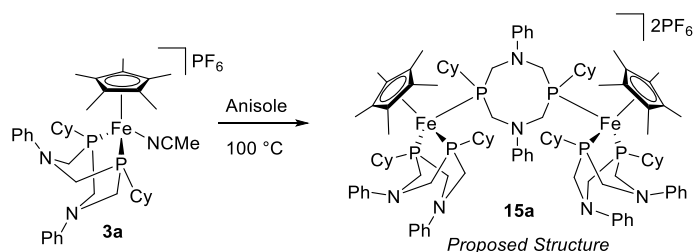
Scheme 5.1: Off-cycle catalyst deactivation

Further experiments should also be carried out to confirm the identity of the potential catalytic intermediates **13a** and **13b**. Low temperature ^{31}P{^{1}H} NMR analysis may slow

the chemical equilibrium enough to help identify the distinct species involved. ^{1}H NMR data may also be diagnostic at cold temperatures, and two large peaks should be evident for the Cp* methyl protons. The coalescence temperature can be used to calculate the equilibrium constant of the proton exchange. ^{15}N NMR analysis would show direct evidence of a protonated nitrogen. This would necessitate the synthesis of an isotopically labelled ligand from ^{15}N-aniline. Since catalytic turnover was observed at 70 °C, high temperature ^{31}P{^{1}H} NMR experiments at gradually increasing temperatures may also be used to determine the barrier of the rate-limiting step in the catalytic cycle.

Deprotonation of the proposed resting-state intermediates should be attempted to inhibit product release and facilitate isolation and characterization (Scheme 5.2). ^{1}H NMR analysis would be essential to elucidate the structure and should exhibit diagnostic signals for the amine and the vinyl protons. The ^{31}P{^{1}H} NMR spectrum should not show a signal for the [PF$_6$]$^-$ anion since the complex would be neutral. MALDI-MS data collected for an isolated product would also prove valuable if the iron-bound heterocycle was detected.

Possible on-cycle intermediate
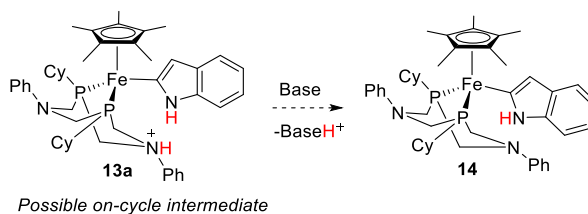
Scheme 5.2: Deprotonation of a proposed cationic intermediate may allow deactivation and isolation.

More substrates should be screened that have the potential to form *exo* products, especially those able to form 7-membered *endo* heterocycles (Scheme 5.3). Such substrates provide an opportunity to test Fe(II) P$^R_2$N$^{R'}_2$ catalysts on challenging substrates that have typically required Os(II) or Ru(II). Successful hydrofunctionalization using Fe(II) would be further evidence of the significant effect that P$^R_2$N$^{R'}_2$ ligands can have on catalysis.
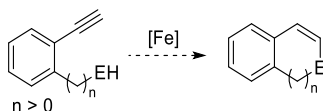
Scheme 5.3: Expanded substrate scope will allow further insight into the mechanism of catalysis.

The isolated vinylidene **7** provides an opportunity to explore the viability of MLC complexes **3a** and **3b** for intermolecular hydrofunctionalization. Amine nucleophiles are known to selectively attack C_α of iron vinylidenes, and stoichiometric reactions with **7** may form carbene products (Scheme 5.4i). Experimentation on the resulting products could determine conditions for product release, which would allow insight into whether *anti*-Markovnikov intermolecular hydrofunctionalization catalysis is feasible with complexes **3a** or **3b** (Scheme 5.4, ii).
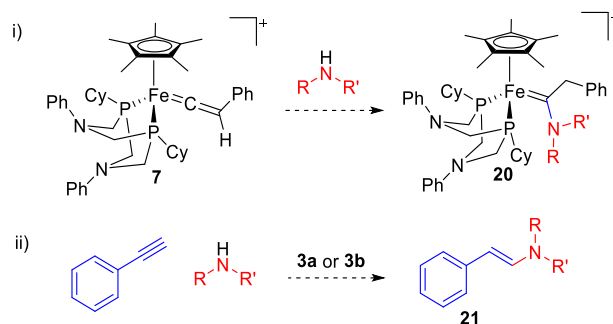
Scheme 5.4: i) Possible reactivity involving vinylidene complex **7** and amine nucleophiles. ii) Proposed catalysis for the intermolecular hydrofunctionalization of alkynes.

Chapter 6

6   Experimental

6.1   General Considerations

Air- and water-sensitive reactions were performed under Ar or N_2 using standard Schlenk line or glovebox techniques, respectively. All glassware was oven dried at 150 °C for at least 4 hours prior to use. Pyrene (98%), 2-ethynylaniline (98%), tetralin (1,2,3,4-tetrahydronaphthalene; 99%), $FeCl_2$ (98%), lithium pentamethylcyclopentadienide, sodium cyclopentadienide (2.0 M in THF), potassium hexafluorophosphate (>99%), and 2-methyltetrahydrofuran (Me-THF; >99% anhydrous) were obtained from Sigma-Aldrich. $CyPH_2$ (97%) and $PhPH_2$ (99%) were obtained from Strem Chemicals. Dichloromethane-d_2 (99.8%) was obtained from Cambridge Isotope Laboratories. [Fe(Cp*)(MeCN)$_3$]PF$_6$ was synthesized following a literature procedure and matched reported characterization data.[84] 2-ethynylbenzyl alcohol, 2-ethynylbenzamide, 2-ethynylbenzylamine, and 2-ethynylbenzeneethanol were synthesized according to literature procedures and matched reported characterization data.[58, 59, 92, 93] Dried and degassed tetrahydrofuran, diethyl ether, dichloromethane, pentane and acetonitrile were obtained from an Innovative Technology 400-5 Solvent Purification System and stored in a glovebox under N_2 over 4 Å molecular sieves with the exception of acetonitrile, which was stored over 3 Å molecular sieves (Fluka and activated at 150 °C for over 12 h). Ethanol and aniline were degassed by bubbling with N_2, and 1,2-dichloroethane (DCE) was degassed by bubbling with N_2 after drying over 4 Å molecular sieves. Dichloromethane-d_2 was dried with 4 Å molecular sieves. All other chemicals were used as received.

Charge-transfer Matrix Assisted Laser Desorption/Ionization (MALDI) mass spectra were collected on an AB Sciex 5800 TOF/TOF mass spectrometer using a pyrene matrix in a 10:1 molar ratio to metal complex. Samples were spotted on the target plate from solutions in DCM. All NMR spectra were recorded on either an Inova 600 MHz or Bruker 400 MHz instrument. ^1H and $^{13}C\{^1H\}$ spectra acquired in CDCl$_3$ and DCM-d_2 were referenced internally against the residual solvent signal (CHCl$_3$ at 7.26 ppm, DCM

at 5.32 ppm) to TMS at 0 ppm. $^{31}P\{^1H\}$ spectra were referenced externally to 85% phosphoric acid at 0.00 ppm. Multiplicities are described as s (singlet), d (doublet), t (triplet), sept (septet), broad (br), and m (multiplet). X-ray diffraction measurements were made on a Bruker Kappa Axis Apex2 diffractometer at a temperature of 110 K. Infrared spectra were collected on solid samples using a Bruker ALPHA II FTIR spectrometer. Quantification of catalytic reactivity was achieved using an Agilent 7890a Gas Chromatograph with a flame ionization detector (GC-FID), fitted with a HP-5 column. Calibration curves of 2-ethynylaniline (**EA**) and indole (**Ind**) were prepared. The response factor for **Ind** with respect to **EA** was 1.06 and this value was applied to quantify in situ yields of **Ind**. A response factor of 1 was assumed for 1*H*-isochromene (**IC**) with respect to 2-ethynylbenzyl alcohol (**EBA**)and this was used to quantify the in situ yields of **IC**.

6.2   Representative Procedure for the Synthesis of P$^{Ph}_2$N$^{Ph}_2$ Ligand (**2a**)

A modified literature procedure was followed.[71] In the glovebox, phenylphosphine (1.176 g, 10.68 mmol) was added to a 100 mL Schlenk flask. The flask was removed from the glovebox and connected to a Schlenk line under argon atmosphere and degassed EtOH (50 mL) was added via cannula. A separate 2-neck 500 mL Schlenk flask containing a stir bar, 37% w/w aqueous paraformaldehyde solution (8.098 g, 99.77 mmol), and EtOH (200 mL) was set up with a reflux condenser on the Schlenk line and the solution was degassed. The primary phosphine solution was then added to the 500 mL Schlenk flask via cannula at room temperature. Degassed EtOH (50 mL) was added via cannula to rinse the 100 mL Schlenk flask, which was then transferred to the 500 mL flask. The 500 mL reaction flask was heated to 70 °C for 3 h, after which an aliquot was transferred to a degassed NMR tube by syringe. The solution was analyzed by unlocked $^{31}P\{^1H\}$ NMR spectroscopy, which showed that all primary phosphine (δ = ca. –120) was consumed and a new singlet had appeared for the hydroxymethyl phosphine intermediate (ca. 100 ppm downfield). Aniline (1.00 mL, 10.5 mmol) was added to the reaction solution dropwise by syringe at a rate of ca. 1 drop/10 seconds. White precipitate was observed on addition of each drop but did not persist until approximately half of the aniline was added. The

reaction was left to stir at 70 °C for 16 h and then cooled to room temperature. The white precipitate was isolated by filtration through a filter frit and dried under vacuum. The resulting white powder was washed with acetonitrile (3×10 mL) to yield $P^{Ph}_2N^{Ph}_2$ ligand (73%). The $P^{Cy}_2N^{Ph}_2$ ligand was synthesized by the same method and isolated in 76% yield. The ^1H and $^{31}P\{^1H\}$ spectra for both ligands matched reported characterization data.[100, 101]

6.3 Synthesis of [Fe(Cp*)(P^R$_2$N^{Ph}$_2$)(MeCN)]PF$_6$ Complexes

General Procedure: Complexes of the type [Fe(Cp*)($P^R_2N^{Ph}_2$)(MeCN)]PF$_6$ were synthesized according to an adapted literature procedure[83] and performed in a glovebox under N_2 atmosphere. To a 20 mL vial with a stir bar, the $P^R_2N^{Ph}_2$ ligand (0.5 mmol, 1 equiv.) and FeCl$_2$ (1.2 equiv.) were added followed by THF (8 mL). The reaction was stirred at room temperature for 1 h until a clear solution was obtained. LiCp* (1.2 equiv.) was added as a suspension in THF (4 mL) and the solution was stirred for 5 minutes. KPF$_6$ (1.2 equiv.) was added and the reaction was stirred for 5 minutes before acetonitrile (5 mL) was added. The reaction was stirred for an additional 2 h, during which an orange suspension had formed. The solvent was removed under reduced pressure and the solids were taken up in acetonitrile (5 mL) then filtered through a glass microfiber plug. The plug was washed with acetonitrile until the washings were clear. The solvent of the filtrate was removed under vacuum and the remaining solids were taken up in DCM (5 mL) and filtered through Celite, which was washed with DCM. The filtrate solvent was removed under vacuum and the remaining solids were washed with Et$_2$O (3×7 mL). The remaining solids were dried under vacuum.

[Fe(Cp*)(P^{Cy}$_2$N^{Ph}$_2$)(MeCN)]PF$_6$ (3a): Yield: 86%, red solid. ^1H (400 MHz, CD$_2$Cl$_2$) δ: 7.33-7.27 (m, Ph-*H*, 4H), 7.07 (d, ^3J = 8.3 Hz, Ph-*H*, 2H), 7.01-6.96 (m, Ph-*H*, 3H), 6.94 (t, ^3J = 7.3 Hz, Ph-*H*, 1H), 3.90-3.82 (m, P-C*H$_2$*-N, 2H), 3.80-3.72 (m, P-C*H$_2$*-N, 2H), 3.23-3.17 (m, P-C*H$_2$*-N, 2H), 2.83-2.74 (m, P-C*H$_2$*-N, 2H), 2.70-2.61 (m, P-C*H*, 2H), 2.39 (s, Fe-NCC*H$_3$*, 3H), 2.17-2.08 (m, C*H$_2$*, 4H), 2.05-1.97 (m, C*H$_2$*, 4H), 1.91-1.84 (m, C*H$_2$*, 2H), 1.68-1.59 (m, C*H$_2$*, 2H), 1.64 (s, C$_5$(C*H$_3$*)$_5$, 15H), 1.59-1.44 (m, C*H$_2$*, 4H), 1.40-1.31

(m, CH_2, 2H), 1.21-1.11 (m, CH_2, 2H). ^{31}P{^{1}H} (162 MHz, CD$_2$Cl$_2$) δ: 52.4 (s, P_{Cy}), −144.5 (sept, $^1J_{P-F}$ = 711.1 Hz, PF_6). ^{13}C{^{1}H} (101 MHz, CD$_2$Cl$_2$) δ: 153.6 (t, $^3J_{C-P}$ = 7.0 Hz, N-C_{Ar}), 152.3 (t, $^3J_{C-P}$ = 9.8 Hz, NC_{Ar}), 132.6 (s, C_{Ar}), 129.89 (s, C_{Ar}), 129.86 (s, Fe-NCCH$_3$), 122.6 (s, C_{Ar}), 121.4 (s, C_{Ar}), 119.0 (s, C_{Ar}), 116.9 (s, C_{Ar}), 88.3 (s, C_5(CH$_3$)$_5$), 46.0 (ABX, P-CH$_2$-N), 45.3 (ABX, P-CH$_2$-N), 39.8 (ABX, P-CH$_{Cy}$), 28.3 (s, CH$_2$), 27.6 (s, CH$_2$), 27.6 (ABX, P-CH-CH$_2$), 27.3 (ABX, P-CH-CH$_2$), 26.5 (s, CH$_2$), 10.3 (s, C$_5$(CH$_3$)$_5$), 5.4 (s, Fe-NCCH$_3$). MALDI MS (pyrene matrix): Calc. *m/z* 657.3 [Fe(Cp*)(P$^{Cy}_2$N$^{Ph}_2$)]$^+$, Obs. *m/z* 657.4. ATR-FTIR (cm^{-1}): ν 1594 (C=C) (phenyl ring).

Procedure for Crystal Growth: Crystals suitable for X-Ray diffraction were grown by dissolving complex **3a** with a minimal amount of DCM in a 4 mL glass vial and layering the solution with pentane.

[Fe(Cp*)(P$^{Ph}_2$N$^{Ph}_2$)(MeCN)]PF$_6$ (3b): Yield: 85%, red solid. ^{1}H (400 MHz, CD$_2$Cl$_2$) δ: 7.72-7.60 (m, Ph-H, 10H), 7.45-7.39 (m, Ph-H, 2H), 7.32-7.26 (m, Ph-H, 2H), 7.23-7.15 (m, Ph-H, 2H), 7.06 (t, ^3J = 7.3 Hz, Ph-H, 1H), 6.89-6.82 (m, Ph-H, 3H), 4.46-4.32 (m, P-CH_2-N, 2H), 3.93-3.82 (m, P-CH_2-N, 2H), 3.81-3.65 (m, P-CH_2-N, 2H), 3.60-3.48 (m, P-CH_2-N, 2H), 2.44 (s, Fe-NCCH_3, 3H), 1.22 (s, C$_5$(CH_3)$_5$, 15H). ^{31}P{^{1}H} (162 MHz, CD$_2$Cl$_2$) δ: 50.2 (s, P_{Ph}), −144.7 (sept, $^1J_{P-F}$ = 710.6 Hz, PF_6). ^{13}C{^{1}H} (101 MHz, CD$_2$Cl$_2$) δ: 152.8 (t, $^3J_{C-P}$ = 9.9 Hz, N-C_{Ar}), 151.7 (t, $^3J_{C-P}$ = 7.3 Hz, N-C_{Ar}), 132.7 (s, C_{Ar}), 132.5 (ABX, P-C_{Ar}), 131.4 (s, Fe-NCCH$_3$), 130.5 (ABX, P-C_{Ar}), 130.2 (ABX, P-C_{Ar}), 130.1 (s, C_{Ar}), 129.8 (s, C_{Ar}), 122.3 (s, C_{Ar}), 121.8 (s, C_{Ar}), 118.1 (s, C_{Ar}), 117.7 (s, C_{Ar}), 89.5 (s, C_5(CH$_3$)$_5$), 53.5 (ABX, P-CH$_2$-N), 46.9 (ABX, P-CH$_2$-N), 9.7 (s, C$_5$(CH$_3$)$_5$), 5.5 (s, Fe-NCCH$_3$). MALDI MS (pyrene matrix): Calc. *m/z* 645.2 [Fe(Cp*)(P$^{Ph}_2$N$^{Ph}_2$)]$^+$, Obs. *m/z* 645.2. ATR-FTIR (cm^{-1}): ν 1595 (C=C, phenyl ring).

6.4   General Procedure for the Catalytic Hydrofunctionalization of Substrates

In a glovebox, stock solutions of substrate (2-ethynylaniline or 2-ethynylbenzyl alcohol, 600 mM) and internal standard (tetralin, 400 mM) were prepared in either DCM, DCE, Me-THF, or anisole and combined in equivalent volumes to give one stock solution with 300 mM substrate and 200 mM internal standard. Catalyst (**3a** or **3b**) was added as a

solution in DCM (25, 50, or 100 μL of 15 mM) to 4 mL vials containing stir bars and the solvent was left to evaporate. The amount of catalyst solution added was varied depending on the desired loading for the trial (0.5, 1.0, or 2.0 mol%). The vials were then charged with the substrate/internal standard stock solution (250 μL) and additional solvent (250 μL DCM, DCE, MeTHF, or anisole), giving a final volume of 500 μL. The final concentrations for all vials was 150 mM in substrate, 100 mM in internal standard, and 0.75, 1.5, or 3.0 mM in catalyst. A final vial was charged with substrate/internal standard stock solution (250 μL) for use as the time = 0 sample. The vials were capped and removed from the glovebox and heated with stirring to various temperatures (40-110 °C). After each desired time, 2 vials were removed from heat and a 20 μL aliquot was immediately diluted to 3 mM (based on substrate) in acetonitrile (980 μL) and analyzed by GC-FID. A 10 μL aliquot of the T0 sample was diluted with acetonitrile (990 μL) and analyzed by GC-FID.

6.5   Procedures for Catalysis Control Reactions

FeCl$_2$ and FeCl$_2$ + P$^{Cy}_2$N$^{Ph}_2$ as Catalysts: FeCl$_2$ (18.5 mg, 146 mmol) was dissolved in THF (9.73 mL) and stirred overnight until a clear colourless solution was obtained. A portion of this FeCl$_2$/THF stock solution (1.543 mL) was added to P$^{Cy}_2$N$^{Ph}_2$ ligand (10.8 mg, 12.8 mmol) and stirred until a clear yellow solution was obtained. Each of the FeCl$_2$ and FeCl$_2$ + P$^{Cy}_2$N$^{Ph}_2$ stock solutions (50 μL of 15 mM for 1.0 mol%) were used in place of the catalyst stock solution in the general procedure for catalytic hydrofunctionalization of substrates and the reaction was analyzed after 1 hour by GC-FID.

1,4-Cyclohexadiene as a Radical Trap: A 1,4-cyclohexadiene stock solution (34 μL, 37 μM) was diluted in anisole (1.664 mL) and used in the general procedure for catalytic hydrofunctionalization of substrates in place of the additional solvent (250 μL) needed to reach the desired total volume of 500 μL. Complex **3a** (25 μL of 15 mM for 0.5 mol%) was used as the catalyst and the reactions were analyzed after 1 h reaction time by GC-FID.

Dark Reaction: Dark reactions were performed according to the general procedure for catalytic hydrofunctionalization of substrates using complex **3a** (25 μL of 15 mM for 0.5

mol%) with vials wrapped in aluminum foil prior to and during heating. Reaction aliquots were analyzed after 1 hour by GC-FID.

Non-Catalytic Control Reaction: In a glovebox, stock solutions of substrate (2-ethynylaniline and indole, 600 mM each) and internal standard (tetralin, 400 mM) were prepared in anisole, combined in equivalent volumes, and diluted with an equivalent volume of anisole to give one stock solution with 150 mM of each substrate and 100 mM internal standard. 4 mL vials containing stir bars were then charged with the substrate/internal standard stock solution (500 μL) and additional solvent (250 μL anisole), giving a final volume of 500 μL. The vials were capped and removed from the glovebox and heated with stirring (110 °C). After each desired time, 2 vials were removed from heat and a 20 μL aliquot was immediately diluted to 3 mM (based on substrate) in acetonitrile (980 μL) and analyzed by GC-FID.

6.6   Synthesis of On-Cycle Intermediates **12/13**

In a glovebox under N_2 atmosphere, complex **3a** (28 mg, 0.033 mmol, 1 equiv) and 2-ethynylaniline (92.3 μL, 0.79 mmol, 24 equiv.) were dissolved in DCM (0.7 mL) and added to an NMR tube. The NMR tube was capped, removed from the glovebox, sealed with parafilm, and heated to 45 °C for 72 hours. $^{31}P\{^{1}H\}$ (400 MHz, CH_2Cl_2) δ: 51.4 ppm (br).

6.7   Synthesis of Catalyst Decomposition Product **15a**

In a glovebox under N_2 atmosphere, complex **3a** (27 mg, 0.032 mmol, 1 equiv) was added to an NMR tube followed by anisole (600 μL) and then 2-ethynylaniline (36 μL, 0.32 mmol, 10 equiv.). The NMR tube was capped, removed from the glovebox, sealed with parafilm, and heated to 70 °C for 48 hours and then 100 °C for 24 hours. Et_2O (1 mL) was added and a red solid precipitated out of solution. The solids were washed with Et_2O and dried under reduced pressure and the resulting product was clean by $^{31}P\{^{1}H\}$ NMR analysis but anisole was evident in the ^{1}H NMR spectrum. $^{31}P\{^{1}H\}$ (400 MHz, CD_2Cl_2) δ: 55.1 ppm (d, J_{P-P} = 48 Hz), 5.4 ppm (t, J_{P-P} = 48 Hz), −144.7 (sept, $^{1}J_{P-F}$ = 711.2 Hz, PF_6).

6.8　Synthesis of [Fe(Cp*)(P$^{Cy}_2$N$^{Ph}_2$)(=C=CHPh)]PF$_6$ (**7**)

In a glovebox, complex **3a** (19 mg, 0.021 mmol, 1 equiv) was added to a 4 mL screw cap vial containing a stir bar. A solution of phenylacetylene (24 mg, 0.23 mmol, 11 equiv.) in DCE (1 mL) was added to the vial, which was capped and sealed with tape. The vial was removed from the glovebox and heated to 70 °C for 2 hours in an oil bath. The reaction was taken into the glovebox and the solvent was removed under vacuum. The resulting solids were washed with Et$_2$O (3 × 3 mL) and dried under vacuum to afford **2a** as an orange solid. Yield: 17 mg, 85%. ^{1}H (400 MHz, CD$_2$Cl$_2$) δ: 7.44-7.36 (m, Ph-*H*, 2H), 7.34-7.26 (m, Ph-*H*, 4H), 7.22-7.11 (m, Ph-*H*, 5H), 7.09-7.00 (m, Ph-*H*, 2H), 6.98-6.90 (m, Ph-*H*, 2H), 6.01 (s, C=C*H*Ph, 1H), 4.02-3.91 (m, P-C*H*$_2$-N, 2H), 3.71-3.60 (m, P-C*H*$_2$-N, 2H), 3.55-3.45 (m, P-C*H*$_2$-N, 2H), 3.37-3.27 (m, P-C*H*$_2$-N, 2H), 2.13-1.75 (m, C*H*$_2$, 10H), 1.86 (s, C$_5$(C*H*$_3$)$_5$, 15H), 1.72-1.60 (m, P-C*H*, 2H), 1.54-1.38 (m, C*H*$_2$, 4H), 1.34-1.19 (m, C*H*$_2$, 4H), 0.96-0.81 (m, C*H*$_2$, 2H). ^{31}P{^{1}H} (162 MHz, CD$_2$Cl$_2$) δ: 51.1 (s, *P*$_{Cy}$), −144.5 (sept, $^1J_{P-F}$ = 710.6 Hz, *P*F$_6$). ^{13}C{^{1}H} (101 MHz, CD$_2$Cl$_2$) δ: 359.6 (Fe=*C*=CHPh, assigned by ^{1}H-^{13}C HMBC), 153.1 (t, $^3J_{C-P}$ = 8.4 Hz, N-*C*$_{Ar}$), 151.4 (t, $^3J_{C-P}$ = 10.1 Hz, N*C*$_{Ar}$), 130.6 (s, *C*$_{Ar}$), 130.2 (s, *C*$_{Ar}$), 130.1 (s, *C*$_{Ar}$), 129.2 (s, *C*$_{Ar}$), 127.2 (s, *C*$_{Ar}$), 126.9 (s, *C*$_{Ar}$), 125.7 (s, Fe=C=*C*HPh), 123.6 (s, *C*$_{Ar}$), 122.6 (s, *C*$_{Ar}$), 119.6 (s, *C*$_{Ar}$), 117.4 (s, *C*$_{Ar}$), 100.8 (s, *C*$_5$(CH$_3$)$_5$), 46.7 (ABX, P-*C*H$_2$-N), 46.2 (ABX, P*C*H$_2$N), 38.7 (ABX, P*C*H$_{Cy}$), 28.8 (s, *C*H$_2$), 27.6 (ABX, PCH*C*H$_2$), 27.4 (ABX, PCH*C*H$_2$), 27.0 (s, *C*H$_2$), 26.0 (s, *C*H$_2$), 10.7 (s, C$_5$(*C*H$_3$)$_5$). MALDI MS (pyrene matrix): Calc. *m/z* 759.4 [Fe(Cp*)(P$^{Cy}_2$N$^{Ph}_2$)(C=CHPh)]$^+$, Obs. *m/z* 759.4. ATR-FTIR (cm^{-1}): ν 1617 (C=C) (vinylidene), 1596 (C=C) (phenyl ring).

Appendices
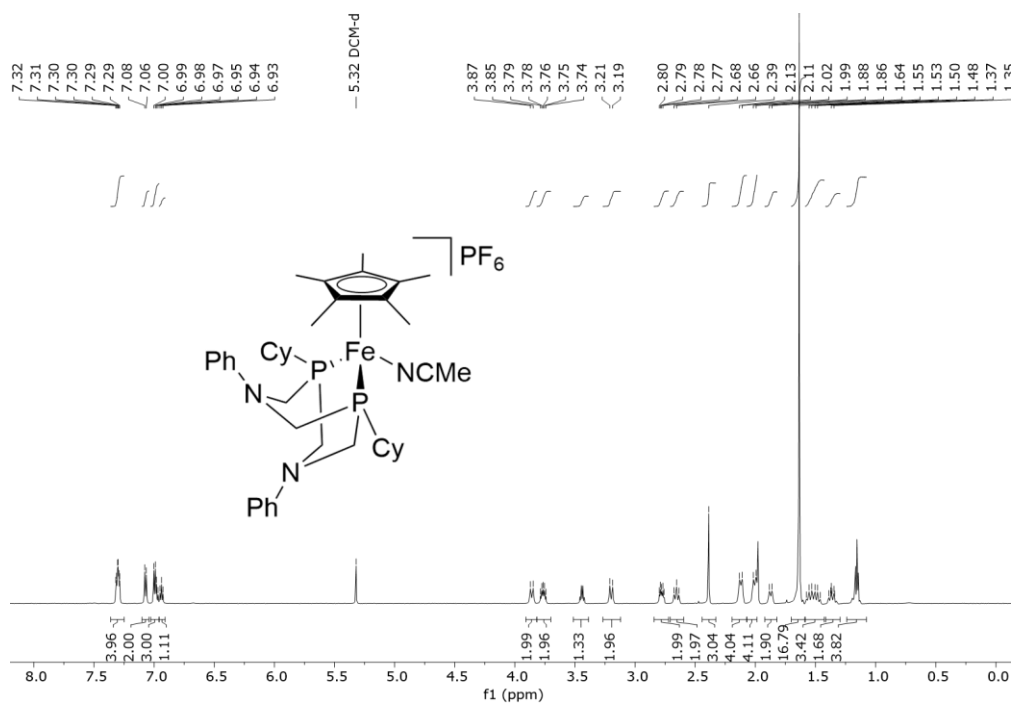
Appendix A.1: ^{1}H NMR spectrum of **3a** (400 MHz, CD$_2$Cl$_2$).
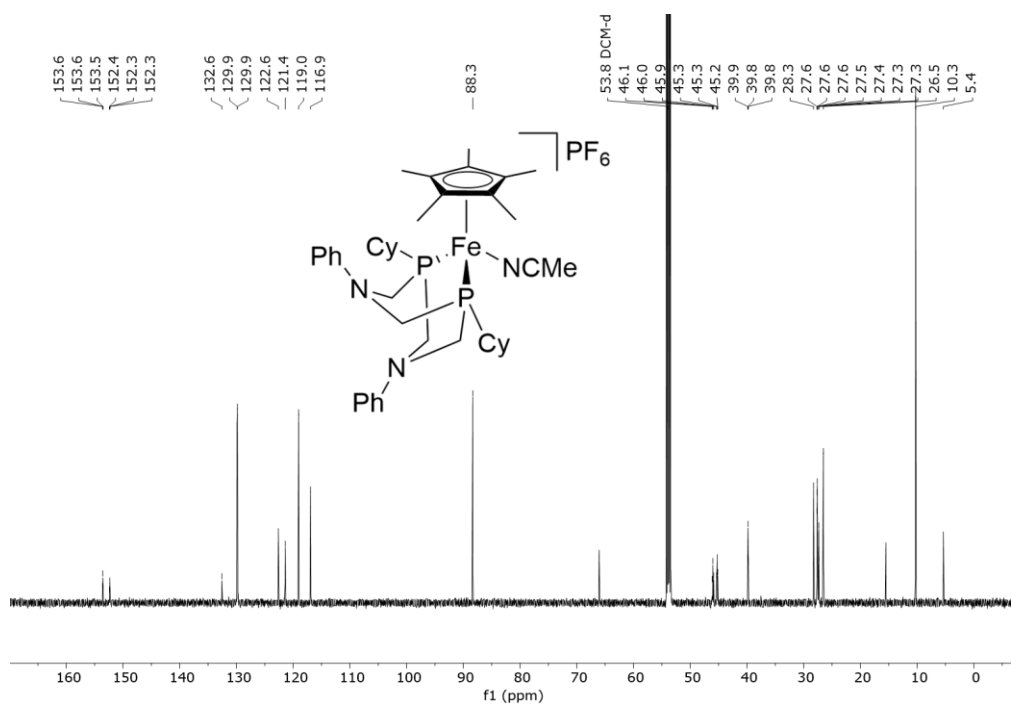
Appendix A.2: ^{13}C{^{1}H} NMR spectrum of **3a** (101 MHz, CD$_2$Cl$_2$).
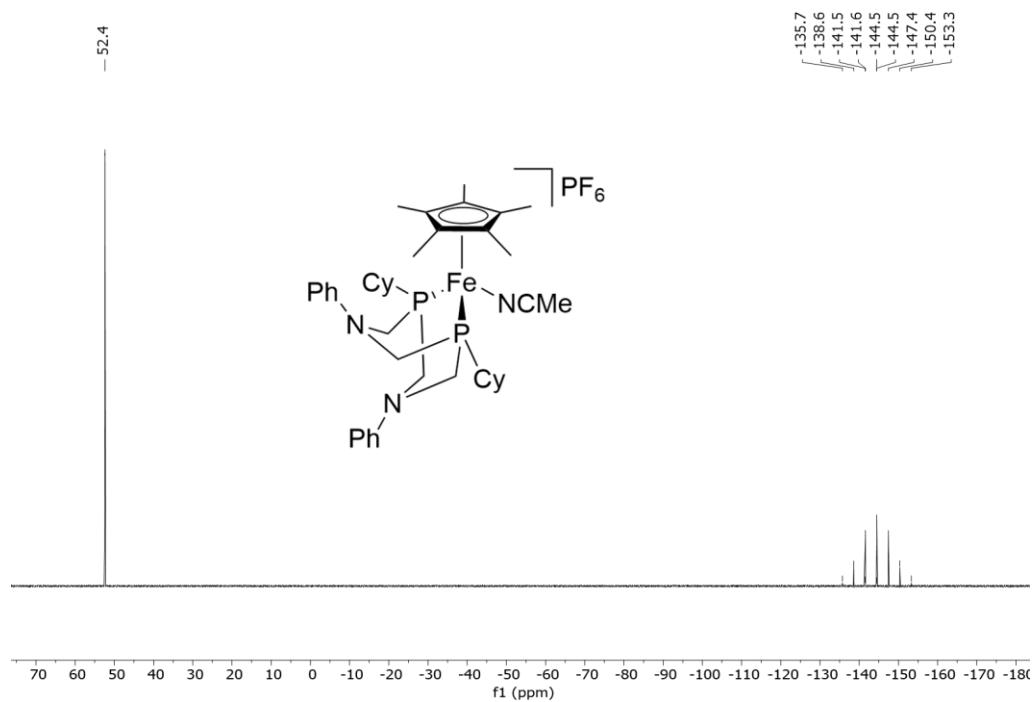
Appendix A.3: ^{31}P{^{1}H} NMR spectrum of **3a** (162 MHz, CD$_2$Cl$_2$).
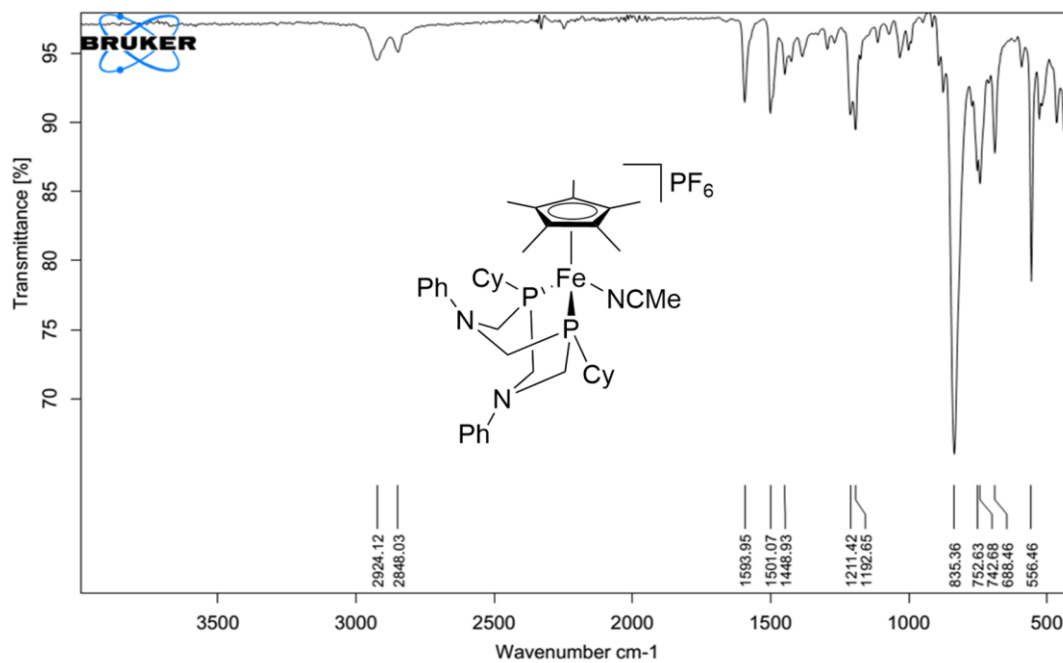
Appendix A.4: ATR-FTIR spectrum of **3a**.
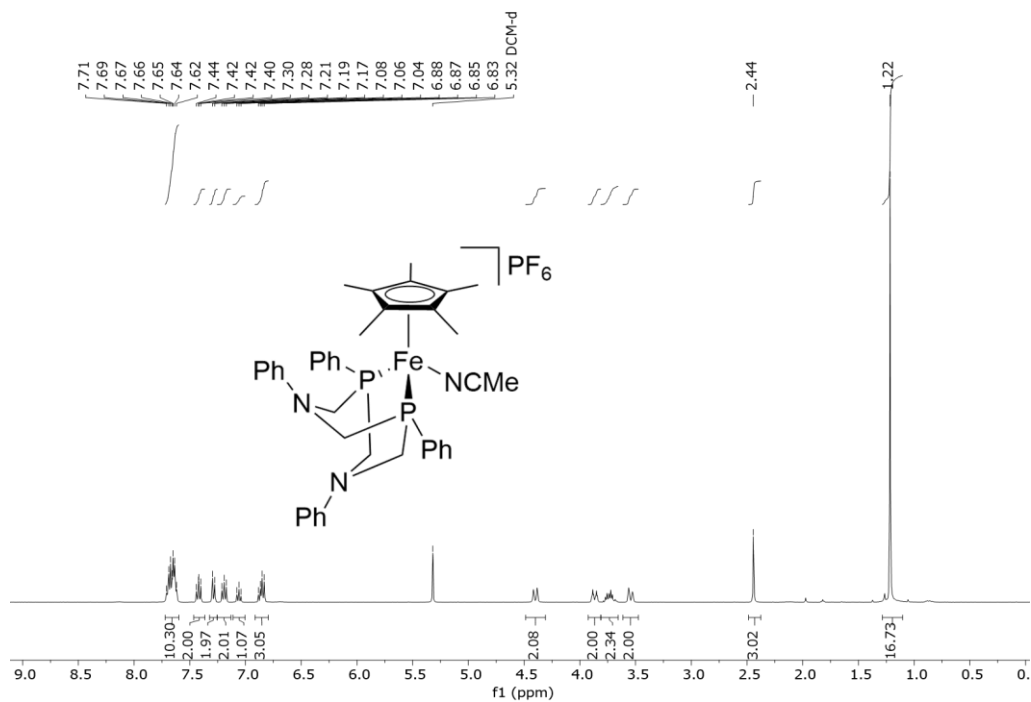
Appendix A.5: ^{1}H NMR spectrum of **3b** (400 MHz, CD$_2$Cl$_2$).
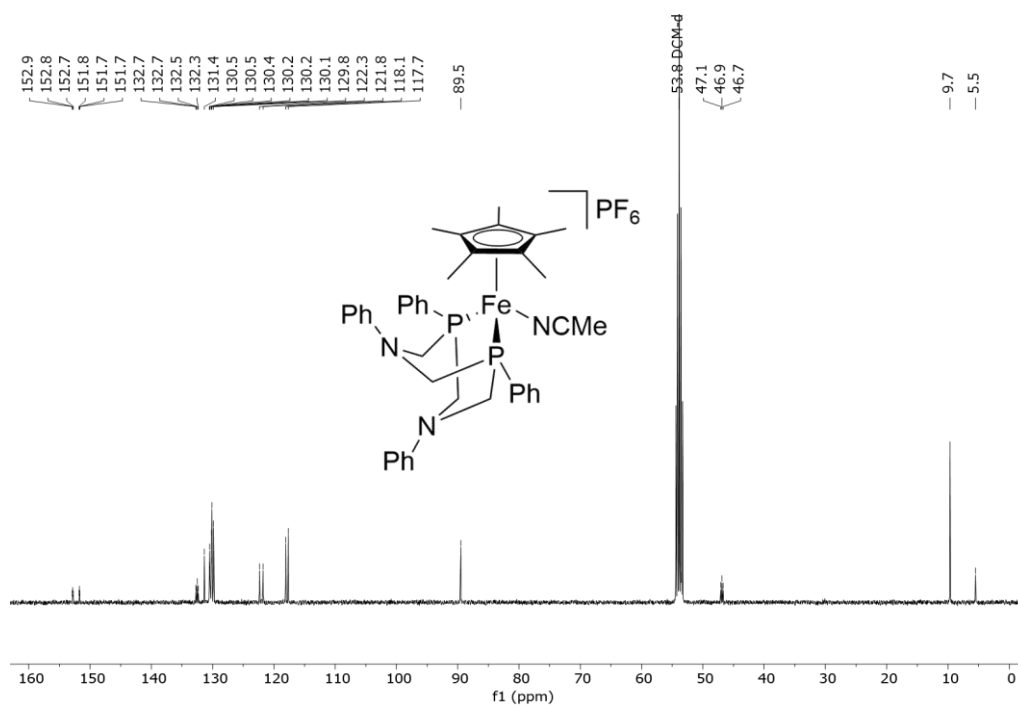
Appendix A.6: ^{13}C{^{1}H} NMR spectrum of **3b** (101 MHz, CD$_2$Cl$_2$).
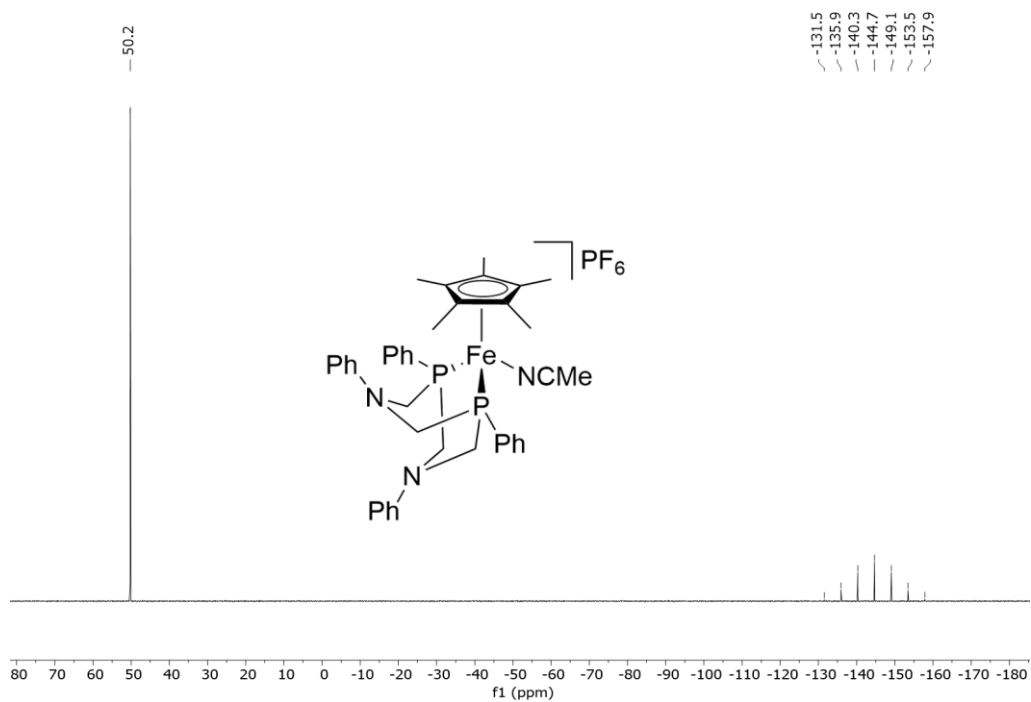
Appendix A.7: $^{31}P\{^1H\}$ NMR spectrum of **3b** (162 MHz, CD$_2$Cl$_2$).
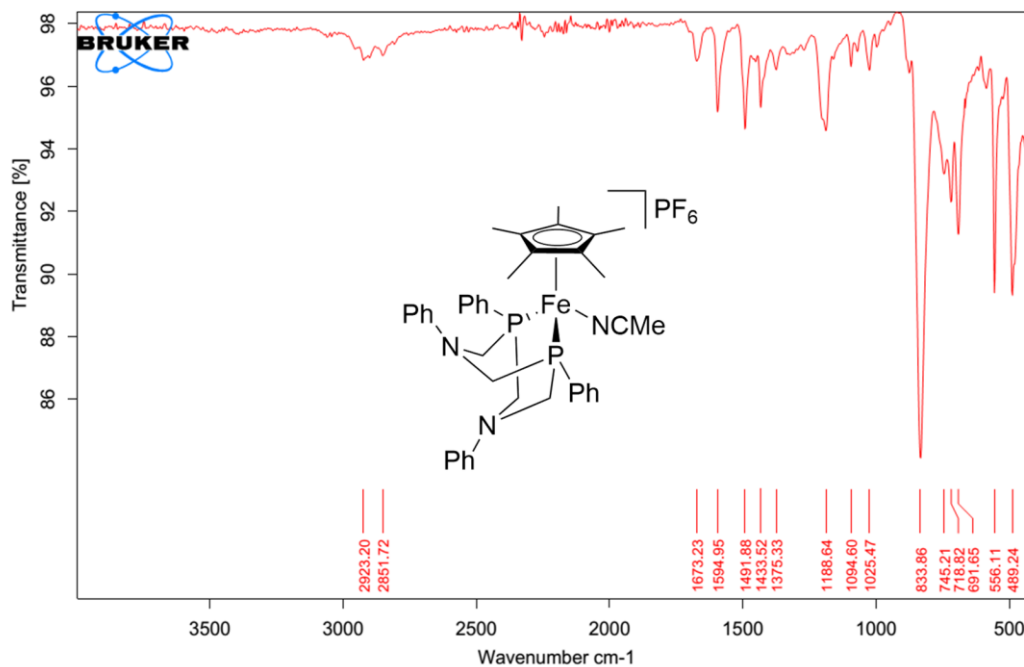
Appendix A.8: ATR-FTIR spectrum of **3b**.
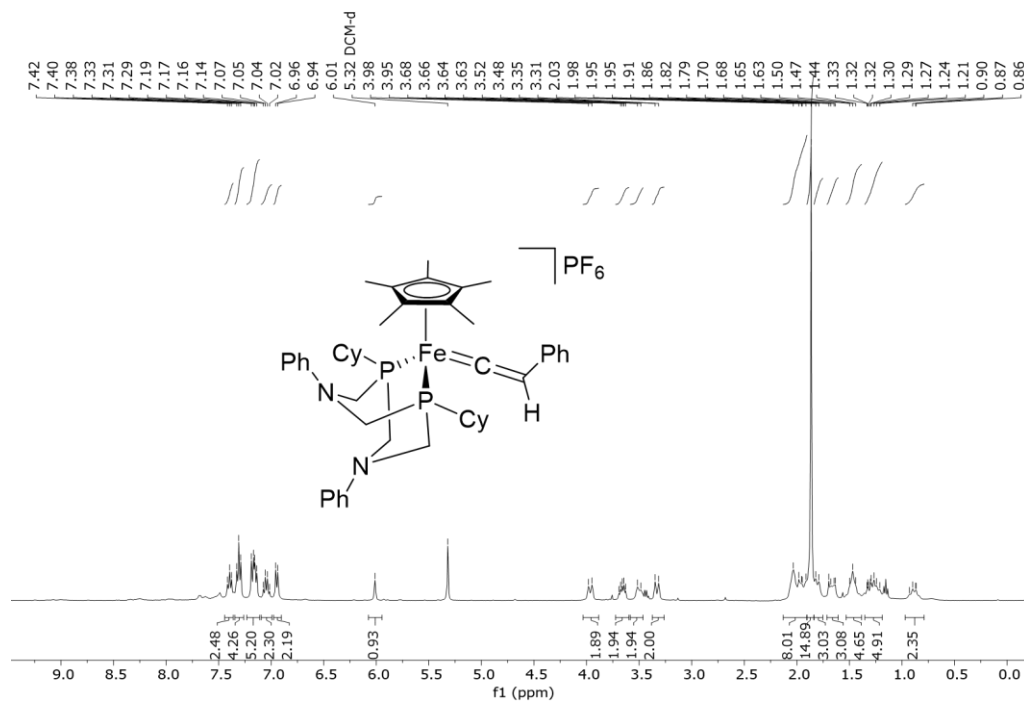
Appendix A.9: ^{1}H NMR spectrum of **7** (400 MHz, CD$_2$Cl$_2$).
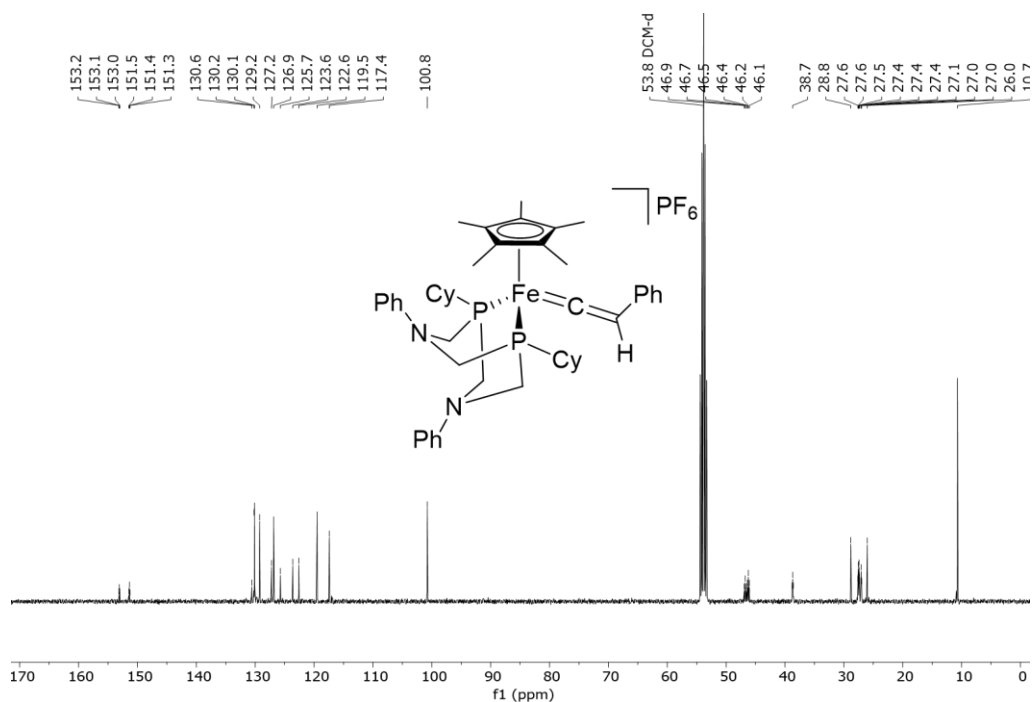
Appendix A.10: ^{13}C{^{1}H} NMR spectrum of **7** (101 MHz, CD$_2$Cl$_2$).
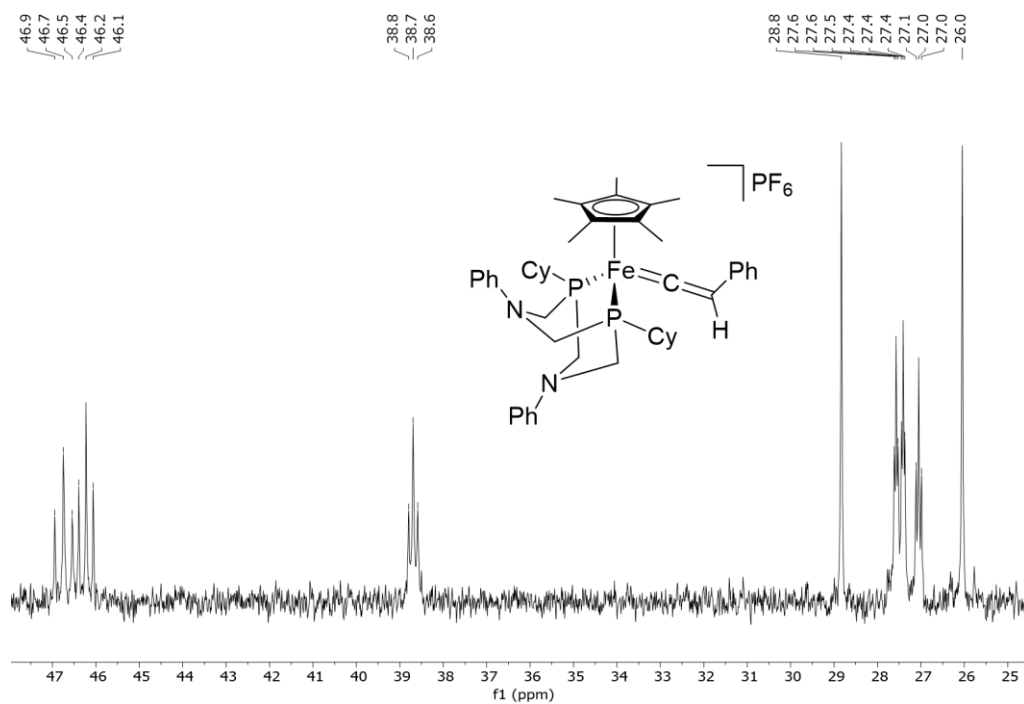
Appendix A.11: Magnified $^{13}C\{^1H\}$ NMR spectrum of **7** (162 MHz, CD_2Cl_2) showing complex multiplets.
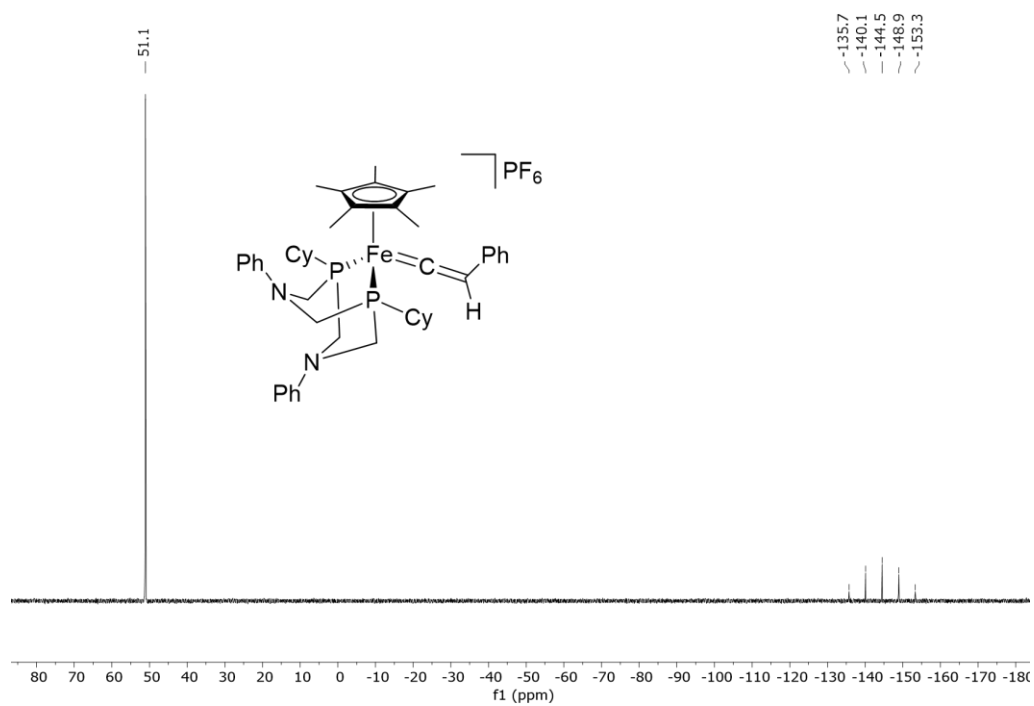
Appendix A.12: $^{31}P\{^1H\}$ NMR spectrum of **7** (162 MHz, CD_2Cl_2).
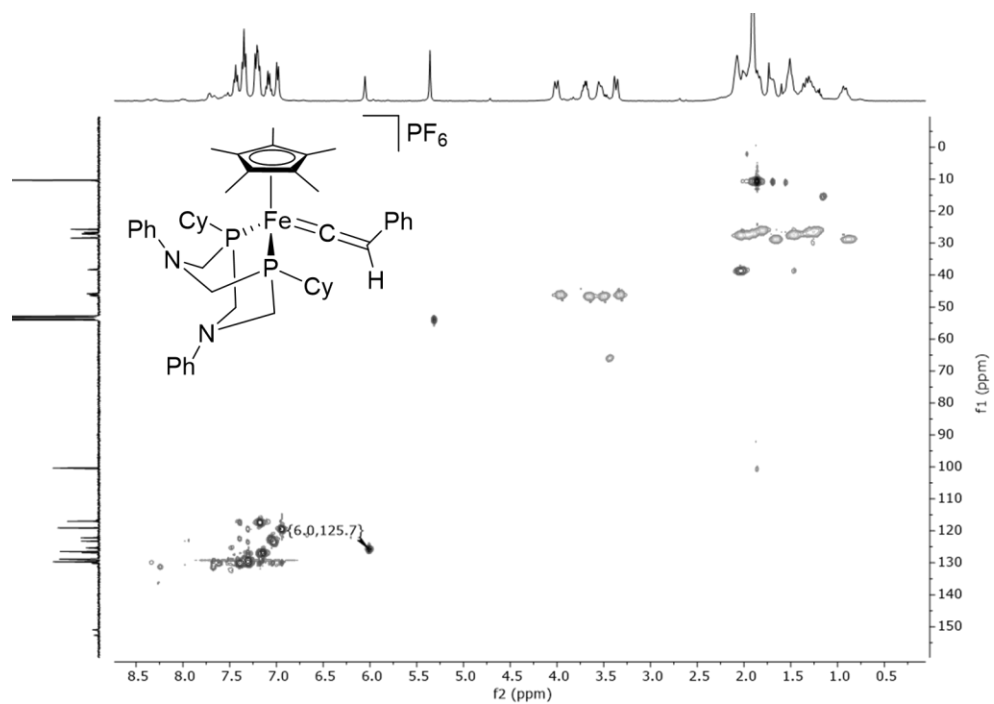
Appendix A.13: ^{1}H-^{13}C HSQC spectrum of **7** (400 MHz, CD$_2$Cl$_2$) showing H$_\beta$ and C$_\beta$ correlation.
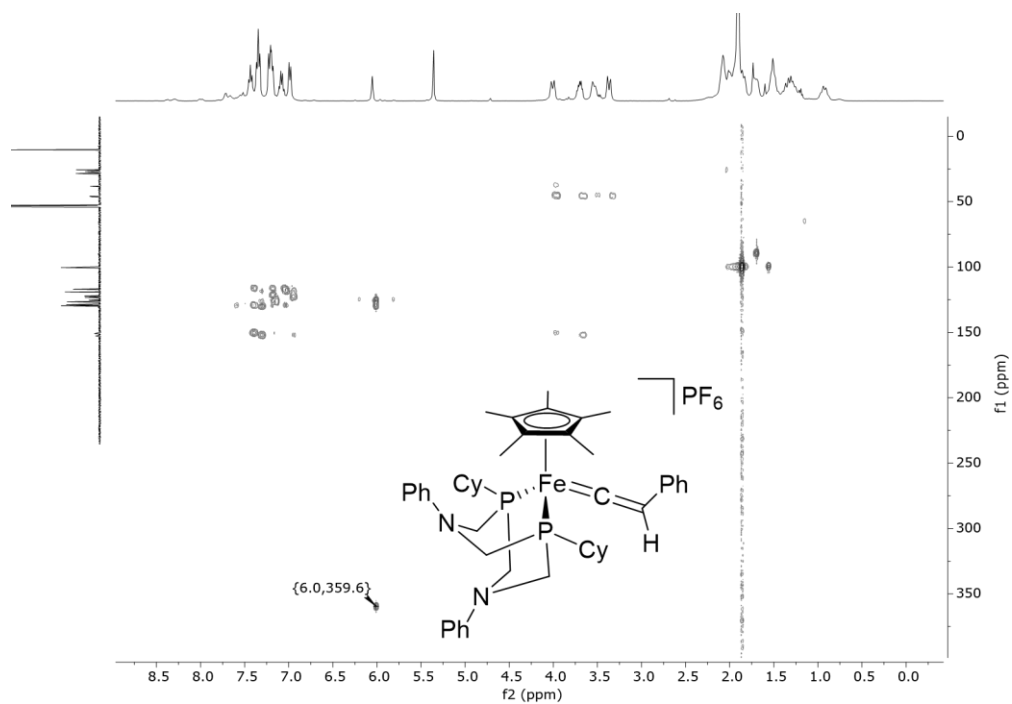
Appendix A.14: ^1H-^{13}C HMBC spectrum of **7** (400 MHz, CD_2Cl_2) showing H_β and C_α correlation.
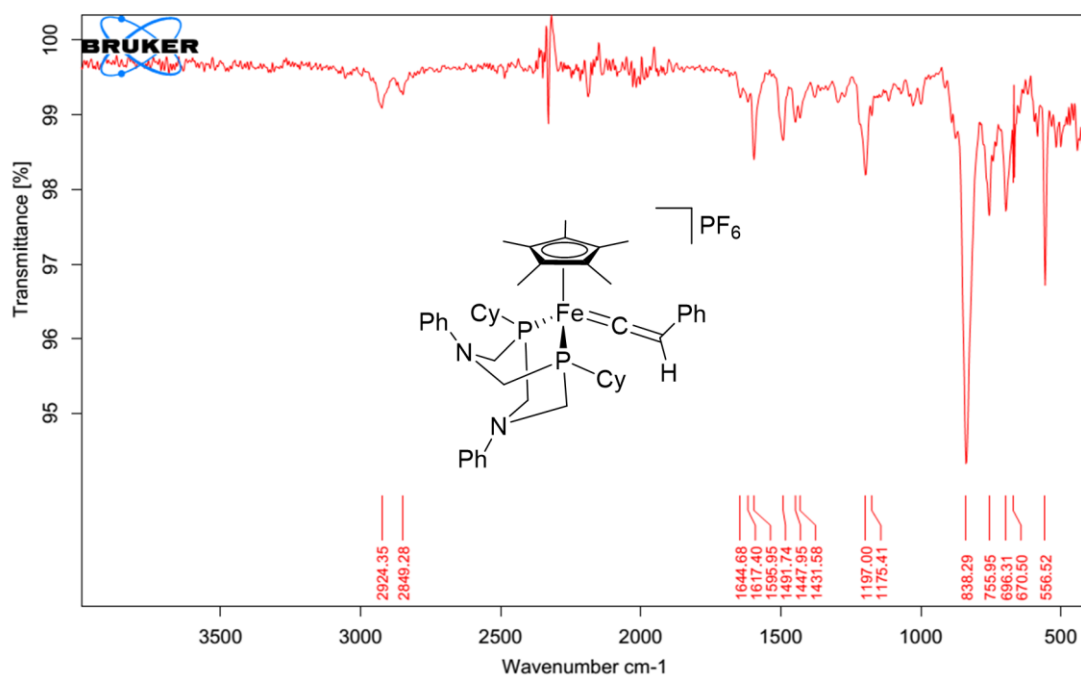
Appendix A.15: ATR-FTIR spectrum of **7**.
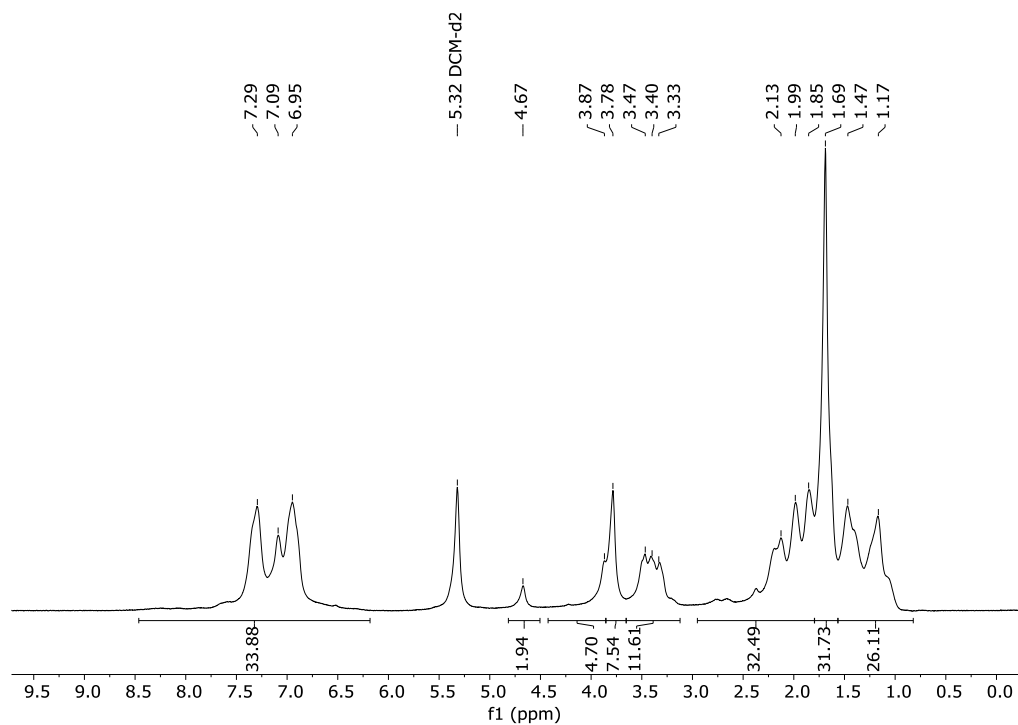
Appendix A.16: ^{1}H NMR spectrum of **15a** (400 MHz, CD$_2$Cl$_2$).
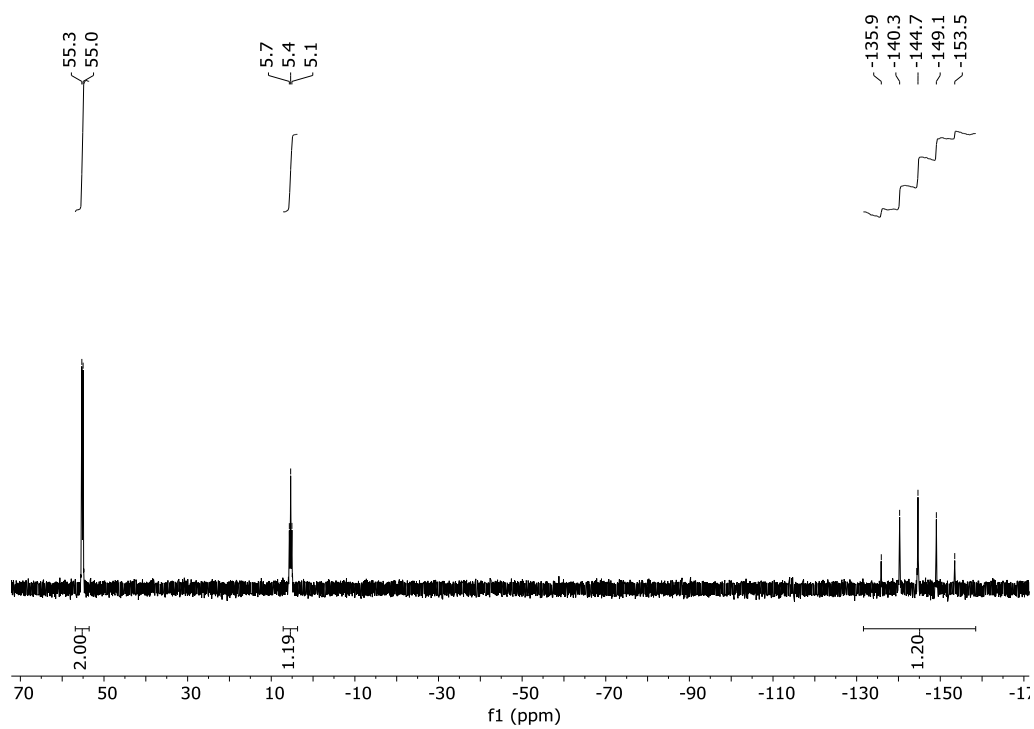
Appendix A.17: ^{31}P{^{1}H} NMR spectrum of **15a** (162 MHz, CD$_2$Cl$_2$).

Appendix A.18: Crystallographic Details

Experimental for C$_{42}$H$_{61}$F$_6$FeN$_4$P$_3$ (3a)

Data Collection and Processing. The sample (**3a**) was submitted by James Stubbs of the Blacquiere research group at the University of Western Ontario. The sample was mounted on a Mitegen polyimide micromount with a small amount of Paratone N oil. All X-ray measurements were made on a Bruker Kappa Axis Apex2 diffractometer at a temperature of 110 K. The unit cell dimensions were determined from a symmetry constrained fit of 9104 reflections with $5.76° < 2\theta < 67.32°$. The data collection strategy was a number of ω and ϕ scans which collected data up to $72.784°$ (2θ). The frame integration was performed using SAINT.[102] The resulting raw data was scaled and absorption corrected using a multi-scan averaging of symmetry equivalent data using SADABS.[103]

Structure Solution and Refinement. The structure was solved by using a dual space methodology using the SHELXT program.[104] All non-hydrogen atoms were obtained from the initial solution. The hydrogen atoms were introduced at idealized positions and were allowed to ride on the parent atom. The structural model was fit to the data using

full matrix least-squares based on F^2. The calculated structure factors included corrections for anomalous dispersion from the usual tabulation. The structure was refined using the SHELXL program from the SHELX suite of crystallographic software.[105] Graphic plots were produced using the Mercury program suite.[106] Additional information and other relevant literature references can be found in the reference section of this website (http://xray.chem.uwo.ca).
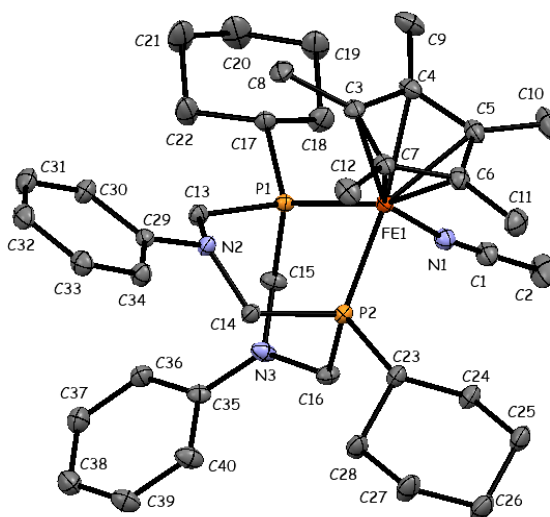
Appendix A.19: ORTEP drawing of **3a** *cation* showing naming and numbering scheme. Ellipsoids are at the 50% probability level and hydrogen atoms were omitted for clarity.
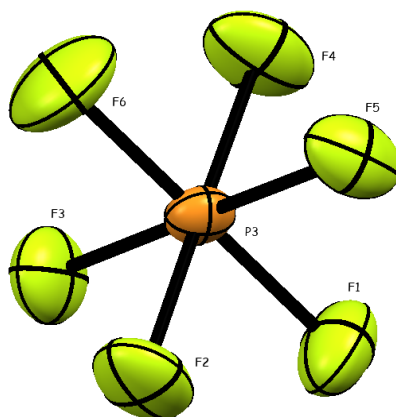
Appendix A.20: ORTEP drawing of **3a** *anion* showing naming and numbering scheme. Ellipsoids are at the 50% probability level.

Appendix A.21: Summary of Crystal Data for **3a**

Formula	$C_{42}H_{61}F_6FeN_4P_3$
Formula Weight (*g/mol*)	884.70
Crystal Dimensions (*mm*)	$0.405 \times 0.302 \times 0.219$
Crystal Color and Habit	red prism
Crystal System	orthorhombic
Space Group	P b c a
Temperature, K	110
a, Å	18.324(6)
b, Å	21.144(7)
c, Å	22.237(6)
α,°	90
β,°	90
γ,°	90
V, Å^3	8615(5)
Number of reflections to determine final unit cell	9104
Min and Max 2θ for cell determination, °	5.76, 67.32
Z	8
F(000)	3728
ρ (*g/cm*)	1.364
λ, Å, (MoKa)	0.71073

μ, (cm^{-1})	0.523
Diffractometer Type	Bruker Kappa Axis Apex2
Scan Type(s)	phi and omega scans
Max 2θ for data collection, °	72.784
Measured fraction of data	0.999
Number of reflections measured	348006
Unique reflections measured	20954
R_{merge}	0.0566
Number of reflections included in refinement	20954
Cut off Threshold Expression	$I > 2sigma(I)$
Structure refined using	full matrix least-squares using F^2
Weighting Scheme	w=1/[sigma^2(Fo^2)+(0.0440P)^2+3.9205P] where P=(Fo^2+2Fc^2)/3
Number of parameters in least-squares	512
R_1	0.0372
wR_2	0.0886
R_1 (all data)	0.0606
wR_2 (all data)	0.1005
GOF	1.006
Maximum shift/error	0.002
Min & Max peak heights on final DF Map (e^-/Å)	-0.452, 0.642

Where:

$R_1 = \Sigma(|F_o| - |F_c|) / \Sigma F_o$

$wR_2 = [\Sigma(w(F_o^2 - F_c^2)^2) / \Sigma(w F_o^4)]^{\frac{1}{2}}$

$GOF = [\Sigma(w(F_o^2 - F_c^2)^2) / (\text{No. of reflns.} - \text{No. of params.})]^{\frac{1}{2}}$

References

1.   Parshall, G. W., *J. Mol. Catal.* **1978**, *4*, 243-270.

2.   Ojima, I.; Tzamarioudaki, M.; Li, Z.; Donovan, R. J., *Chem. Rev.* **1996**, *96*, 635-662.

3.   Bolm, C.; Legros, J.; Le Paih, J.; Zani, L., *Chem. Rev.* **2004**, *104*, 6217-6254.

4.   Ananikov, V. P.; Beletskaya, I. P., *Organometallics* **2012**, *31*, 1595-1604.

5.   Behr, A.; Vorholt, A. J.; Seidensticker, T., *ChemBioEng Reviews* **2015**, *2*, 6-21.

6.   Bender, T. A.; Dabrowski, J. A.; Gagné, M. R., *Nature Reviews Chemistry* **2018**, *2*, 35-46.

7.   Shelke, Y. G.; Yashmeen, A.; Gholap, A. V. A.; Gharpure, S. J.; Kapdi, A. R., *Chem. Asian J.* **2018**, *13*, 2991-3013.

8.   Cai, Y.; Zhang, J.-W.; Li, F.; Liu, J.-M.; Shi, S.-L., *ACS Catalysis* **2019**, *9*, 1-6.

9.   Hayler, J. D.; Leahy, D. K.; Simmons, E. M., *Organometallics* **2019**, *38*, 36-46.

10.   Lu, C.; Du, J.; Su, X.-J.; Zhang, M.-T.; Xu, X.; Meyer, T. J.; Chen, Z., *ACS Catalysis* **2016**, *6*, 77-83.

11.   Das, U. K.; Ben-David, Y.; Leitus, G.; Diskin-Posner, Y.; Milstein, D., *ACS Catalysis* **2019**, *9*, 479-484.

12.   Fürstner, A., *ACS Central Science* **2016**, *2*, 778-789.

13.   Coles, N. T.; Webster, R. L., *Isr. J. Chem.* **2017**, *57*, 1070-1081.

14.   Gao, R.; Sun, W.-H.; Redshaw, C., *Catalysis Science & Technology* **2013**, *3*, 1172-1179.

15.   Sun, C.-L.; Li, B.-J.; Shi, Z.-J., *Chem. Rev.* **2011**, *111*, 1293-1314.

16.   Ananikov, V. P., *ACS Catalysis* **2015**, *5*, 1964-1971.

17.   Wei, D.; Darcel, C., *Chem. Rev.* **2019**, *119*, 2550-2610.

18.   Rummelt, S. M.; Darmon, J. M.; Yu, R. P.; Viereck, P.; Pabst, T. P.; Turner, Z. R.; Margulieux, G. W.; Gu, S.; Chirik, P. J., *Organometallics* **2019**, *38*, 3159-3168.

19.   Bauer, I.; Knölker, H.-J., *Chem. Rev.* **2015**, *115*, 3170-3387.

20.   Zweig, J. E.; Kim, D. E.; Newhouse, T. R., *Chem. Rev.* **2017**, *117*, 11680-11752.

21.   El-Sepelgy, O.; Brzozowska, A.; Azofra, L. M.; Jang, Y. K.; Cavallo, L.; Rueping, M., *Angew. Chem. Int. Ed.* **2017**, *56*, 14863-14867.

22.   Mastalir, M.; Glatz, M.; Pittenauer, E.; Allmaier, G.; Kirchner, K., *J. Am. Chem. Soc.* **2016**, *138*, 15543-15546.

23.   Wang, Y.; Zhu, J.; Durham, A. C.; Lindberg, H.; Wang, Y.-M., *J. Am. Chem. Soc.* **2019**, *141*, 19594-19599.

24.   Ananikov, V. P.; Tanaka, M., *Topics in Organometallic Chemistry* **2012**, *43*, 19.

25.   Li, D. Y.; Shi, K. J.; Mao, X. F.; Zhao, Z. L.; Wu, X. Y.; Liu, P. N., *Tetrahedron* **2014**, *70*, 7022-7031.

26.   Challinor, A. J.; Calin, M.; Nichol, G. S.; Carter, N. B.; Thomas, S. P., *Adv. Synth. Catal.* **2016**, *358*, 2404-2409.

27.   El-Sepelgy, O.; Brzozowska, A.; Sklyaruk, J.; Jang, Y. K.; Zubar, V.; Rueping, M., *Org. Lett.* **2018**, *20*, 696-699.

28.   Greenhalgh, M. D.; Jones, A. S.; Thomas, S. P., *ChemCatChem* **2015**, *7*, 190-222.

29.   Huang, L.; Arndt, M.; Gooßen, K.; Heydt, H.; Gooßen, L. J., *Chem. Rev.* **2015**, *115*, 2596-2697.

30.   Huo, J.; He, G.; Chen, W.; Hu, X.; Deng, Q.; Chen, D., *BMC Chemistry* **2019**, *13*, 89.

31.   Müller, T. E.; Grosche, M.; Herdtweck, E.; Pleier, A.-K.; Walter, E.; Yan, Y.-K., *Organometallics* **2000**, *19*, 170-183.

32.   Müller, T. E.; Hultzsch, K. C.; Yus, M.; Foubelo, F.; Tada, M., *Chem. Rev.* **2008**, *108*, 3795-3892.

33.   Severin, R.; Doye, S., *Chem. Soc. Rev.* **2007**, *36*, 1407-1420.

34.   Praveen, C.; Iyyappan, C.; Perumal, P. T., *Tetrahedron Lett.* **2010**, *51*, 4767-4771.

35.   Ding, D.; Mou, T.; Xue, J.; Jiang, X., *Chem. Commun.* **2017**, *53*, 5279-5282.

36.   Liu, R.; Li, M.; Xie, W.; Zhou, H.; Zhang, Y.; Qiu, G., *J. Org. Chem.* **2019**, *84*, 11763-11773.

37.   Wang, Y.; Bi, X.; Li, D.; Liao, P.; Wang, Y.; Yang, J.; Zhang, Q.; Liu, Q., *Chem. Commun.* **2011**, *47*, 809-811.

38.   Guo, X.; Pan, S.; Liu, J.; Li, Z., *J. Org. Chem.* **2009**, *74*, 8848-8851.

39.   Xu, X.; Liu, J.; Liang, L.; Li, H.; Li, Y., *Adv. Synth. Catal.* **2009**, *351*, 2599-2604.

40.   Lehnherr, D.; Ji, Y.; Neel, A. J.; Cohen, R. D.; Brunskill, A. P. J.; Yang, J.; Reibarkh, M., *J. Am. Chem. Soc.* **2018**, *140*, 13843-13853.

41.   Gunanathan, C.; Milstein, D., *Acc. Chem. Res.* **2011**, *44*, 588-602.

42.   Gunanathan, C.; Milstein, D., *Chem. Rev.* **2014**, *114*, 12024-12087.

43.   Hou, C.; Jiang, J.; Li, Y.; Zhao, C.; Ke, Z., *ACS Catalysis* **2017**, *7*, 786-795.

44.   Khusnutdinova, J. R.; Milstein, D., *Angew. Chem. Int. Ed.* **2015**, *54*, 12236-12273.

45.   Milstein, D., *Philos. Trans. R. Soc. A.* **2015**, *373*, 20140189.

46.   Werkmeister, S.; Neumann, J.; Junge, K.; Beller, M., *Chem. Eur. J.* **2015**, *21*, 12226-12250.

47.   Ikeda, Y.; Yamaguchi, T.; Kanao, K.; Kimura, K.; Kamimura, S.; Mutoh, Y.; Tanabe, Y.; Ishii, Y., *J. Am. Chem. Soc.* **2008**, *130*, 16856-16857.

48.   Mutoh, Y.; Ikeda, Y.; Kimura, Y.; Ishii, Y., *Chem. Lett.* **2009**, *38*, 534-535.

49.   Mutoh, Y.; Imai, K.; Kimura, Y.; Ikeda, Y.; Ishii, Y., *Organometallics* **2011**, *30*, 204-207.

50.   Singh, V. K.; Bustelo, E.; de los Ríos, I.; Macías-Arce, I.; Puerta, M. C.; Valerga, P.; Ortuño, M. Á.; Ujaque, G.; Lledós, A., *Organometallics* **2011**, *30*, 4014-4031.

51.   Ikeda, Y.; Kodama, S.; Tsuchida, N.; Ishii, Y., *Dalton Trans.* **2015**, *44*, 17448-17452.

52.   Otsuka, M.; Tsuchida, N.; Ikeda, Y.; Lambert, N.; Nakamura, R.; Mutoh, Y.; Ishii, Y.; Takano, K., *Organometallics* **2015**, *34*, 3934-3943.

53.   Watanabe, T.; Mutoh, Y.; Saito, S., *J. Am. Chem. Soc.* **2017**, *139*, 7749-7752.

54.   Kuwabara, T.; Sakajiri, K.; Oyama, Y.; Kodama, S.; Ishii, Y., *Organometallics* **2019**, *38*, 1560-1566.

55.   Roh, S. W.; Choi, K.; Lee, C., *Chem. Rev.* **2019**, *119*, 4293-4356.

56.   Cai, T.; Yang, Y.; Li, W.-W.; Qin, W.-B.; Wen, T.-B., *Chem. Eur. J.* **2018**, *24*, 1606-1618.

57.   Álvarez-Pérez, A.; González-Rodríguez, C.; García-Yebra, C.; Varela, J. A.; Oñate, E.; Esteruelas, M. A.; Saá, C., *Angew. Chem. Int. Ed.* **2015**, *54*, 13357-13361.

58.   Varela-Fernández, A.; Varela, J. A.; Saá, C., *Adv. Synth. Catal.* **2011**, *353*, 1933-1937.

59.   Varela-Fernández, A.; García-Yebra, C.; Varela, J. A.; Esteruelas, M. A.; Saá, C., *Angew. Chem. Int. Ed.* **2010**, *49*, 4278-4281.

60.   Varela-Fernández, A.; González-Rodríguez, C.; Varela, J. A.; Castedo, L.; Saá, C., *Org. Lett.* **2009**, *11*, 5350-5353.

61.   Chung, L.-H.; Yeung, C.-F.; Wong, C.-Y., *Chem. Eur. J.* **2020**, *26*, 6102-6112.

62.   Trost, B. M.; Rhee, Y. H., *J. Am. Chem. Soc.* **2002**, *124*, 2528-2533.

63.   Grotjahn, D. B., *Chem. Eur. J.* **2005**, *11*, 7146-7153.

64.   Grotjahn, D. B.; Incarvito, C. D.; Rheingold, A. L., *Angew. Chem. Int. Ed.* **2001**, *40*, 3884-3887.

65.   Grotjahn, D. B.; Lev, D. A., *J. Am. Chem. Soc.* **2004**, *126*, 12232-12233.

66.   Nair, R. N.; Lee, P. J.; Rheingold, A. L.; Grotjahn, D. B., *Chem. Eur. J.* **2010**, *16*, 7992-7995.

67.   Grotjahn, D. B., *Top. Catal.* **2010**, *53*, 1009-1014.

68.   Arita, A. J.; Cantada, J.; Grotjahn, D. B.; Cooksy, A. L., *Organometallics* **2013**, *32*, 6867-6870.

69.   Stubbs, J. M.; Bow, J. P. J.; Hazlehurst, R. J.; Blacquiere, J. M., *Dalton Trans.* **2016**, *45*, 17100-17103.

70.   Stubbs, J. M.; Bridge, B. J.; Blacquiere, J. M., *Dalton Trans.* **2019**, *48*, 7928-7937.

71.   Stubbs, J. M.; Chapple, D. E.; Boyle, P. D.; Blacquiere, J. M., *ChemCatChem* **2018**, *10*, 4001-4009.

72.   Liang, Q.; Osten, K. M.; Song, D., *Angew. Chem. Int. Ed.* **2017**, *56*, 6317-6320.

73.   Gorgas, N.; Stöger, B.; Veiros, L. F.; Kirchner, K., *ACS Catalysis* **2018**, *8*, 7973-7982.

74.   Gorgas, N.; Alves, L. G.; Stöger, B.; Martins, A. M.; Veiros, L. F.; Kirchner, K., *J. Am. Chem. Soc.* **2017**, *139*, 8130-8133.

75.   Brenna, D.; Villa, M.; Gieshoff, T. N.; Fischer, F.; Hapke, M.; Jacobi von Wangelin, A., *Angew. Chem. Int. Ed.* **2017**, *56*, 8451-8454.

76.   Hughes, D. L.; Leigh, G. J.; Jimenez-Tenorio, M.; Rowley, A. T., *J. Chem. Soc., Dalton Trans.* **1993**, 75-82.

77.   Boland-Lussier, B. E.; Churchill, M. R.; Hughes, R. P.; Rheingold, A. L., *Organometallics* **1982**, *1*, 628-634.

78.   Albertin, G.; Antoniutti, S.; Bordignon, E.; Del Ministro, E.; Ianelli, S.; Pelizzi, G., *J. Chem. Soc., Dalton Trans.* **1995**, 1783-1789.

79.   Bellerby, J. M.; Mays, M. J., *J. Organomet. Chem.* **1976**, *117*, C21-C22.

80.   Liu, T.; DuBois, D. L.; Bullock, R. M., *Nature Chemistry* **2013**, *5*, 228-233.

81.   Liu, T.; Wang, X.; Hoffmann, C.; DuBois, D. L.; Bullock, R. M., *Angew. Chem. Int. Ed.* **2014**, *53*, 5300-5304.

82.   Liu, T.; Chen, S.; O'Hagan, M. J.; Rakowski DuBois, M.; Bullock, R. M.; DuBois, D. L., *J. Am. Chem. Soc.* **2012**, *134*, 6257-6272.

83.   Weber, K.; Weyhermüller, T.; Bill, E.; Erdem, Ö. F.; Lubitz, W., *Inorg. Chem.* **2015**, *54*, 6928-6937.

84.   Zhang, F.; Jia, J.; Dong, S.; Wang, W.; Tung, C.-H., *Organometallics* **2016**, *35*, 1151-1159.

85.   Catheline, D.; Astruc, D., *Organometallics* **1984**, *3*, 1094-1100.

86.   Patiny, L.; Borel, A., *J. Chem. Inf. Model* **2013**, *53*, 1223-1228.

87.   Chapple, D. E.; Boyle, P. D.; Blacquiere, J. M., *Manuscript in Preparation* **2020**.

88.   Brackemeyer, T.; Erker, G.; Fröhlich, R.; Prigge, J.; Peuchert, U., *Chem. Ber.* **1997**, *130*, 899-902.

89.   Brandon, J. B.; Dixon, K. R., *Can. J. Chem.* **1981**, *59*, 1188-1200.

90.   Li, L.; Reginato, N.; Urschey, M.; Stradiotto, M.; Liarakos, J. D., *Can. J. Chem.* **2003**, *81*, 468-475.

91.   Pechmann, T.; Brandt, C. D.; Werner, H., *Dalton Trans.* **2004**, 959-966.

92.   Wang, L.; Liu, L.; Chang, W.; Li, J., *J. Org. Chem.* **2018**, *83*, 7799-7813.

93.   Mancuso, R.; Ziccarelli, I.; Armentano, D.; Marino, N.; Giofrè, S. V.; Gabriele, B., *J. Org. Chem.* **2014**, *79*, 3506-3518.

94.   Jiang, G.; Fang, S.; Hu, W.; Li, J.; Zhu, C.; Wu, W.; Jiang, H., *Adv. Synth. Catal.* **2018**, *360*, 2297-2302.

95.   Aouissi, A.; Al-Deyab, S. S.; Al-Shahri, H., *Molecules* **2010**, *15*, 1398-1407.

96.   Solovyev, A.; Lacôte, E.; Curran, D. P., *Dalton Trans.* **2013**, *42*, 695-700.

97.   Wang, Y.; Diallo, A. K.; Ornelas, C.; Ruiz, J.; Astruc, D., *Inorg. Chem.* **2012**, *51*, 119-127.

98.   Reger, D. L.; Coleman, C. J.; McElligott, P. J., *J. Organomet. Chem.* **1979**, *171*, 73-84.

99.   Reger, D. L.; Coleman, C. J., *Inorg. Chem.* **1979**, *18*, 3155-3160.

100.   Fihri, A.; Luart, D.; Len, C.; Solhy, A.; Chevrin, C.; Polshettiwar, V., *Dalton Trans.* **2011**, *40*, 3116-3121.

101.   G. Märkl, V.; Jin, G. Y.; Schoerner, C., *Tetrahedron Lett.* **1980**, *21*, 1409-1412.

102.   Bruker-AXS, SAINT version 2013.8, **2013**, Bruker-AXS, Madison, WI 53711, USA.

103.   Bruker-AXS, SADABS version 2012.1, **2012**, Bruker-AXS, Madison, WI 53711, USA.

104.   Sheldrick, G. M., *Acta Cryst.* **2015**, *A71*, 3-8.

105.   Sheldrick, G. M., *Acta Cryst.* **2015**, *C71*, 3-8.

106.   Macrae, C. F. B., I. J.; Chisholm, J. A.; Edington, P. R.; McCabe, P.; Pidcock, E.; Rodriguez-Monge, L.; Taylor, R.; van de Streek, J. and Wood, P. A. J., *Appl. Cryst.* **2008**, *41*, 466-470.

Curriculum Vitae

Name:	Benjamin Bridge	
Post-secondary Education:	B.Sc. University of Western Ontario London, Ontario, Canada	2014-2018
Honours and Awards:	OGS Master's Scholarship NSERC CGS-M Scholarship NSERC USRA Dean's Honour List	2019-2020 2018-2019 2017 2015-2018
Related Work Experience	Teaching Assistant Chemistry 2213A - UWO Teaching Assistant Chemistry 1302B - UWO Undergraduate Research Assistant - UWO	2019 2019 2016-2017

Publications:

4. B.J. Bridge, P.D. Boyle, J.M. Blacquiere. 'Endo-Selective Iron Catalysts for Intramolecular Alkyne Hydrofunctionalization' *Submitted*, **2020**, om-2020-00307s.

3. J.M. Stubbs, B.J. Bridge, J.M. Blacquiere. 'Optimizing Ligand Structure for Low-Loading and Fast Catalysis for Alkynyl-Alcohol and -Amine Cyclization' *Dalton Trans.*, **2019**, *48*, 7928-7937.

2. K.M.K. Jackman, B.J. Bridge, E.R. Sauvé, C.N. Rowley, C.H.M. Zheng, J.M. Stubbs, P.D. Boyle, J.M. Blacquiere. 'C(sp^3)-C(sp^3) Coupling with a Pd(II) Complex Bearing a Structurally Responsive Ligand' *Organometallics*, **2019**, *38*, 1677.

1. J.M. Stubbs, K.F. Firth, B.J. Bridge, K.J. Berger, R.J. Hazlehurst, P.D. Boyle, J.M. Blacquiere. 'Phosphine-Imine and -Enamido Ligands for Acceptorless Dehydrogenation Catalysis' *Dalton Trans.*, **2017**, *46*, 647.

Presentations:

4. B.J. Bridge, P.D. Boyle, J.M. Blacquiere. $P^R_2N^{R'}_2$ Iron (II) Complexes for Intramolecular Hydroamination (Poster). *Canadian Chemistry Conference and Exhibition*, Quebec, QC, June 2019.

3. B.J. Bridge, J.M. Stubbs, J.M. Blacquiere. Synthesis of Iron $P^R_2N^{R'}_2$ Complexes for Cyclization Catalysis (Poster). *Inorganic Discussion Weekend*, Waterloo, ON, Oct 2018.

2. B.J. Bridge, M.A. Kerr. Progress Towards the Formal Synthesis of Chanoclavine I (Oral). *SOUSCC*, Waterloo, ON, March 2018.

1. E.R. Sauvé, B.J. Bridge, C.H.M. Zheng, H. Yoon, P.D. Boyle, and J.M. Blacquiere. Reductive Elimination of Ethane Induced by Coordinative Unsaturation of a Mono-Methyl Pd(II) Complex (Poster). *CSC Conference*, Toronto, ON, May 2017.

Graduate Courses	9503R Advanced NMR Spectroscopy I	0.25 credits
	9563Q Total Synthesis	0.25 credits
	9603T Advanced NMR Spectroscopy II	0.25 credits
	9651S Organometallic Bond Activation	0.25 credits
	9657Y Graduate Seminar Course	0.50 credits